KU LEUVEN

FACULTY OF SCIENCE

Unravelling the role of ROCK in the pathological retina

Insights from expression and inhibition studies on mouse and pig retinal cell and explant models

Lien VEYS

Supervisor: Prof. Dr. L. Moons

Co-supervisor: Dr. Inge Van Hove

Mentor: Evy Lefevere

Thesis presented in fulfillment of the requirements for the degree of Master of Science in Biology

Academic year 2015-2016

Dankwoord

Utile dulci, deze Latijnse zegswijze, afkomstig uit de Ars Poetica van Horatius, is niet enkel voor literairen, maar ook voor wetenschappers een inspirerende gedachte. Vrij vertaald kan je het interpreteren als: 'het nuttige aan het aangename koppelen'. Deze woorden vond ik wel passend om mijn thesis en tevens het laatste hoofdstuk van mijn studieloopbaan in te leiden. Tijdens de afgelopen vijf jaar biologie koppelde ik dan ook het nuttige - het opsteken van kennis met betrekking tot alle mogelijke aspecten van de biologie en het behalen van een diploma - aan het aangename - een groeiende verwondering voor de complexiteit van mens en natuur naast het verwerven en delen van nieuwe inzichten met een leuke en hechte groep medestudenten -. In mijn thesisjaar was dat niet anders, na een weloverwogen zoektocht naar een boeiend project vond ik een onderwerp dat me écht interesseerde. Het werken aan de thesis vormde een heuse uitdaging, maar uiteindelijk blik ik toch tevreden terug op een goed thesisjaar en kan ik toch wel met enige trots mijn proefschrift voorleggen. Hierbij wil ik niet nalaten enkele mensen te bedanken.

In de eerste plaats wil ik graag mijn promotor Lieve Moons bedanken voor de kans die ze me gaf om op een stimulerende werkplek onderzoek te verrichten en voor het nalezen van mijn thesis. Ook Evy en Inge, mijn twee begeleidsters, ben ik dankbaar voor het vele verbeterwerk, maar ook voor alle labotechnieken en de schrijfvaardigheden die ze me dit jaar bijgebracht hebben (én voor de brownies!). Alle andere mensen van het labo, in het bijzonder Lut, hielpen me verder met nuttige tips en antwoorden op vragen die opdoken tijdens mijn experimenten in het labo. Verder wil ik graag de andere thesisstudenten vermelden, namelijk Asmin, Astrid, Eline, Jolien, Lore, Marie-Anne, Sophie, Wout, Charlotte en Nathan, bij wie ik af en toe mijn hart kon luchten. Zonder hun steun en vriendschap, de thesisavondjes en pauzemomentjes in het park met onze "Thesis Crew" zou het jaar lang niet zo "*dulci*" geweest zijn.

Tot slot wil ik ons vertrouwde en hechte gezin, mijn broers en zussen: Joke, Koen, Kaat en Bart, bedanken voor hun geduld met mij tijdens dit drukke jaar en om de weekends leuk te maken. Mama en papa wil ik niet alleen bedanken voor hun steun, zorg en aanmoediging maar ook voor het bekostigen van mijn kot en mijn studies. Ik weet dat ik op hen kan rekenen als het nodig is: om bijvoorbeeld op een late vrijdagavond een grieperig thesisstudentje van het labo naar huis te brengen, om mij telefonisch moed in te spreken of gewoon een klankbord te bieden. Joey, die na 5 jaar ook al echt deel uitmaakt van ons gezin, was op vele momenten een belangrijk steun- en rustpunt; zijn geduld, zijn talent om mij heel veel te doen lachen en om te relativeren: "stap voor stap, dan kom je er wel", zijn tips voor het bijschaven van mijn Engels, waren onvervangbaar.

Dank jullie wel allemaal, *let's roll with ROCK*!

Table of Contents

Samenvatting

Als gevolg van de toenemende levensverwachting, dreigen meer en meer personen te lijden aan meestal onomkeerbare neurodegeneratieve aandoeningen van het centraal zenuwstelsel, zoals de ziekte van Alzheimer en Parkinson, maar ook glaucoom en diabetische retinopathie. Omdat dergelijke ziekten de levenskwaliteit negatief beïnvloeden en de huidige behandelingen ze niet voldoende kunnen stoppen of genezen, is het ontwikkelen van nieuwe strategieën, waaronder neuroprotectieve en axon regeneratieve therapieën, zeer dringend en wenselijk. Hiervoor is het optische circuit een ideaal modelsysteem omdat het goed gekarakteriseerd, anatomisch eenvoudig en makkelijk te manipuleren is. Recent werd de inhibitie van *Rho-associated coiled-coil kinase* (ROCK) naar voor geschoven als een efficiënte en veelbelovende strategie om neuronale overleving en axonale regeneratie te bewerkstellingen. Omdat zijn exacte werkingsmechanismen echter nog niet gekend zijn, is het doel van deze thesis om de rol van ROCK gedetailleerder te ontrafelen op cellulair niveau in de gezonde en pathologische retina. Aangezien het exacte expressiepatroon in de retina nog niet volledig gekarakteriseerd is, werden eerst de expressielevels van ROCK1 en ROCK2 bestudeerd in gezonde en gestresseerde retinale cellen, geïsoleerd uit varkensogen. Dit toonde een duidelijke aanwezigheid van ROCK in gezonde Müller glia aan en vroege, differentiële veranderingen in expressieniveau van beide isovormen onder stress. Verder werden varkens retinale explanten geoptimaliseerd en gevalideerd om te dienen als model voor neurodegereratie, door neuronale overleving en gliale reactiviteit in kaart te brengen. Tot slot werden postnatale muis retinale explanten gebruikt om ROCK2 te lokaliseren in gliale vezels en neurieten en om het effect van neurotropines en ROCK inhibitors en de combinatie van beiden op neurietuitgroei bloot te leggen.

Summary

As a consequence of the increased life expectancy, more people are likely to suffer from mostly irreversible neurodegenerative diseases, such as Parkinson's and Alzheimer's disease, but also glaucoma and diabetic retinopathy. Because these diseases reduce the quality of life and current treatments fail to prevent or reverse neurodegeneration, the development of novel strategies, including neuroprotective and axon regenerative therapies, is urgent and highly desirable. The optical circuit is an ideal model system for this, because it is well-charactarised, anatomically simple and easy to manipulate. Recently, the inhibition of Rho-associated coiled-coil kinase (ROCK) was put forward as an efficient and promising strategy to effectuate neuronal survival and axonal regeneration. However, because its exact working mechanism remains elusive, the main objective of this thesis is to unravel the role of ROCK in more detail on a cellular level in the healthy and pathological retina. Since the exact ROCK expression pattern in the retina remains elusive, firstly the expression levels for ROCK1 and ROCK2 were studied in healthy and stressed retinal cells isolated from porcine eyes. This study demonstrated a clear presence of ROCK in healthy Müller glia and an early differential upregulation of both isoforms in response to stress. Furthermore, a porcine retinal explant was optimised and validated to serve as a neurodegeneration mimicking, model by examining neuronal survival and glial reactivity. Finally, postnatal mouse retinal explants were used to demonstrate the localisation of ROCK2 in glial fibres and neurites and to uncover the stimulatory and differential neurite outgrowth capacities of neurotrophins and ROCK inhibition and the combination of both.

List of abbreviations

Ab	Antibody
AD	Aqua destillata
AH	Aqueous humour
ALS	Amyotrophic lateral sclerosis
AMA	AMA0428
BDNF	Brain-derived neurotrophic factor
BRB	Blood-retinal barrier
BSA	Bovine Serum Albumin
cAMP	Cyclic adenosine monophosphate
Cdc42	Cell division cycle 42
CNS	Central nervous system
CNTF	Ciliary neurotrophic factor
CRMP-2	Collapsin response mediator protein-2
CSPG	Chondroitin sulphate proteoglycan
DAPI	4',6-diamidino-2-phenylindole
DIV	Days *in vitro*
DMSO	Dimethyl sulfoxide
DPBS	Dulbecco's phosphate buffered saline
DPX	Distyrene Plasticizer Xylene
DR	Diabetic retinopathy
ECM	Extracellular matrix
EGF	Epidermal growth factor
ERM	Erzin/radixin/moesin
EtOH	Ethanol
GAM	Goat anti mouse

GAP	GTPase activating protein
GAP-43	Growth-associated protein-43
GAR	Goat anti rabbit
GCC	Ganglion cell complex
GCL	Ganglion cell layer
GDP	Guanosine diphosphate
GEF	Guanine nucleotide exchange factor
GFAP	Glial fibrillary acidic protein
GON	Glaucomatous optic neuropathies
GS	Glutamine synthetase
GTP	Guanosine triphosphate
H&E	Hematoxilin & Eosin
hiFBS	Heat inactivated foetal bovine serum
HIV	Hours *in vitro*
HSE	Health, Safety and Environment
Iba-1	Ionised calcium-binding adapter molecule 1
ICC	Immunocytochemistry
IHC	Immunohistochemistry
ILM	Inner limiting membrane
IL	Interleukin
INA	Immunodetected neurite area
INL	Inner nuclear layer
IOP	Intraocular pressure
IPL	Inner plexiform layer
L	Containment level
LGN	Lateral geniculate nucleus
LP	Lava purple

LIMK	LIM kinases
MAG	Myelin-assosiated glycoprotein
MAP	Microtubule-associated protein
MLC	Myosin light chain
MLCP	Myosin light chain phosphatase
mTOR	Mechanistic target of rapamycin
MQ	Milli-Q
NaAz	Sodium azide
NeuN	Neuronal nuclei
NF	Neurofilament
NFL	Nerve fibre layer
NMDA	N-methyl-D-aspartate
NOA	Neurite outgrowth area
Nogo	Neurite outgrowth inhibitor
NPDR	Non-proliferative diabetic retinopathy
NTG	Normal tension glaucoma
OLM	Outer limiting membrane
OMgp	Oligodendrocyte-myelin glycoprotein
ONC	Optic nerve crush
ONH	Optic nerve head
ONL	Outer nuclear layer
OPL	Outer plexiform layer
P	Postnatal day
PBS	Phosphate buffered saline
PDR	Proliferative diabetic retinopathy
Pen/Strep	Penicillin/Streptomycin
PFA	Paraformaldehyde

PlGF	Placental growth factor
PNS	Peripheral nervous system
PTEN	Phosphate and tensin homolog
Rac1	Ras-related C3 botulinum toxin substrate 1
RBPMS	RNA-binding protein with multiple splicing
RGC	Retinal ganglion cell
ROCK	Rho-associated coiled-coil kinase
ROS	Reactive oxygen species
RPE	Retinal pigment epithelium
rpm	Rotations per minute
RT	Room temperature
RT-PCR	Real time PCR
SDS	Sodium dodecyl sulphate
SEM	Standard error of the mean
SOCS3	Suppressor of cytokine singaling 3
TBS	Tris buffered saline
TM	Trabecular meshwork
TNB	Tris NaCl buffer
TNF-α	Tumor necrosis factor α
TUNEL	Terminal deoxynucleotidyl transferase dUTP nick-end labeling
VEGF	Vascular endothelial growth factor
WB	Western Blot
Y2	Y-27632
Y3	Y-39983

1 Literature study

An increasing group of people is affected by age-related diseases like neurodegenerative diseases. The current treatments only focus on reducing the symptoms, relieving the pain or increasing mobility, but they do not interfere with the progression of the disease itself (Frank, 2015; Tezel, 2006). Therefore, studying the cellular and molecular pathways underlying neurodegeneration, until now poorly understood, is necessary to further develop novel therapeutic approaches in CNS injuries or diseases. Some of these pathways, for example protein degradation pathways, the intrinsic mitochondrial apoptotic pathway and extrinsic apoptotic pathways have been key players in the search for therapeutic strategies for over a decade (Bredesen et al., 2006; Rubinsztein, 2006; Thompson, 2008). However, novel players arrive on the neurodegenerative research scene. One of these novel potential therapeutic strategies involves the Rho-ROCK pathway. Several reports demonstrate that this pathway might be involved in the pathogenesis of neurodegenerative diseases (Van de Velde et al., 2015). During the course of this Masters' thesis, the focus will be on the protease ROCK and its potential role in the development of glaucoma and diabetic retinopathy (DR). Both are neurodegenerative eye disorders that can lead to permanent vision loss and eventually blindness. In glaucoma, loss of retinal ganglion cells (RGCs) and their axons first leads to a decline of peripheral vision, followed by a gradual decline of central vision (Bear et al., 2007). In DR, poor blood sugar control due to diabetes damages the tiny blood vessels in the retina, which results in edema and distorts central vision (Schmidt et al., 2008).

1.1 The human visual system

The ability to see is an efficient way to perceive stimuli in our surroundings. Seeing requires a complex interplay between the eyes and the brain through several components, collectively called the visual system. Injury to the visual system will lead to vision loss. The visual pathway, shown in Figure 1, starts at the level of the eyes, where visual information enters as light energy (Bear et al., 2007). Photoreceptors of the retina convert this form of energy into electrical energy and neural activity is generated. These signals propagate through the optic nerve, which consists of axons from RGCs, the

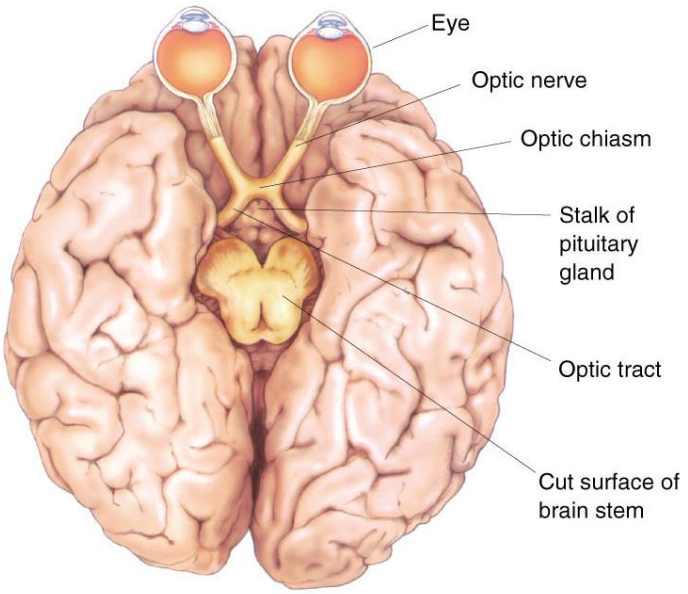

Figure 1: Bottom view of the brain showing the optic nerves, optic chiasm and optic tract (Bear et al., 2007).

projection neurons, via the optic chiasm, where most axons cross over to the contralateral side of the brain and others remain at the ipsilateral side of the brain. Thereafter, visual stimuli are transmitted through the optical tracts to (sub)thalamic brain regions, such as the superior colliculus and the lateral geniculate nucleus (LGN). The LGN is an important visual processing center in the thalamus, where signals are processed before they are passed along to the primary visual cortex.

1.1.1 The eye

The mammalian eye consists of the actual eyeball and additional structures, e.g. the eye muscles, the eyelids and the lacrimal glands. The nerve fibres connecting the eye and the brain form the optic nerve. Together with bloodvessels, they leave the eye trough a hole in the sclera that is covered with a mesh-like structure, the lamina cribrosa (Kiel, 2010). The eyeball, as shown in Figure 2 is made up of three layers: the fibrous tunic, the vascular tunic and the nervous tunic (Perkins, 2015).

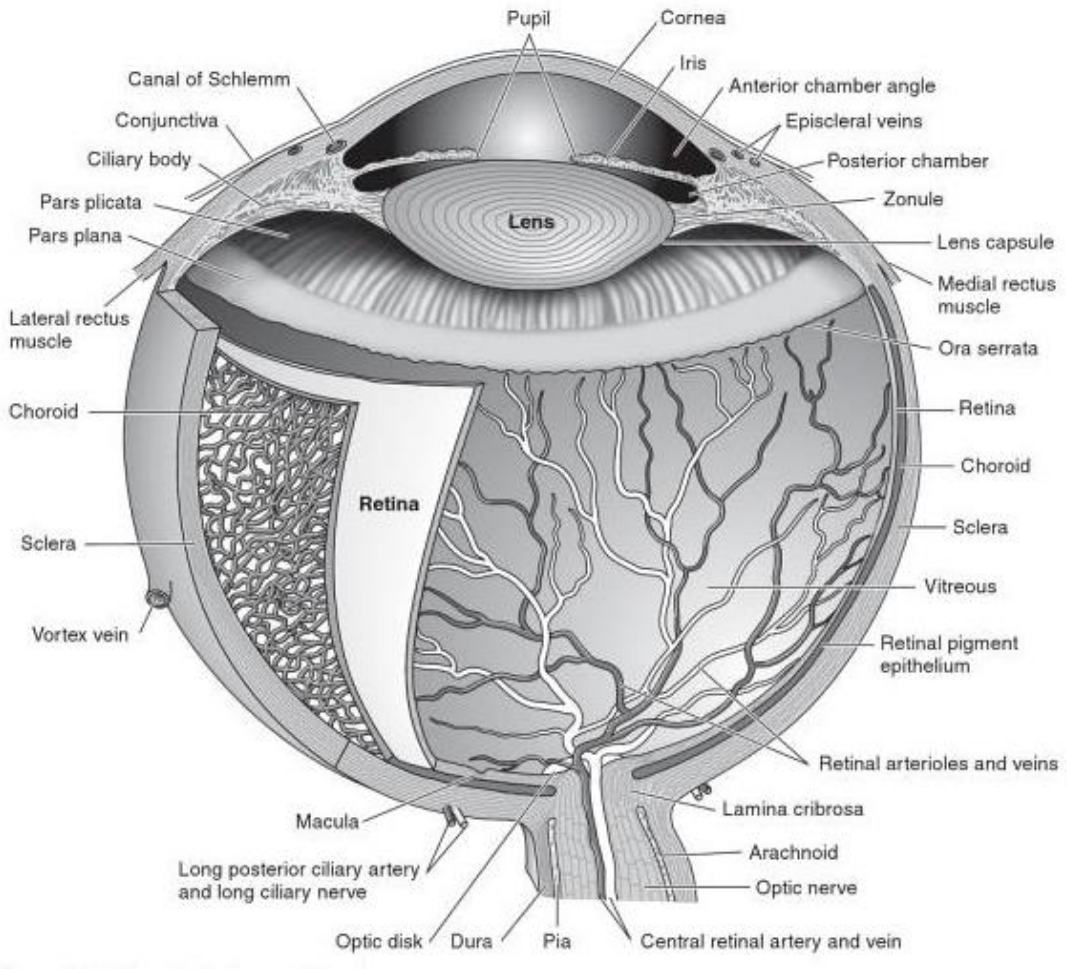

Figure 2: Anatomy of the human eye. The eyeball is made up of three layers: the fibrous tunic (sclera and cornea), the vascular tunic (blood vessels, iris, ciliary body and choroid) and the nervous tunic (retina and optic nerve). (Riordan-Eva & Cunningham, 2011).

Firstly, the **fibrous tunic** consists of the sclera and the cornea, which are continuous. The **cornea** is the transparent surface on the anterior part of the eye, while the **sclera** is made up of strong connective tissue that covers the rest of the eye. These two parts are essential structural components of the eye, since they ensure solidity.

Second, the **vascular tunic**, also called the uvea, is the middle layer and consists of the iris, the ciliary body and the choroid. The **iris**, adjacent to the cornea, consists of two muscles surrounding the pupil and is strongly pigmented. The **ciliary body** is a complex and highly specialised tissue that is built up of ciliary muscles and pigmented and non-pigmented ciliary epithelium. Relaxation and contraction of the ciliary muscles can change the shape of the lens. Further, the ciliary epithelium produces the aqueous humour (AH). The AH fills the anterior- and posterior chamber of the eye and has an important function in nourishment of the lens and the cornea and it permits inflammatory cells and mediators to circulate in the eye in pathological conditions (Junqueira & Carneiro, 2005). The anterior chamber is the fluid-filled space between the iris and the cornea. The posterior chamber includes the space between the iris and the connection between the lens and the ciliary body. On the contrary, the posterior cavity of the eye, called the vitreal chamber, is filled with vitreous humour, which is a gelatinous, transparent mass composed of a highly-hydrated double network of protein fibrils and charged polysaccharide chains. It is mainly produced before birth by the non-pigmented cells of the ciliary body and is important in maintaining the structural stability of the eye and keeping the retina in its place. The **choroid** lies between the retina and the sclera and contains connective tissue and choroid vessels, which supply blood and provides oxygen and metabolic substrates to the inner layers of the retina. These choroid vessels originate from the posterior ciliary arteries (Kiel, 2010). The next layer, separates the choroid from the retina and is called **Bruch's membrane**, which is a pentalaminar membrane that is composed of elastic fibres and acts as a regulator of the exchange of biomolecules, nutrients, oxygen, fluids and metabolic waste products between the retina and the general circulation via the blood vessels of the choroid (Booij et al., 2010).

Thirdly, the inner layer of the eye comprises the **nervous tunic** and is also called the **retina**, which is considered a part of the central nervous system (CNS) (Perkins, 2015).

1.1.1.1 The retina

1.1.1.1.1 Retinal cell types

The mammalian retina is located at the posterior side of the eye and contains a set of specific cell types. Its main purpose is to convert light to electrochemical signals, which are percieved in the brain as vision. Most of these cells, as shown in Figure 3, can be classified into 5 distinct classes of cells: the vascular cells, the macroglia, the neurons, the microglia and the retinal pigment epithelial (RPE) cells (Gardner et al., 2002). The **vascular cells** consist of

pericytes and endothelial cells. The first are modified smooth muscle cells, able to contract and relax to regulate the vascular blood flow of the eye, while the endothelial cells are one of the major components of the blood-retinal barrier (BRB). The **macroglia** (Müller glia and astrocytes) are cells of neuroectodermic origin. They support the retinal blood vessels and neurons, and they regulate the retinal metabolism (Cavallotti & Cerullo, 2008). The Müller glia are the most prominent glial cells in the retina (Reichenbach & Bringmann, 2010). They have very important functions in the support of the other retinal structures, in providing neuronal support and in the maintenance of a homeostatic retinal extracellular environment. Furthermore, they regulate the balance of ions, water, neurotransmitter molecules and pH. Müller glia may also be involved in the control of angiogenesis, and the regulation of retinal blood flow (Fruttiger, 2007). These cells span across the retina from the inner limiting membrane (ILM) to the outer limiting membrane (OLM), where they ensheath and contact every type of neuron in the retina (Bringmann et al., 2006). This morphological relationship enables functional interactions between neurons and Müller glia. Importantly, most retinal diseases are associated with Müller glia gliosis, in which the cells are in a reactive state and known to be highly involved in the development of retinal edema and neuronal cell death (Bringmann et al., 2006). In contrast to the long Müller glia, astrocytes are star shaped cells that only reside in the inner part of the retina, where they fold around blood vessels and RGCs.

The third class of cells, the **neurons**, consists of approximately 55 different cell types in mammals (Masland, 2001). They are separated in different cell types: RGCs, amacrine cells, bipolar cells, horizontal cells and photoreceptors.

Next to macroglia, also

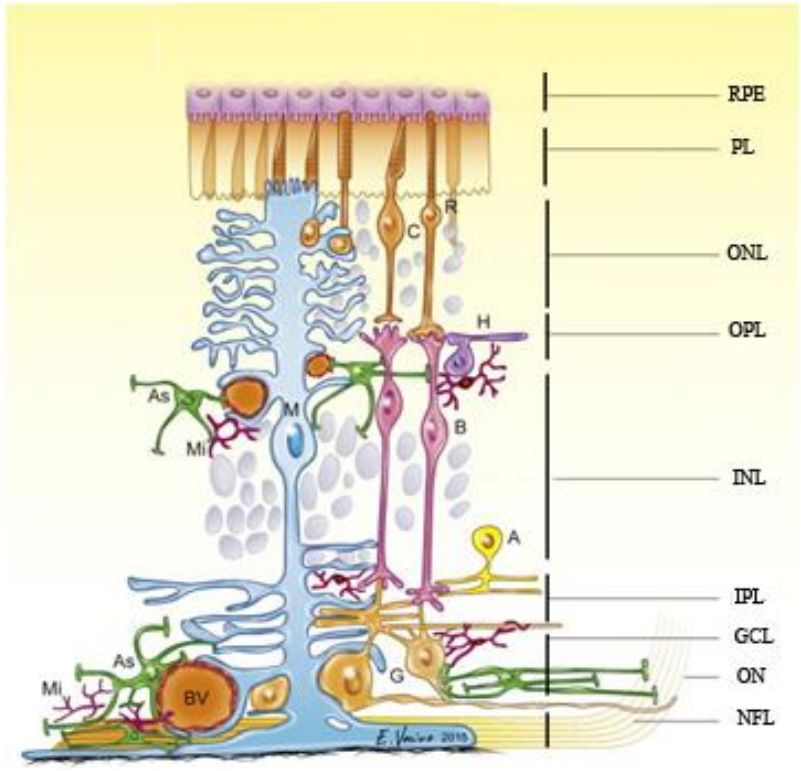

Figure 3: Schematic drawing of the retinal cell types. First, the blood vessels (BV) supply oxygen and nutrients to the other cells. Second, the macroglia consist of Müller glia in blue (M) and astrocytes in green (As). Third, the neurons consist of cone (C) and rod (R) photoreceptors, bipolar cells (B), amacrine cells (A) and retinal ganglion cells (G), which send their axons to the brain via the optic nerve (ON). Fourth, there are the microglia in red (Mi). These different cell types are arranged in different layers (from the most internal to the outer layers): the nerve fibre layer (NFL), the ganglion cell layer (GCL), the inner plexiform layer (IPL), the inner nuclear layer (INL), the outer plexiform layer (OPL), the outer nuclear layer (ONL), the photoreceptor layer (PL) and retinal pigment epithelium (RPE). Adapted from Vecino et al. (2015).

microglia provide structural support to the retina and have an important function in the tissue surveillance. As blood-born immunologic cells cannot penetrate the retina under physiological conditions, due to the BRB, these resident macrophages act as a first line of active immune defence in the CNS by becoming phagocytotic in response to homeostatic disturbances by invading microorganisms or cell damage. During this transition, their appearance will change from ramified microglia to amoeboid microglia. Moreover, the microglia are involved in cell degeneration, RGC apoptosis and removal of dead cells. Another important function of microglia is the communication with neurons and glial cells by secreting factors that pass on information about the functional or pathological state of the eye (Vecino et al., 2015). Some examples of such secretory molecules are chemokines, cytokines, reactive oxygen species (ROS), growth factors and neurotrophic factors like brain-derived neurotrophic factor (BDNF) (Jha et al., 2013). An additional cell type is the **RPE cell** that lies within the RPE. These cells are pigmented granule-containing hexagonal epithelial cells and mainly have a function in epithelial transport, light absorption, immune modulation and ion balancing. Diseases like macular degeneration or retinitis pigmentosa are associated with an impaired RPE function (Klimanskaya, 2006). The interactions and functional integration of all these cell types are required for normal vision.

1.1.1.1.2 Retinal layers

The aforementioned retinal cell types are organised in ten distinct layers, through which the light is converted to energy. The outermost layer is the RPE, followed by the photoreceptor layer, the OLM, the outer nuclear layer (ONL), the outer plexiform layer (OPL), the inner nuclear layer (INL), the inner plexiform layer (IPL), the ganglion cell layer (GCL), the nerve fibre layer (NFL) and the innermost ILM, as shown in Figure 3.

The multifunctional and essential **RPE** is composed of RPE cells and is attached to the choroid. Just below the RPE lies the **photoreceptor layer** (rods and cones), which contains the inner and outer segments, but not the nuclei of photoreceptor cells. Rods are elongated cylindrical cells that are very sensitive to low light intensity, while cones are conical or flask shaped, both connected to the OLM (Swaroop et al., 2010). The cones are responsible for colour vision and are less sensitive to low light intensity levels. The third layer, the **OLM**, is the boundary between the photoreceptor layer and the ONL. This OLM plays a major role in maintaining the structure of the retina through a series of adherens junctions between photoreceptors and neighboring Müller glia that serve to determine apical-basal polarity in photoreceptor cells (Omri et al., 2010). The fourth layer, the **ONL**, contains the nuclei of the photoreceptor cells. In the next layer, the **OPL**, neuronal synapses are formed between dendrites of horizontal and bipolar cells from the INL and photoreceptor dendrites from the ONL. The sixth layer, the **INL**, contains cell bodies of bipolar, amacrine and horizontal cells. Furthermore, the **IPL** is the layer where axons of bipolar cells and amacrine cells synapse

with dendrites of RGCs. The cell bodies of these RGCs are contained in the next layer, the **GCL**, but also a small number of "displaced amacrine cells" are present (MacNeil & Masland, 1998). The RGCs extend their axons into the optic NFL and they leave the eyeball at the optic disc. The retinal **NFL** is a very sensitive structure that lies in between the GCL and the ILM. It gradually becomes thicker around the optic nerve head (ONH), where the nerve fibres pass the lamina cribrosa and continue their way to the brain. In the optic disc, several blood vessels erupt and the long axons from the RGCs converge in the optic nerve. No visual stimuli can be perceived at this spot, also called the blind spot (Perkins, 2015). The most inner layer of the retina, as the name states, is the **ILM**. It is a very thin layer formed by the footplates of Müller glia and astrocytes and it is the border between the retina and the vitreous body (Gelman et al., 2015).

1.1.1.1.3 Phototransduction

All these celltypes and cell layers play a specific role in maintaining retinal function and support the neuronal conversion of light energy into neuronal activity. Photoreceptors (rods or cones) contain a set of proteins called opsins and use those proteins for phototransduction, the process of converting light energy into electrical signals. In practice, the opsins will absorb a photon, which results in the hyperpolarisation of the photoreceptor cell. Next, the photoreceptor carries the signal to the neighbouring cell by making a synaptic connection. The basic circuitry of the retina incorporates a three-neuron chain: photoreceptor to bipolar cell to RGC. This chain can be extended by horizontal cells, amacrine cells, other bipolar cells and other RGCs (Masland, 2001).

1.1.1.1.4 Vasculature

The delivery of metabolic substrates and oxygen to the retina is accomplished by 2 independent vascular systems: the retinal and the choroidal vessels (Runkle & Antonetti, 2011). More specifically, 85% of the retinal blood flow originates from the choroidal vessels, while the central retinal artery, which nourishes the inner retinal layers, provides the remaining 15%. The central retinal artery branches from the optic nerve and runs through the optic nerve head to reach the retina (Erickson et al., 2007; Pournaras et al., 2008). The venous circulation follows a similar pattern and drains the metabolic waste products (Kiel, 2010). However, not all retinal areas are equally covered with blood vessels. The macula lutea or the yellow spot is characterised by a lack of blood vessels, and represents a spot with improved quality of vision (Perkins, 2015). The fovea is a dark spot in the center of the macula without rods, but only cone-like photoreceptors, which enables a very detailed and sharp colour vision in bright light.

1.2 The visual system of the mouse and the pig

The visual system of rodents and higher-order mammals is structurally and functionally similar, which is why rodents like mice and rats are heavily used as animal models for ocular

diseases (Levkovitch-Verbin, 2004). However, there are some differences which must be considered (Wang & Burkhalter, 2007). A notable first difference is the lateral placement of rodent eyes, resulting in a larger visual field, but a smaller binocular visual field. As a consequence, less than 10% of the RGC axons remain at the ipsilateral side of the brain when passing through the optic chiasm, whereas in humans 50% project ipsilaterally (Hübener, 2003; Levkovitch-Verbin, 2004). Secondly, the vast majority of rodent RGCs projects their axon to the superior colliculus and only a small minority projects to other targets like the LGN, whereas in humans it is the other way around (Hübener, 2003). Furthermore, rodent lenses are rounder, less flexible and occupy a larger portion of the eye, the lamina cribrosa is not present and 97% of the photoreceptors in the retina are rods, which are essential for the rodent's nightlife, while 95% of human photoreceptors are rods (Tkatchenko et al., 2010). More primitive mammals like mice also lack a macular region and fovea, although they posses a residue of an evolutionary ancient fovea, the visual streak, an area characterised by high RGC densities (Azuma, 2000).

The porcine eye is similar to the human eye in terms of anatomy, vasculature, and photoreceptor distribution. Therefore it provides an attractive animal model for retinal disease research (Guduric-Fuchs et al., 2009). However the major difference is the lack of a fovea, although a visual streak is present (Azuma, 2000).

1.3 Neurodegenerative diseases

Neurodegenerative diseases of the CNS like Parkinson's, Alzheimer's and Huntington disease, amylotrophic lateral sclerosis (ALS) and glaucoma are characterised by accelerated neuronal loss, axonal degeneration and trans-synaptic degeneration (Beal et al., 2005), and their progression increases with age. These diseases seriously affect quality of life and human wellbeing (MIT, 2014). With the ageing population in the more economically developed countries (Gavrilova & Gavrilov, 2009), an increasing group of people is affected by age-related diseases like neurodegenerative diseases. The current treatments for these neurodegenerative diseases only focus on reducing the symptoms, relieving the pain or increasing mobility, but they do not interfere with the progression of the disease itself (Frank, 2015; Tezel, 2006). Therefore, studying the pathological mechanisms underlying neurodegeneration, until now poorly understood, is necessary to further develop novel therapeutic approaches in CNS injuries or diseases.

Even though the various neurodegenerative diseases show different symptoms and their causes remain unclear, the degenerative mechanisms might be shared (Nieoullon, 2011). Common factors that may play a role in neuronal cell death are free radicals and antioxidants produced by various cells in the brain, mitochondrial and metabolic dysfunction, excitoxicity, induced by abnormal regulation of glutamate transporters, calcium binding proteins,

neurotrophic factors, protein misfolding, cellular defence mechanisms, oxidatively damaged DNA repair, compounds acting on ion channels, metals, inflammation, etc. (Beal et al., 2005).

Because the retina is considered a part of the CNS, the visual system is a powerful and easily accessible modelsystem to study CNS neurodegeneration.

1.3.1 Glaucoma

1.3.1.1 General introduction

Glaucoma is a heterogenous group of glaucomatous optic neuropathies (GONs), diseases commonly characterised by age-related progressive degeneration of the optic nerve and apoptosis of RGC somata. As shown in Figure 4, this leads to loss of vision, which starts in the periphery and progresses towards the center of the visual field (Bear et al., 2007). Glaucoma is the second leading cause of irreversible blindness worldwide. In 2010, around 60 million people were diagnosed with glaucoma, and the numbers are ever increasing (Nickells et al., 2012; Resnikoff et al., 2008). Formerly, glaucoma was considered a disease of the eye, however, more recent studies showed that glaucoma is a disease of the whole visual system, including intracranial optic nerve, LGN, and visual cortex (Dekeyster et al., 2015; Gupta et al., 2006).

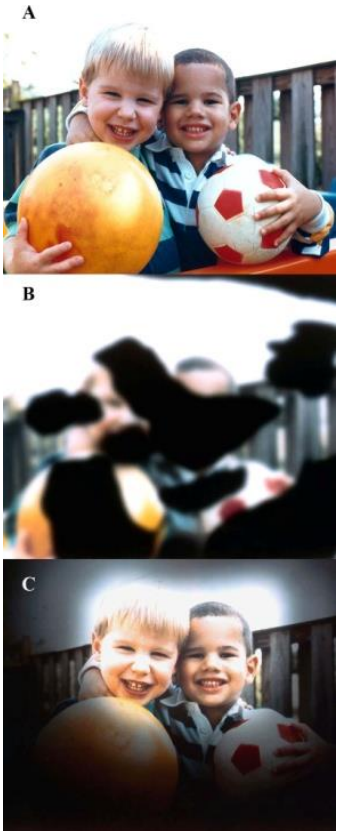

Figure 4: A: normal vision, B: vision of a patient with diabetic retinopathy, C: vision of an advanced glaucomatous patient (Bear et al., 2007).

1.3.1.2 Pathogenesis of glaucoma

Despite the prevalence of this group of diseases, its pathophysiology remains rather vague, because several risk factors, separately or simultaneously, contribute to the disease's progression. The best studied risk factor and the only treatable one is a high intraocular pressure (IOP) (Weinreb & Khaw, 2004). However, glaucomatous vision loss can likewise occur without elevated IOP and the disease might progress despite succesfull IOP lowering therapies. Other important risk factors are age, family history, gender, ethnic background, severe myopia, disturbed cerebrospinal fluid pressure and vascular disorders (Van de Velde et al., 2015). Furthermore, several underlying mechanisms can play a central role in inducing glaucomatous degeneration, e.g. affected glial cells, local ischemia-hypoxia, excitotoxicity, defective axonal transport, increased oxidative stress, an aberrant immune system, inflammatory cytokines, etc. One of the hypothetical cascades of the multifactorial pathogenesis leading to glaucomatous RGC apoptosis is shown in Figure 5. Both mechanical and/or ischemic insults may cause mitochondrial dysfunction, thereby resulting in oxidative stress and subsequent RGC apoptosis due to oxidative damage.

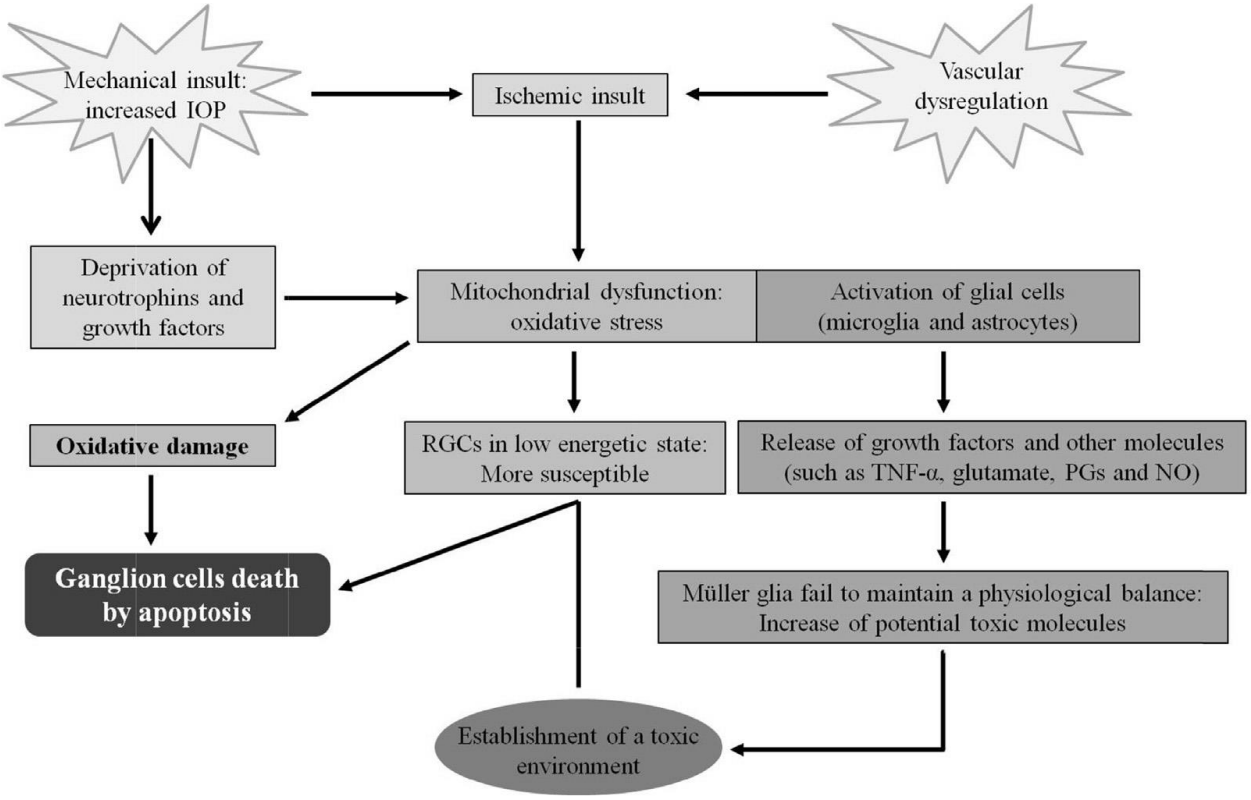

Figure 5: Hypothetical cascade of the events leading to glaucomatous RGC death. Both mechanical and/or ischemic insults may cause mitochondrial dysfunction, thereby resulting in oxidative stress and subsequent RGC apoptosis due to oxidative damage. Mitochondrial dysfunction leads to an activation of glial cells, causing a gradual release of growth factors and other molecules (tumor necrosis factor-α (TNF-α), glutamate, prostaglandins (PGs) and nitric oxide (NO)). Initially, Müller glia will try to maintain a physiological balance, but eventually they will fail. A gradual increase in the level of these potential harmful molecules will lead to establishment of a toxic environment. The RGCs are already in a decreased energetic state, so they are even more susceptible to further injury, thereby also these RGCs will be triggered to death via apoptosis (Van de Velde et al., 2015).

Mitochondrial dysfunction also leads to an activation of glial cells, causing a gradual release of growth factors and other molecules. Initially, Müller glia will try to maintain a physiological balance, but eventually they will fail. A gradual increase in the level of potential harmful molecules will lead to establishment of a toxic environment. Because the RGCs already are in a decreased energetic state, they are even more susceptible to further injury, and as such these RGCs will be triggered to death via apoptosis (Van de Velde et al., 2015).

In the paragraphs below, the important risk factors IOP, vascular insufficiency, oxidative stress and excitotoxic damage will be discussed, followed by the role of glia in the pathogenesis of glaucoma.

Historically, an **elevated IOP** is considered to be a key element in glaucomatous pathophysiology. The AH is produced in the cilliary body, where it migrates via a pressure gradient from the posterior chamber to the anterior chamber and leaves the eye via two outflow pathways, the trabecular meshwork (TM) pathway and the uveoscleral pathway (Figure 2) (Murgatroyd & Bembridge, 2008). The TM is a sieve like structure that allows the AH to be drained by Schlemm's canal. This outflow pathway, as shown in Figure 6, accounts for 90% of the total AH outflow. Another outflow route is provided by the uveoscleral pathway, were the AH passes the supraciliar space and is drained by the venous circulation of the ciliary body and the sclera (Johnson & Erickson, 2000). An imbalance between AH production and outflow leads to an increase or decrease of the IOP. TM degeneration or obstruction, as can occur in glaucoma, then results in a decreased outflow and leads to a primary consequence of glaucoma: elevated IOP. The IOP elevation subsequently generates mechanical stress on the posterior structures of the eye and causes the deformation or remodeling of the ONH (Figure 2), resulting in optic nerve 'cupping' and RGC axon damage (Burgoyne, 2015). Furthermore, mechanical axonal damage and **disruption of axonal transport** will interfere with retrograde delivery of essential trophic factors to RGCs from the brain (Weinreb et al., 2014). This axon transport failure will eventually lead to ischaemia, increased oxidative stress and a secondary wave of **RGC apoptosis**. The apoptosis of RGCs is regulated by intrinsic pathways in which BAX is upregulated, leading to elevated permeability of the mitochondrial membrane. This mitochondrial permeability will evoke the release of cytochrome *c* and the formation of an aposome, with subsequent activation of the caspase cascade (Nickells, 2012).

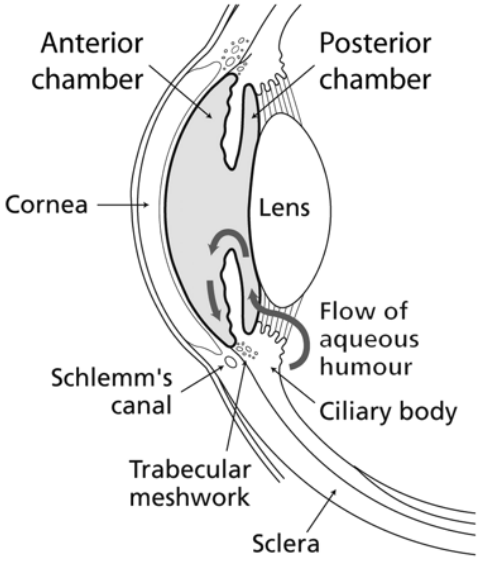

Figure 6: Flow of the aqueous humour in a healthy eye (Murgatroyd & Bembridge, 2008).

In a healthy eye, a normal and continuous vascular flow is essential to provide metabolites and oxygen to the vital parts of the eye. The perfusion rate of the blood flow of the eye is autoregulated by both IOP and local arterial blood pressure (Cursiefen et al., 2000). Vasoconstriction and subsequent reduction in blood pressure on one hand or elevated IOP on the other hand can reduce that vascular flow. A decline in cerebral and ocular perfusion has been observed to coincide with **vascular dysregulation** induced by mechanical stress or age. The failure of autoregulation then often leads to ocular ischaemia (Agarwal et al., 2009).

Excessive ROS formation is an important risk factor in several neurodegenerative ocular diseases, e.g. age-related macular degeneration and glaucoma (Yildirim et al., 2004). ROS, including peroxides, superoxide, hydroxyl radicals and singlet oxygen, are constantly

produced by the cellular metabolism as a consequence of mitochondrial dysfunction, abnormal protein folding, vascular dysregulation and defects in protein degeneration and aerobic metabolism (Tezel, 2006). Controlled amounts of ROS are essential in cell signaling and regulation and the eye is protected from an oxidative stress excess, but when antioxidant potential is out of balance, surplus of ROS will lead to the accumulation of **oxidative stress**. Moreover, glaucoma patients show a diminished antioxidant capacity (Ferreira et al., 2004). In certain forms of glaucoma, vascular dysregulation, together with oxidative stress evoke changes in TM cells, thereby increasing outflow resistance and elevating IOP. Besides TM changes, elevated NO levels also lead to an increased glutamate release, which results in neuronal toxicity (Agarwal et al., 2009). The long axons of RGCs are particularly sensitive to energy loss and oxidative stress. Moreover, if axons are damaged, the trophic factors BDNF and ciliary neurotrophic factor (CNTF), produced by target neurons from the brain, will not be able to reach the RGCs, which will as a result become even more prone to cell death (Weinreb et al., 2014).

Glutamate-mediated toxicity, or glutamate **excitotoxicity**, is another known factor in the pathogenesis of glaucoma. Glutamate is the most prominent excitatory neurotransmitter in the CNS and glutamate neurotransmission is mediated via metabolotropic (G protein-linked) and ionotropic (N-methyl-D-aspartate (NMDA)) receptors. Elevated glutamate levels result in the failure of the intracellular calcium homeostasis, mitochondrial dysfunction, generation of ROS and loss of mitochondrial membrane potential (Agarwal et al., 2009). Mytochondrial dysfunction causes insufficient energy supply and can lead to even higher levels of ROS and makes the cells more vulnerable to apoptosis (Prentice et al., 2015). An excess calcium influx will activate pro-apoptotic signaling cascades in neurons and induces membrane depolarisation (Almasieh et al., 2012; Dong et al., 2008). Moreover, damaged RGCs release glutamate in the extracellular space, which will stimulate excitotoxicity in other RGCs and contribute to a positive feedback loop (Sucher et al., 1997).

The exact mechanism underlying damage to RGC axons by glial cells remains to be elucidated. Most retinal neurodegenerative diseases are associated with a **reactive Müller glia gliosis**, leading to morphological, biochemical and physiological changes depending on the type and severity of the pathology. Müller gliosis has a dual role in neuronal survival. On the one hand, Müller glia support the survival of retinal neurons by releasing neurotrophic factors that protect neurons, the uptake and degradation of glutamate, the secretion of antioxidants, the facilitation of neovascularisation or by transdifferentiating into cells with neuronal phenotype. On the other hand, gliotic Müller glia may accelerate the progress of neuronal degeneration by dysregulating various neuronsupportive functions and secreting toxic factors that can influence neighbouring axons, they can contribute to edema

development and glial scar formation (Bringmann et al., 2009a; Bringmann et al., 2006; Chong & Martin, 2015).

Astrocytes can also become gliotic in response to disturbances. Müller glia and astrocytes modulate both neurotransmitter levels and excitotoxicity by removing the majority of glutamate from the extracellular space in the retina. When glutamate transport into Müller glia is reduced, for example in pathological conditions, more glutamate is transported into the neurons (Bringmann et al., 2009b).

Finally, also **microglia** become activated and migrate to the site of injury in the early disease stages, even before RGC damage, so they clearly contribute to the disease onset or progression (Bosco et al., 2011). Furthermore, induced IOP elevation results in an early increase in microglial activity and density in the retina, optic nerve and optic tract (Ebneter et al., 2010). This activation can lead to a secretion of proinflammatory cytokines, thereby negatively influencing RGC survival. Healthy RGCs can temper microglial reactivity, while a chronic activation of microglia occurs when RGCs are damaged (Chong & Martin, 2015).

1.3.1.3 Treatment of Glaucoma

The currently available therapies to treat glaucoma only decrease the symptoms or the risk of glaucomatous vision loss. Lowering elevated IOP is currently the only successful therapy. Results from different clinical trails have demonstrated the benefit of IOP lowering in glaucoma (Easthope & Perry, 2002; Higginbotham et al., 2004).

Several categories of IOP lowering treatments are used. A first group includes eyedrops and stimulate the removal of AH from the eye. They are able to reduce the IOP by about 30% in glaucomatous patients, which leads to less structural and functional damage of the RGCs (Linden & Alm, 1999). However, when the therapy appears to be ineffective, if too many side effects occur, or when the patient is not compliant, other more invasive measures will have to be taken. Laser trabeculoplasty lowers IOP by increasing AH outflow via laser induced biological changes in the TM (Patel et al., 2015). During filtration surgery, parts of the TM and adjacent structures are cut out, to encourage draining via this route . Other less invasive strategies have been proposed to lower IOP, such as devices to drain AH to an external reservoir.

However, IOP lowering operations are not always successful, because surgical complications and inappropriate wound healing can occur, leading to still a progressive visual loss in treated patients (Rulli et al., 2013; Weinreb et al., 2014). Despite medical or surgical treatment, the progression of the disease is often slowed down, but not completely stopped (Agarwal et al., 2009). Given the current limitations in glaucoma therapy, it is clearly necessary to develop novel IOP-independent therapies to prevent RGC damage. Moreover, 30-40% of glaucomatous patiens have a normal IOP, also called normal tension glaucoma (NTG).

Despite the multifactoriality GONs, they are all characterised by RGC degeneration and axonal loss, which is why nowadays, neuroprotective strategies, that focus directly on protecting RGCs, are put forward as an alternative or additional therapy to accommodate all GON patients (Agarwal et al., 2009).

1.3.2 Diabetic retinopathy

1.3.2.1 General introduction

DR is a common complication of *diabetes mellitus* type 1 and 2 as a consequence of hyperglycemia, but the disease can also have other pathological causes, such as oxidative stress, advanced glycation end products, protein kinase C and inflammation (Frank, 2015; Tapp et al., 2003; Wan et al., 2015). It is the major cause of blindness among adults in their working age worldwide, but also affects people in other age classes (Wan et al., 2015). Poor blood sugar control due to diabetes disturbes a number of metabolic pathways and leads to damage of the tiny blood vessels in the retina, thereby distorting vision as shown in Figure 4 (Schmidt et al., 2008).

Several risk factors contribute to the development of the disease e.g. duration of diabetes, systolic blood pressure, genetic factors, glycemic control and urinary albumin (Tapp et al., 2003; Xu et al., 2012).

1.3.2.2 Pathogenesis of diabetic retinopathy

DR pathology can be subdivided into non-proliferative diabetic retinopathy (NPDR) and the more advanced proliferative diabetic retinopathy (PDR), wich is characterised by retinal and choroidal neovascularisation (Tapp et al., 2003). During the disease's progression in PDR, the damaged tissues and angiogenic factors result in the provocation of novel vessel outgrowth.

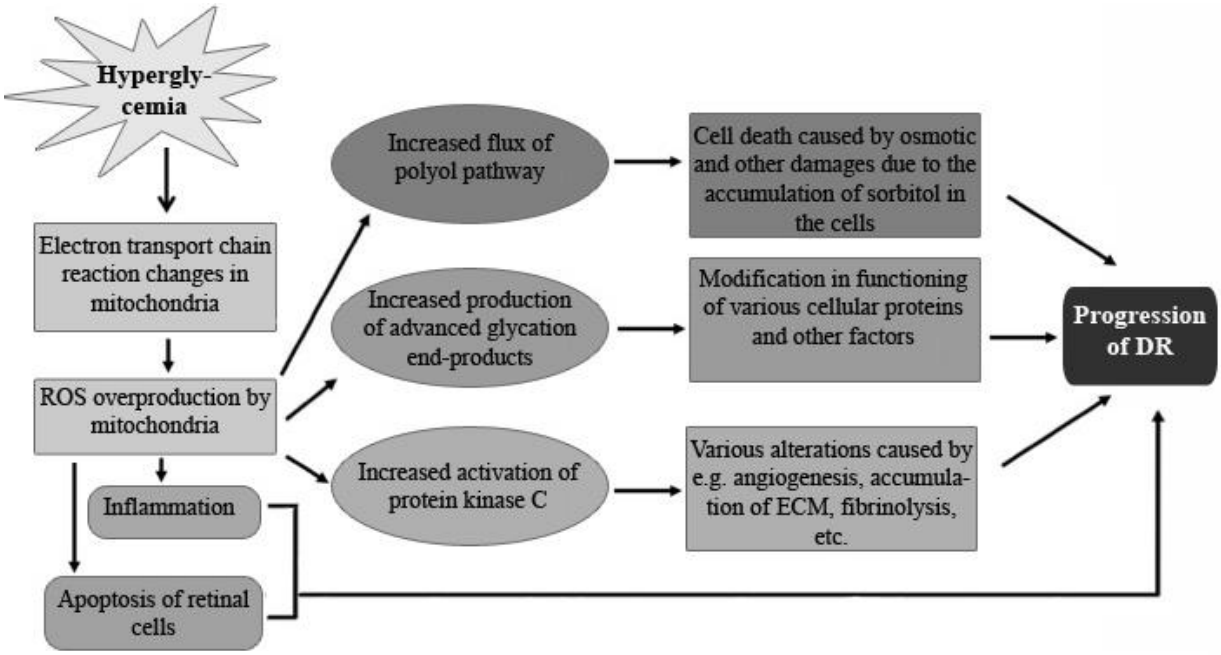

Figure 7: Hypothetical cascade of events leading to the progression of diabetic retinopathy. Adapted from Behl et al. (2015).

These vessels will not normalise and will be more susceptible to damage, and can for example lead to vitreous heamorrages. In NPDR, microaneurisms are more common, leading to the formation of exudates that can also potentially cause haemorrages (Behl et al., 2015). The exact pathological mechanisms of DR are not fully understood yet, but hypotheses are made as shown in Figure 7. ROS production due to hyperglycemia could lead to inflammation, apoptosis of retinal cells and stimulation of the polyol pathway, advanced glycation end product production and protein kinase C activation, all encouraging DR progression.

DR is characterised by leaky vessels, microaneurysms, capillary apoptosis and new blood vessels sprouting (neovascularisation) in the retina. This leads to inter-retinal edema, ocular hemorrhage and eventually closure of the retinal vessels and decrease of blood perfusion (Tian et al., 2015). However, DR is not only characterised by **vascular problems**, but also fibrosis, inflammation and **neurodegeneration** have been observed in patients. Furthermore, not only photoreceptors are affected, but also other retinal cell types such as RGCs and glia encounter metabolic discrepancies, which can lead to apoptosis of both RGCs and photoreceptors (Adamiec-Mroczek et al., 2015; Cuenca et al., 2014; Kern & Berkowitz, 2015). As a consequence, thinning of retinal layers and disturbance of retinal homeostasis will occur, which leads to loss of visual function (Barber, 2015). Very recently, axon loss has been implicated in DR, together with astrocyte reactivity and myelin alterations in the distal part of the ON (Dorfman et al., 2015). However, the timing and exact location of early neurodegeneration is still debated (Cuenca et al., 2014).

Although the pathogenesis is not clear yet, a strong correlation has been demonstrated between DR and **hyperglycemia**, or elevated blood sugar levels. Elevated glucose levels in the blood plasma seem to have a negative effect on different tissues and cells, such as RPE cells, vascular cells, photoreceptors and glia in the retina, (Ola & Alhomida, 2014; Xu et al., 2011). In retinal vascular cells, this effect is very distinct and results in proliferation of endothelial cells and swelling of retinal blood vessels. Several consequences, such as loss of pericytes and endothelial cells, can lead to dysfunction of the BRB, capillary apoptosis and microaneurisms. Chronic hyperglycemia is also associated with inflammation, cellular injury, RPE damage and thickening of the basement membranes in the retinal blood vessels, which will cause closing of the capillaries, leading to hypoxia, tissue ischaemia, release of angiogenic factors (e.g. vascular endothelial growth factor (VEGF) and placental growth factor (PlGF)) (Behl et al., 2015; Wan et al., 2015; Xu et al., 2011).

Since DR is also a metabolic disease, levels of several metabolites will change, like glutamate, ROS and neurotrophic factors. **Oxidative stress** can be induced by higher ROS levels in DR and contributes to the pathogenesis of the disease (Wan et al., 2015). ROS are responsible for the destruction of cellular structures and alter several other pathways and mechanisms, for example, ROS in the retina can lead to augmented advanced glycation end

products and activated protein kinase C. Moreover, oxidative stress is implicated to be involved in the osmotic swelling of Müller glia, which may contribute to development of edema in the eye (Krugel et al., 2011). Furthermore oxidative stress can contribute to the development of inflammation (Friedlander, 2007). As such, ROS can increase the susceptibility to damage in the retina. The aforementioned mechanisms work in a synergistic way and thereby damage the endothelial cells even more (Behl et al., 2015).

Inflammation of blood-born leukocytes is implicated in the pathology of DR, however, little is known about the contribution of the inflammatory process to this disease. Multiple mediators play important roles in inflammation, including proinflammatory cytokines (e.g. interleukin (IL) -6 and tumor necrosis factor-α (TNF-α)) and chemokines. Capillary non-perfusion, capillary loss, advanced glycation end products and oxidative stress lead to hypoxia (Stitt et al., 2013), which will in turn activate endothelial cells and lead to release of inflammatory cytokines. Leukocytes make hypoxia worse by further obstructing retinal capillaries, leading to even more severe hypoxia, wich induces expression of angiogenic growth factors and neovascularisation in PDR (Semeraro et al., 2015). Inflammation is associated with deterioration of the BRB and leads to endothelial dysfunction and pathological events like vessel sprouting, leaky vessels, thickening of the basal membrane, which results in the progression of the disease (Behl et al., 2015; Wan et al., 2015; Yu et al., 2015b).

Furthermore, inflammatory processes are indicated to **activate microglia** and **Müller glia**, which will in turn secrete pro-inflammatory and apoptotic molecules and reinforce inflammatory effects in the eye (Grigsby et al., 2014). Gliotic microglia are associated with thinning of the GCL and the NFL (Grigsby et al., 2014; Karlstetter et al., 2015). The gliotic Müller glia will undergo changes, and will have a dual role in the development of DR, similar tho their dual role in the development of glaucoma (Bringmann et al., 2009a; Chong & Martin, 2015). However, the mechanisms causing glial changes in response to hyperglycemia are still unclear.

1.3.2.3 Treatment of diabetic retinopathy

For DR, the most important therapeutic strategy remains the combined control of glucose levels, blood pressure and serum levels. Several other treatments are available, such as laser photocoagulation, vitroretinal surgery, corticosteroids and anti-VEGF therapies (Tian et al., 2015). Laser photocoagulation implies the cauterisation of ocular blood vessels and reduces visual loss from macular edema and PDR (Klein et al., 1987). However, the lost vision cannot be restored and it can cause decreased adaptation to light intensity, loss of visual acquity and peripheral vision and a change in color detection. Vitroretinal surgery can be used to remove epiretinal membranes in case of for example retinal detachment, to re-attach the retina. However, complications can develop, e.g. hypotony and a higher incidence of

endophthalmitis (Taylor & Aylward, 2005). A commonly used drug to treat DR is anti-VEGF injection, which is already more efficient than laser therapy for vision improvement, but most patients do not show complete resolution of edema and vision improvement. Yet, retinal detachment, hypertensia and cardiovascular diseases can develop after injection, and several patients do not respond to VEGF therapy (Das et al., 2015; Zhang et al., 2011b). Corticosteroids are mainly used for their anti-inflammatory effects, however, corticosteroid-induced IOP rise could be a side effect and corticoid therapy is known to cause secondary cataract formation (Ciulla et al., 2014; Hussain & Ciulla, 2015). Since every therapeutic option seems to have its disadvantages, the demand for novel therapies is rising. Furthermore, because DR is not only a vascular disease, but also a neurodegenerative disease, neuroprotective strategies can be put forward, targeting the preservation of neurons and visual function.

1.4 Neuroprotection and axonal regeneration as a novel therapy for neurodegenerative eye diseases

The currently available therapies target the symptoms and try to slow down the progression of neurodegenerative eye diseases. However, until now, no real neuroprotective and regenerative therapy is available. Because of current limitations, there is a distinct need for novel and alternative treatment strategies that protect the retinal neurons or have the potential to repair previously damaged neurons. Glaucoma and DR, like other neurodegenerative diseases, are characterised by neuronal cell death and/or axonal degeneration. Therefore a novel neuroprotective or regenerative approach can be of great therapeutic interest, not only for patients suffering from glaucoma and DR, but also for patients suffering from other neurodegenerative diseases in the CNS.

1.4.1 Neuroprotection

Experimental animal studies have shown several therapeutic agents, such as neurotrophic factors, NMDA antagonists, nitric oxide synthase inhibitors and antioxidants to have effective neuroprotective qualities (Danesh-Meyer, 2011; Johnson et al., 2011; Kertmen et al., 2015; Reglodi et al., 2015; Salerno et al., 2002). Neurotrophic factors, including BDNF and CNTF have been shown to be neuroprotective in animal models of glaucoma and of mechanic optic nerve injury (Johnson et al., 2011). For example, a study in rats showed that intravitreal injection of BDNF enhanced RGC survival following optic nerve crush (ONC) (Bikbova et al., 2014; Chen & Weber, 2004). However, developing methods to deliver those biologically active factors in a safe and sustained way seems to be the stumbling stone to bring this therapeutic possibility into clinical use (Johnson et al., 2011). Indeed, a pilot phase 2 study with CNTF did not show to be as successful as expected (Zhang et al., 2011a). Furthermore, NMDA antagonists are promising therapeutic targets in neurodegenerative diseases like Alzheimer's, Parkinson's, glaucoma and several other diseases in which excitotoxicity plays a

role. However, most of the antagonists failed in clinical trials, because NMDA receptors are essential in normal neurotransmission. When all receptors are blocked, physiological neurotransmission will be inhibited and neuronal function will be disturbed. The NMDA antagonist memantine has shown to selectively block excessive receptor activation, while leaving the normal receptors unchanged (Danesh-Meyer, 2011). Memantine has then been approved for use in Alzheimer's disease and is one of the few neuroprotective agents that came on the drug market to treat neurodegeneration. However in a clinical trial, memantine treatment did not improve visual function in glaucoma (Agarwal et al., 2009; Van de Velde et al., 2015). The second clinical trial to evaluate neuroprotection was performed with the selective α2 antagonist, brimonidine, which modulates NMDA receptor function and upregulates neurotrophic factors. Despite good preclinical results, the briomidine clinical trial did not provide sufficient evidence for use in patients (Lindsey et al., 2015). Thus, although many positive results are obtained in preclinical research, no retinal neuroprotective agents are on the market yet.

1.4.2 Axonal regeneration

While neuroprotection is of utmost importance, on its own, it is not sufficient to restore damaged neuronal circuits. Indeed, many neurodegenerative diseases are highly characterised by axonal degeneration. As such, the search for molecules that promote axonal regeneration in the CNS is an important challenge in scientific research. In the adult peripheral nervous system (PNS), long- distance axon regeneration and substantial functional recovery can occur (Huebner & Strittmatter, 2009). However, in the CNS, regeneration after injury is extremely limited and appears to be an obstacle in developing effective therapies for neurodegenerative diseases, which needs to be overcome.

1.4.2.1 Limitations for axon regeneration

The regenerative limitation of the adult CNS is attributed to both intrinsic and extrinsic factors. The three most common causes of CNS regeneration failure from extrinsic sources are the formation of the glial scar, the large amount of inhibitory components in the extracellular matrix (ECM), which is released from degenerating myelin or the glial scar, and the deprivation of growth factors (Benowitz & Yin, 2008; Bosse, 2012; Huebner & Strittmatter, 2009). The major difference between the CNS and PNS is the presence of different myelinating cells; Schwann cells in the PNS and oligodendrocytes in the CNS (Dezawa, 2002; Filbin, 2003). Schwann cells cease to express myelin proteins and myelin inhibitors with injury and assist in clearing myelin debris, while oligodendrocytes continue to express myelin proteins, resulting in a rise in myelin debris (Dezawa, 2002). Furthermore, less inflammatory cells are present in the CNS, e.g. macrophages, which remove myelin debris after injury, which in turn blocks axonal regrowth and re-myelination in the CNS.

1.4.2.1.1 Intrinsic factors

In the mature CNS, part of the limited regeneration can be attributed to a loss of intrinsic growth ability of the neurons with ageing. Several proteins are up- or downregulated in different phases of life, such as growth-associated protein-43 (GAP-43), which is highly expressed during development and after injury, when RGCs extend their axons. Such expression shifts lead to a limited intrinsic growth capacity in the later stages of the CNS neurons (Bosse, 2012; Goldberg et al., 2002).

1.4.2.1.2 Extrinsic factors

The **glial scar** serves as a major barrier for regenerating axons of the CNS. It is formed by astrogliosis at the lesion site whereby reactive astrocytes, microglia and oligodendrocyte precursors are recruited (Yiu & He, 2006). Astrogliosis is positive for isolating the injury site and minimising the area of inflammation and cellular degeneration, but can also have negative effects in terms of regeneration inhibition and the formation of physical and chemical barriers (Faulkner et al., 2004). Hypertrophic, reactive astrocytes in the glial scar release inhibitory ECM molecules, such as proteoglycans (for example the chondroitin sulphate proteoglycan (CSPG) family) and myelin associated inhibitors, at the site of injury. Though, the mechanism underlying CSPG induced axonal regeneration inhibition in the adult mammalian CNS is not completely exposed (Yiu & He, 2006).

Several **inhibitory components** can be released from **degenerating myelin** or the glial scar, for example neurite outgrowth inhibitor (Nogo), myelin-associated glycoprotein (MAG), oligodendrocyte-myelin glycoprotein (OMgp) and CSPGs. Nogo is a transmembrane protein that inhibits neurite outgrowth and causes neurite growth cone collapse (GrandPre et al., 2000). OMgp is a glycosylphosphatidylinositol-anchored CNS myelin protein that is expressed by neurons and oligodendrocytes and for which a role in axon sprouting has been suggested (Fujita & Yamashita, 2014; Wang et al., 2002). Furthermore, the transmembrane protein MAG has a role in glia-axon interactions and is more highly expressed in the CNS than in the PNS. The cellular cyclic adenosine monophosphate (cAMP) levels determine MAGs' effect on axon outgrowth. Knowing that cAMP levels decrease with age, the effect shifts from outgrowth promotion to outgrowth inhibition. The three aforementioned inhibitors bind the same receptor complex with the Nogo receptor-1, neurotrophin receptor p75NTR and leucine-rich repeat and Ig domain containing 1 (Venkatesh et al., 2007).

When axons are damaged after nerve injury in the CNS, retrograde transport to the nerve cells can be blocked, which leads to **deprivation of endogenous growth factors**. Neurotrophic factors (e.g. CNTF and BDNF) have been shown to exert neuroprotective and axon regenerative effects, which is why deprivation of these factors implicates axon regeneration impairment (Johnson et al., 2011; Lykissas et al., 2007; Weinreb et al., 2014).

1.4.2.2 Role of glial and inflammatory cells

As stated earlier, the glial cells play a role in axon regeneration in the CNS. Acute activation of neural glia appears to be neuroprotective, while prolonged activation has a detrimental role in axonal regeneration. Retinal activated Müller glia and astrocytes secrete neurotrophic factors, growth factors and cytokines, which have stimulatory effects on RGCs and photoreceptors (Bringmann et al., 2009a). Part of their effects are rather direct, while others are indirect, mediated by interaction of neurotrophic factors with Müller glia and a subsequent release of direct neurotrophic factors by these glial cells (Benowitz & Yin, 2008; Bringmann et al., 2009a).

Furthermore, resident microglia, astrocytes, Müller glia, neutrophils and infiltrating macrophages mediate the innate immune response and release inflammatory cytokines, chemokines, etc. (Bringmann et al., 2009a). Activation of microglia can lead to the production of pro- and anti-inflammatory factors. Some of these factors can thus have neurotoxic effects, while others can induce a controlled inflammatory response, which is implicated in enhanced neuronal cell survival and establishment of axonal regeneration (Suzumura, 2013). Upon neuronal damage, inflammatory molecules (e.g. TNF-α, ILs, ROS) are released, which evoke microglial activation and recruitment to the site of injury. Subsequent neuroinflammation is characterised by this microglial recruitment and the infiltration of blood-borne inflammatory cells to the site of neuronal injury and can cause the RGCs to regain an active growth state and extend their axons (Jha et al., 2013; Yin et al., 2009). The molecular basis of this positive effect of inflammation on regeneration assistance and the role of glial reactivity is still unclear and previous literature reports are contradictory (Hauk et al., 2008). However, the calcium bindin protein oncomodulin has been identified as a molecule that could link inflammation and RGC regeneration. This molecule promotes axon growth in RGCs. Inflammation causes recruited immune cells to secrete high oncomodulin levels. Furthermore, anti-oncomodulin agents suppress axon regeneration, indicating that it serves as a growth-promoting signal between innate immunity and RGCs (Benowitz & Popovich, 2011; Yin et al., 2009).

1.4.2.3 Strategies towards axonal regeneration

Several strategies targeting both intrinsic and extrinsic factors have been proposed to tackle regeneration limitations including targeting of the inhibiting ligands, peripheral nerve graft transplantation, intraocular injection of neurotrophic factors, induction of controlled inflammation and targeting of intracellular signaling pathways. One option concerning targeting intrinsic factors, is aiming on several intracellular signaling pathways involved in intrinsic growth control, e.g. JAK/STAT, PI3K/Akt en MAPK/ERK. Deletion or activation of several inhibitory molecules can be another strategy to interfere in these pathways, for example by deletion of phosphatase and tensin homolog (PTEN) or suppressor of cytokine singaling 3 (SOCS3), activation of the mechanistic target of rapamycin (mTOR) pathway,

etc.(de Lima et al., 2012; Diekmann et al., 2015; Sun et al., 2011). Concerning targeting extrinsic factors, directly aiming to inhibit molecules derived from myelin or the glial scar, e.g. NogoA, had limited success (Fischer et al., 2004). Transplantation of a part of the nerve from the PNS to the site of lesion showed to promote RGC axon regeneration, caused by the presence of less inhibiting molecules and more growth factors, e.g. neurotrophic factors (Berry et al., 1996). These neurotrophic factors such as CNTF can also be administered via other routes and do promote regeneration of RGC axons (Leaver et al., 2006; Pernet et al., 2013). Moreover, inflammation and associated glial reactivity are also linked to neuroprotection, axon outgrowth and axon elongation (Benowitz & Popovich, 2011; Lorber et al., 2009). Controlled inflammation can be induced by intravitreal zymosan injection (Ahmed et al., 2010; Hauk et al., 2008; Yin et al., 2006). Overall, despite many promising strategies have been developed in animal models, the current experimental treatments in rodents are not readily translatable to human clinical trials (Benowitz & Yin, 2007).

1.5 Rho-associated coiled-coil kinase (ROCK)

Rho GTPases are members of the Ras superfamily of the monomeric GTPases and regulate various aspects of the cell shape, motility, proliferation and apoptosis in all eukaryotic cells (Wang & Chang, 2014). Rho functions as a molecular swich between the inactive guanosine triphosphate (GDP) bound state and the active guanosine triphosphate (GTP) bound conformation. Guanine nucleotide exchange factors (GEF) regulate activation by catalyzing the exchange of GDP to GTP. On the other hand, GTPase activating proteins (GAP) inactivate Rho by stimulating the hydrolysis of GTP to GDP as shown in the upper part of Figure 8. Upon activation, effector molecules become activated and subsequently interact with downstream molecules. At least twenty members of the Rho family of GTPases are

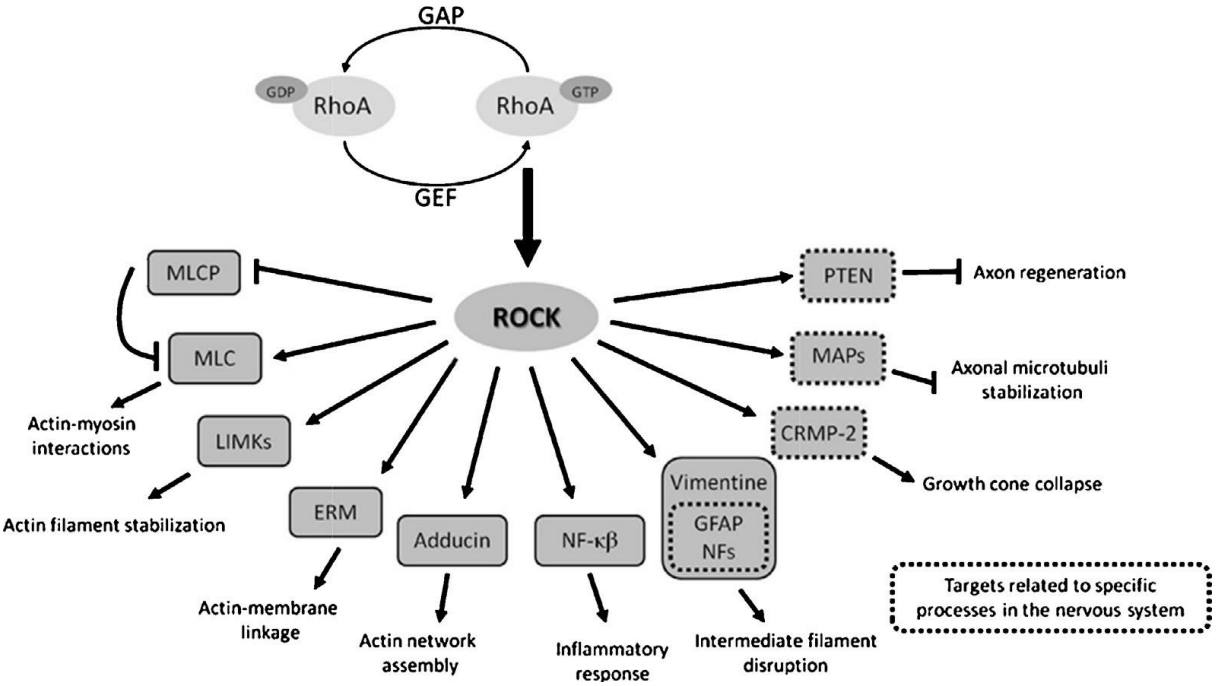

Figure 8: The Rho-ROCK pathway with the main ROCK effectors and their function (Van de Velde et al., 2015).

present in mammals with Rho, Ras-related C3 botulinum toxin substrate 1 (Rac1) and cell division cycle 42 (Cdc42) as the three best characterised members of the family (Amano et al., 2010). Rho can interact with more then 60 effectors in its active form. Rho-associated coiled-coil kinase (ROCK) was the first Rho effector to be discovered. ROCK is a protein serine/threonine kinases that shares a fair percentage of homology to other actin cytoskeletal binding kinases (Noma et al., 2006). ROCK is composed of an N-terminal catalytic domain, a central coiled-coil domain, which is interrupted by a Rho-binding domain, and a C-terminal pleckstrin homology domain, interrupted by a Cys-rich domain as shown in Figure 9 (Ishizaki et al., 1997; Schofield & Bernard, 2013). Two ROCK isoforms have been identified in mammalian systems, namely ROCK1 and ROCK2, which are highly homologous.

1.5.1 ROCK isoforms and their differential expression

ROCK1 and ROCK2 share 64% amino acid sequence identity and their kinase domains are circa 92% identical (Figure 9) (Nakagawa et al., 1996). ROCK1 is located on chromosome 18 and encodes a 1354-amino acid protein in human and mice and is located on chromosome 6 and encodes a slightly larger protein in pigs. Whereas ROCK2 was the first isoform to be identified and is located on chromosome 12 in human and mice and on chromosome 3 in pigs and contains 1388 amino acids (Liao et al., 2007).

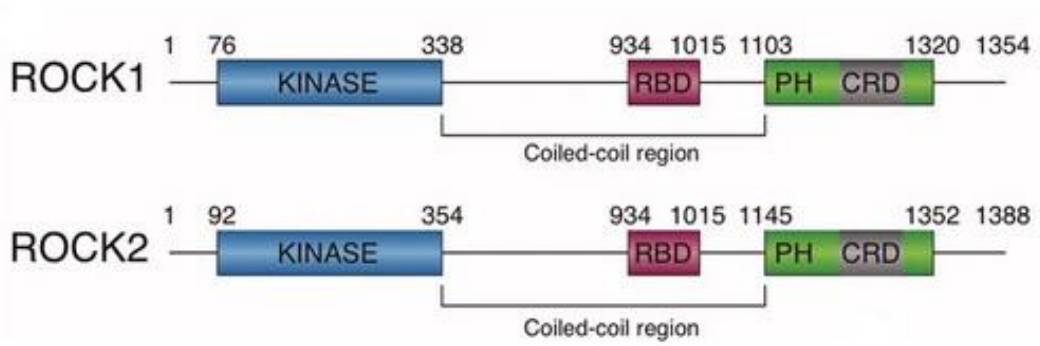

Figure 9: Structural comparison of isoforms ROCK1 and ROCK2, both containing an amino-terminal kinase domain, a coiled-coil region that contains a Rho-binding domain (RBD). The carboxyl-terminal region contains a pleckstrin homology (PH) domain that flanks an internal cysteine-rich domain (CRD) (Schofield & Bernard, 2013).

Nakagawa et al. (1996) suggested that ROCK1 is ubiquitously expressed except in the CNS and in muscles and that ROCK2 is abundantly expressed in CNS, muscle, heart, lung and placenta in the mouse (Nakagawa et al., 1996). In rat, ROCK2 was abundantly expressed in the cerebrum and cerebellum, but also in the heart and lungs. However, ROCK2 was only expressed at lower levels in skeletal muscle, spleen, liver, kidney and pancreas of the rat (Matsui et al., 1996). Immunohistochemical staining revealed the localisation of ROCK2 throughout the rat embryo, including the dorsal root ganglions, heart, liver, umbilical blood vessels and placental layers (Thumkeo et al., 2003). ROCK1 localisation was shown in the

aorta, dorsal root ganglia, heart, skin, and umbilical blood vessels of rat embryos (Shimizu et al., 2005).

ROCK1 and ROCK2 also differ in subcellular organisation, as ROCK2 is distributed mainly in the cytoplasm and can be found in smaller amounts in membranes (Leung et al., 1995; Matsui et al., 1996). The subcellular organisation of ROCK1 is less known, but is thought to be associated with the catenin/epithelial-cadherin complex and with centrosomes (Schofield & Bernard, 2013).

ROCK is highly expressed in the CNS and particularly ROCK2 expression in the CNS is documented (Koch et al., 2014a; Schofield & Bernard, 2013). In the rabbit retinofugal system, ROCK1 and ROCK2 are both expressed in the healthy and diseased optic nerve (Yu et al., 2015a), which shows that ROCK1 is expressed in the CNS, in contrast to the earlier suggestion of Nakagawa (1996). Furthermore ROCK expression can differ in healthy and diseased cells (Schofield & Bernard, 2013). Trabecular meshwork cells also express both ROCK1 and ROCK2 (Wang et al., 2013). Abovementioned results testify that differential ROCK expression in many celltypes in the CNS is still unknown and still debated in literature.

1.5.2 Downstream effectors of ROCK

After activation, ROCK can phosphorylate multiple substrates, which almost all play an important role in regulating cytoskeletal dynamics (Figure 8) (Van de Velde et al., 2015). Some of the important downstream effectors and their function will be summed up here. First, cytoskeletal regulator myosin light chain (MLC) stimulates actin-myosin interactions and is downregulated by MLC phosphatase (MLCP) (Kaneko-Kawano et al., 2012). ROCK can also regulate MLC indirectly by inhibiting MLC-downregulation by MLCP (Amano et al., 2010). The LIM kinases (LIMK) are actin-binding kinases, which, after activation by ROCK, aid actin filament stabilisation and in an active state, they can bind cofilin, thereby leading to an increased number of actin filaments (Kardassis et al., 2009; Scott & Olson, 2007). The erzin/radixin/moesin (ERM) family acts in actin-membrane linkage upon activation by ROCK (Tsukita & Yonemura, 1999; Yonemura et al., 2002). Furthermore, activated adducin, a filamentous actin-finding protein, plays a role in cell motility. Intermediate filament proteins like glial fibrillary acidic protein (GFAP), vimentin and neurofilaments (NFs) are effectors of ROCK, and are important for maintaining cell integrity and mechanical strength (Kimura et al., 1998; Riento & Ridley, 2003). NF-κβ, another ROCK effector, is involved in the inflammatory response and will regulate transcription of pro-inflammatory molecules, such as ILs and TNF-α, in different proinflammatory cells (Montaner et al., 1998; Van de Velde et al., 2015).

1.5.3 ROCK in the CNS

Several downstream components of the Rho-ROCK pathway are expressed in the CNS (as shown by the dotted lines in Figure 8), and are known to play a crucial role in various neural processes, including neuronal death, axonal (mis)guidance and outgrowth (Van de Velde et al., 2015). One of ROCK's targets are the intermediate filaments, such as neurofilament, which is highly expressed in axons, or GFAP in macroglia. Neurofilament activation by ROCK results in intermediate filament disassembly and subsequent changes in axon integrity and axonal growth dynamics, wich makes ROCK a negative regulator of neurite outgrowth. GFAP is a glial intermediate filament protein, which is important in the formation of the glial scar and repair post-injury (Kimura et al., 1998; Riento & Ridley, 2003; Van de Velde et al., 2015). Another ROCK effector in the CNS is collapsin response mediator protein-2 (CRMP-2), which plays a role in disruption of axon guidance and in growth cone collapse (Arimura et al., 2000). Also microtubule-associated proteins (MAPs), such as MAP-2 and Tau, can be activated by ROCK and play a role in neuronal morphology by changing microtubule dynamics, which also leads to a negative effect on neurite outgrowth (Amano et al., 2010). Another interesting downstream target of ROCK in the CNS is PTEN, which negatively regulates the PIP3/Akt/mTOR pathway, thereby also negatively regulating neuronal survival and axonal regeneration (Li et al., 2005). As such, ROCK is a negative regulator of neurite outgrowth and extension and that its activation results in axon retraction and growth cone collapse during axon regeneration. However, a variety of downstream components of the ROCK pathway are still unknown and the elucidation of downstream components would lead to a better understanding of the overall impact of ROCK.

Notably, also several upstream components of the Rho-ROCK pathways are involved in regeneration failure, such as myelin-associated inhibitory molecules, components of the glial scar, cytokines, etc. (Koch et al., 2014b). The myelin-associated inhibitory molecules (Nogo, MAG and OMgp) bind to the Nogo receptor, which activates RhoGTPase via the p75 neurotrophin receptor. RhoGTPase activates ROCK and this results in growth cone collapse and neurite outgrowth inhibition (Kaplan & Miller, 2003). CSPGs are associated with reactive astrocytes in the glial scar, and they interact with the ROCK pathway, resulting in growth inhibition (Gopalakrishnan et al., 2008).

An additional link was found between ROCK2 and caspase-3 activity, which plays a major role in apoptosis. Calpain might link ROCK2 and the apoptotic pathway, because ROCK2 inhibition leads to a decreased calpain activity in RGCs, and thus a decrease in caspase-3 activity and decreased apoptosis (Koch et al., 2014a). As such, ROCK is also assumed to exert a negative effect on neuronal survival.

1.5.4 ROCK inhibion as a potential strategy for novel therapies

Because the Rho-ROCK pathway is involved in oncology, cardiovascular diseases and neurological diseases, inhibition of this pathway can be beneficial as a therapy for these diseases and has already been extensively studied (Liao et al., 2007; Noma et al., 2006). ROCK1 inhibition for example proved to be an interesting therapy for glioma, the most common type of cancer in the CNS (Wan et al., 2014). Several ROCK inhibitors have been developed, such as fasudil, ripasudil, hydroxyfasudil, Y-27632, Y-39983, AMA0076, RKI1447 and Wf536 (Pan et al., 2013). Fasudil, Y-27632, RKI1447 or Wf536 have shown to have an inhibitory effect on tumor growth, progression and metastasis in oncologic research in rodents. In cardiovascular research, Y-27632 and fasudil can have a role in regulating blood pressure in hypertensive rat and human. Fasudil also has pharmacological effects and can prevent diabetes development in rat, modulate regression of arteriosclerotic coronary lesions in pig, suppress left ventricular cavity dilatation and dysfunction in myocardial infarctions in human. In the CNS, the ROCK inhibitors fasudil and Y-27632 can play an important axon regenerative or neuroprotective role in the prevention and therapy of spinal chord injury and Alzheimer's disease in mouse, rat and human (Pan et al., 2013). In the eye, neurodegenerative diseases like glaucoma and DR might also benefit from ROCK inhibition. Fasudil for instance protects the vascular endothelium in DR rat models by reducing neutrophil adhesion and neutrophil-induced endothelial injury (Arita et al., 2009). Moreover, a wide range of ROCK inhibitors have been developed and are now being tested in several animal models and clinical trials for glaucoma, including dimethylfasudil, Y-27632, the more potent Y-39983 and AMA0428 (Feng et al., 2015; Koch et al., 2014a; Lingor et al., 2007; Van de Velde et al., 2014; Watabe et al., 2011).

Despite many promising preclinical results, fasudil and ripasudil are the only clinically approved ROCK inhibitors (Feng et al., 2015). Fasudil inactivates ROCK1 and ROCK2 by binding to its ATP binding site and is used to treat cerebral vasospasm (Feng et al., 2015; Saito et al., 2015; Satoh et al., 2014). Ripasudil is a highly selective and potent ROCK1 and ROCK2 inhibitor and is used to treat glaucoma, because it is an outflow-promoting drug which reduces IOP by stimulating AH drainage through the TM (Garnock-Jones, 2014).

As multiple factors are involved in the restricted axonal regeneration in the CNS, targeting a variety of these factors is very complex. In this regard, targetting the intracellular pathways that are common to several inhibitory sources would be an more efficient approach (Yiu & He, 2006). The Rho-ROCK pathway is an interesting target as it plays a key role in different cellular processes. Moreover, several studies have already shown that ROCK inhibition or knockdown promotes neurite outgrowth and guidance, axonal regeneration and neuronal survival in several experimental models for glaucoma, which makes ROCK a promising target for a variety of neurological disorders (Van de Velde et al., 2015).

1.6 Aims

Due to the increasing life expectancy, more and more people are at risk of developing neurodegenerative diseases. Up till now, *in vitro*, *ex vivo* and *in vivo* studies identified ROCK as a negative regulator of neurite outgrowth, axon guidance and neuronal survival. Therefore the Rho-ROCK pathway was put forward as an important target in retinal neurodegenerative diseases. However, until now the cellular players in the Rho-ROCK pathway are unknown and expression studies of the separate isoforms of ROCK in the retina in different cell types are lacking. Therefore, the central goal of this thesis is to unravel the underlying cellular mechanisms of ROCK2 and ROCK1 in the healthy and pathological retina. The first approach is to develop and optimise models, which mimic the pathological state of the neurodegenerative retina and can be used for future study of neuroprotective capacities of ROCK inhibition. The second approach targets axon regeneration.

First, an *in vitro* model of primary porcine retinal Müller glia and microglia will be optimized, after which different stressors, such as excitotoxicity, oxidative stress and hyperglycemia, will be applied to mimic the pathological retinal environment as a neurodegenerative model. This stress induction will be validated via vimentin expression. Additionally, expression levels for ROCK1 and ROCK2 will be determined in a healthy versus pathological state, to further unravel differential expression of both ROCK isoforms in porcine Müller glia and microglia.

Another goal of this thesis is the development and optimisation of an *ex vivo* model that mimics neurodegeneration, characterised by a slow and progressive decline in neuronal cell survival and an increase in glial reactivity. Therefore porcine retinal explants will be cultured up to one week, after which they will be validated; neuronal cell survival will be assessed via the expression of several RGC markers, glial reactivity will be determined via GFAP and vimentin expression and ther morphology will be evaluated with an H&E staining.

Finally, postnatal mouse retinal explants will be used to study axon regeneration. Initially, we aim to localise the cellular origin of ROCK2 by determining the colocalisation with GFAP and β-tubulin. Subsequently, neurite outgrowth initiation and elongation capacities of neurotrophins and ROCK inhibitors and the combination of both will be investigated with the use of a new automated neurite outgrowth Fiji script that will be developed and optimised and compared with an older used Axiovision script.

2 Materials & methods

2.1 Laboratory animals

2.1.1 *Mus musculus*

The C57B16/N mice (*Mus musculus*) from the inhouse breeding colonies of the KU Leuven were housed in the local animal facilities of the Section of Animal Physiology and Neurobiology in plastic transparent cages. Water and pelleted food were available *at libitum*, sawdust was used as bedding material, and cages were supplemented with environmental enrichment. The animal rooms had a controlled temperature between 20°C and 22°C, a relative humidity between 40 and 60% and a 12h light/dark cycle. These mice were used at postnatal day 3 (P3), the third day after birth (P0), for the mouse retinal explant experiments.

2.1.2 *Sus scrofa domesticus*

Pig (*Sus scrofa domesticus*) eyes were obtained from *Slachthuis Genk NV*, Belgium. Immediately after sacrificing adult pigs from approximately 3 to 5 months old, fresh porcine eyes were collected without harming the eyeball. The porcine eyes were transferred to the lab in cold saline (0.9% NaCl), where the eyes were cleaned, disinfected with 70% ethanol (EtOH) and cells or tissues were extracted within 4h after collection, for the pig retinal *in vitro* and *ex vivo* experiments.

All animal experiments were approved by the Institutional Ethical Committee of KU Leuven and were conducted in strict accordance with the European Communities Council Directive of September 22, 2010 (2010/63/EU) and with the Belgian legislation (Royal order concerning the protection of laboratory animals of May 29, 2013).

2.2 Neuroprotection

2.2.1 *In vitro* retinal cell models

In vitro experiments were performed in order to examine ROCK1 and ROCK2 expression in healthy and stressed retinal Müller glia and microglia.

2.2.1.1 Isolation of porcine retinal glial cells

After removal of excess tissue from the eyeball and disinfecting it in 70% EtOH, primary Müller glia and microglia were isolated from fresh porcine retinae for further cultivation under the laminar flow cabinet. The eyeball was transferred to a petridish containing 1x Phosphate buffered saline (PBS) (10x PBS (pH 7,4) (80mM Na2HPO4.2H2O (Merck), 20mM KH2PO4 (Merck), 1,5M NaCl (Fisher chemical) and 30mM KCl (Acros organics)) in aqua destillata (AD)) with 1x Penicillin/Streptomycin (Pen/Strep) (Life technologies Invitrogen) and an incision was made at the rim of the cornea with a scalpel, after which the cornea was removed by cutting on the rim using small scissors. Then the vitreous humour was

removed by squeezing it out of the eye. The retina was carefully dissected and transferred to an autoclaved tissue grinder with 5 ml separation medium and grinded thoroughly. The mixture was poured via a 40 µm cell strainer (Fisherbrand, Fisher scientific) into a 50 ml tube (Sarstedt) and centrifuged for 5 min at 1200 rotations per minute (rpm) on room temperature (RT). All the following manipulations with the cells are conducted under a sterile horizontal flow cabinet (BioAir). Subsequently, the supernatant was discarded and the cell pellet was washed with 5 ml separation medium (1x Pen/Strep and 1% Glutamax (Life technologies) in DMEM medium (Life technologies)). This washing step was repeated two more times, after which the pellet was resuspended in 20 ml Müller growth medium (10% heat inactivated foetal bovine serum (hiFBS) (Gibco, Life technologies) and 4 ng/ml epidermal growth factor (EGF) (Life technologies) in Separation medium), transferred to a Cellbind T75 cell culture flask (Sarstedt) and incubated undisturbed for a week at 37°C, 5% CO_2. After the first week, the cells were washed with sterile Dulbecco's phosphate buffered saline (DPBS) without Ca^{2+} and Mg^{2+} (Gibco, Life technologies) and the medium was replaced by 10 ml fresh Müller growth medium. Later, this medium was refreshed once a week.

2.2.1.2 Cell culture Müller glia

Müller glia are adherent cells, meaning they grow attached to a surface, and are cultured in Müller growth medium. When the cells were approximately 80% confluent, as visualised after microscopic examination, they were passaged to new T75 culture flasks (on average every 2 weeks). To passage the cells, old medium was removed, the cells were rinsed three times with DPBS without Ca^{2+} and Mg^{2+} to wash away the residual Müller growth medium. Next, the cells were incubated in 2 ml 0.25% trypsin/EDTA solution (Sigma) for a few minutes in order to dissociate cells from each other and from the surface of the culture flask using the proteolytic enzyme trypsin. To stop the trypsinisation reaction, 5 ml Müller growth medium was added. Subsequently, the cells were transferred to a centrifuge tube and spun down for 5 min at 1200 rpm on RT. The supernatant was discarded and the cell pellet was resuspended in fresh Müller growth medium and incubated at 37°C, 5% CO_2.

To freeze the Müller glia for later use, freezing medium containing 20% dimethyl sulfoxide (DMSO) in Müller growth medium was prepared and put at 4°C. Cells were frozen after passage 1 or 2. Before freezing the cells, they were trypsinised and spun down for 5 min at 1200 rpm at RT. The supernatant was then discarded and the pellet was resuspended in half of the total volume needed for freezing, reaching a cell density of 400 000 cells/ml. The density was counted, using a 1/1 dilution of the cells in Trypan blue in a cell counter (Bürker). Subsequently, the cold freezing medium, which was half of the total volume needed for freezing, was added slowly and dropwise to the cell suspension and aliquots of 1 ml were made in cryogenic vials. The vials were stored overnight in a CoolCell cell freezing container in a -80°C freezer and then stored in a -196°C liquid nitrogen freezer.

To thaw the Müller glia, Müller growth medium was used and preheated at 37°C. The vial was allowed to thaw quickly in a 37°C water bath. Then the content was transferred to a 15 ml tube, resuspended in 10 ml Müller growth medium, transferred into a new T75 cell culture flask and incubated at 37°C, 5% CO_2.

2.2.1.3 Seed Müller glia

Müller glia of passage 3-4 were used for stress experiments and for Western Blot (WB) and Immunocytochemistry (ICC). For WB, the cell suspension was transferred to Cellbind T25 cell culture flasks (Falcon, BD). For Immunocytochemistry (ICC), 1 ml per well of the cell suspension, with a concentration around 20 000 to 40 000 cells/ml, was transferred into 4-well dishes (culture area 1.9 cm^2) (Nunc, Thermo Scientific) with sterile coverslips at the bottom. After the transfer, the T25 flasks and the 4-well dishes were incubated at 37°C, 5% CO_2 for 4-5 days, after which the cells were exposed to a stressor.

2.2.1.4 Cell culture microglia

Previously described culturing procedures allow microglia to grow in the Müller glia culture too, in Müller growth medium. They are non-adherent to the flask and loosely attached to the Müller glia. That is why no trypsinisation was needed to bring the cells in suspension. Firm tapping against the side of the flask was sufficient to break the weak connections between the Müller glia and the microglia (Klettner et al., 2014). Then the microglia were seeded for experiments, still using the Müller growth medium.

2.2.1.5 Seed microglia

Microglia in a Müller gla culture of passage 1-2 were used for stress experiments, after which WB and ICC experiments were conducted. They were separated from the Müller glia and the culture medium, containing microglia, was transferred to a centrifuge tube and spun down for 5 min at 1200 rpm on RT. The supernatant was discarded and the cell pellet was resuspended in fresh Müller growth medium, to reach a concentration of at least 40 000 cells/ml. The cell suspension was transferred to T25 flasks for WB and 4-well dishes with sterile circular cover slips for ICC. After the transfer, the T25 flasks and 4-well dishes were incubated at 37°C, 5% CO_2 for 4-5 days, after which the cells were exposed to a stressor.

2.2.1.6 Stressors

To induce excitotoxic stress, the Müller glia were exposed to Müller growth medium supplemented with 0, 5, 10 or 20 mM L-Glutamic acid ($C_5H_9NO_4$, MW 147.1, Sigma) for 6 hours *in vitro* (HIV) or 24 HIV. To induce oxidative stress, the Müller glia were exposed to Müller growth medium supplemented with 0 or 100µM Cobalt (II) chloride hexahydrate ($CoCl_2.6H_2O$, MW 237.9, Sigma) or H_2O_2 30% (Sigma) for 6 HIV or 24 HIV. To induce hyperglycemia, the microglia or Müller glia were exposed to Müller growth medium supplemented with 25mM glucose ($C_6H_{12}O_6$, MW 198.17, Sigma) for 24HIV. The Müller

growth medium already contained 5mM glucose, necessary for the cell to proliferate, meaning total glucose concentrations were 5mM (control) or 30mM glucose.

2.2.1.7 Immunocytochemistry (ICC)

2.2.1.7.1 Fixate cells

After induction of stress, the cells in the 4-well dishes were fixated. First the culture medium was removed and the cells were washed with DPBS. Then the cells were fixed for 15 min in 4% paraformaldehyde (PFA) 0.1 M (Sigma) in 1x PBS. After fixation they were washed with 1x PBS and stored in PBS supplemented with 0.01% sodium azide (NaAz) (Sigma) in 1x PBS.

2.2.1.7.2 General principles of immunostaining

ICC is a technique used to localise antigens in fixed cells, based on epitope detection by antibodies. It differs from immunohistochemistry (IHC) that localises antigens in fixed tissue sections in stead of in cells. In the direct fluorescensce method in immunostainings, an epitope binding antibody (Ab) is conjugated with an enzyme or a fluorophore that can catalyse a colour producing reaction or become fluorescent. However, this detection method is less sensitive and is not applied in this thesis. According to the indirect fluorescence method, the primary Ab will bind to the epitope. The secondary Ab will bind the primary Ab and is conjugated with an enzyme or a fluorophore. In a simple staining, one antigen is detected with one primary and secondary Ab. In a double staining, two different antigens are detected with two sets of Abs, in which the secondary Abs carry a different fluorophore.

2.2.1.7.3 ICC

A simple indirect fluorescence method was used to detect ROCK2, ionised calcium-binding adapter molecule 1 (Iba-1), glutamine synthetase (GS) and vimentin in Müller glia and microglia, in 4-well plates. Iba-1 is a microglia specific marker, while GS is a Müller glia specific marker. Vimentin is an IF protein that is specifically expressed in Müller glia in the porcine retina (Ghosh & Arner, 2010), while its expression can be upregulated in certain porcine models of the pathological retina (Johansson et al., 2010). To get started, PBS was aspirated and the wells were incubated in 500 µl permeabilisation solution (0.2% Triton X-100 (VWR) in 1x PBS) for 10 min and then washed for 5 min with PBS. Next, the cells were blocked in 300 µl blocking solution (2% Bovine Serum Albumin (BSA) 10 mg/ml (Thermo) in 1x PBS) per well. Subsequently, the cells were incubated overnight at 4°C in 250 µl of the primary antibody (Table 1), diluted in Ab dilution solution (0.05% Tween-20 (Merck), 1% BSA in 1x PBS). The next morning, the primary Ab was removed and the cells were washed 4 times in washing solution (0.05% Tween-20 in 1x PBS). A fluorophore labelled secondary Ab (Table 1) was also diluted in Ab dilution buffer and the cells were incubated in 500 µl of the solution for 1h in absence of light. Then, the secondary Ab, either goat anti-mouse IgG (GAM)-Alexa 488 (A-11001, Invitrogen) or goat anti-rabbit IgG (GAR)-Alexa 488 (A-11008,

Invitrogen) was aspirated and the cells were washed 4 times with washing solution. The last step included adding a nuclei staining compound, 4',6-diamidino-2-fenylindool (DAPI) (always diluted 1/1000 in 1x PBS) for 30 min in absence of light. Next, the remaining wash fluid was removed and the coverslips the cells were resided on were mounted with mowiol in order to preserve the fluorescence better on Superfrost plus slides (Thermo Scientific). The slides were stored in absence of light at 4°C.

Representative pictures were taken with a Zeiss Imager Z1 microscope (Carl Zeiss) with an AxioCam MR3 black and white camera using a 10x objective and Zen Pro software, for the vimentin stained cells. For the Iba-1, GS and ROCK2 stained cells, representative pictures were taken with an inverted confocal fluorescence microscope, FV1000 IX-82 (Olympus), with a motorised stage using a 20x objective. The DAPI stain was excited by a 405 nm laser, while the Alexa 488 fluorophore was excited by a 488 nm laser.

Table 1: Primary and corresponding secondary Abs and their dilution for ICC staining of Iba-1, GS, Vimentin and ROCK2 proteins in cells.

Detected antigen	Primary Ab	Firm	Product number	Dilution	Secondary Ab	Dilution
Iba-1	Polyclonal rabbin anti-Iba-1	Wako	019-19741	1/500	GAR-Alexa 488	1/200
GS	monoclonal mouse anti-GS	Millipore	MAB302	1/200	GAM-Alexa 488	1/200
Vimentin	monoclonal mouse anti-vimentin	Sigma	v5255	1/200	GAM-Alexa 488	1/200
ROCK2	polyclonal rabbit anti-ROCK2	Abcam	ab71598	1/500	GAR-Alexa 488	1/200

2.2.1.8 Western blot

2.2.1.8.1 Lysis of the cells

Immediately after the period of stress exposure, the cells in the T25 flasks were lysed. First the culture medium was removed and the cells were washed two times with cold 1x PBS. Then 200 µl/flask of cold RIPA lysis buffer (150 mM NaCl (Fisher chemical), 1% Igepal (Fluka), 0.5% sodiumdeoxycholate (Sigma), 0.1% sodium dodecyl sulphate (SDS) (DNase, RNase, Protease free) (Acros organics) in 50 mM Tris-HCl (pH 8) (Tris 50 mM (Acros organics) in MiliQ (Millipore) with HCl to pH 8)) supplemented with 1 mini tablet EDTA-free protease inhibitor cocktail (Roche Diagnostics) per 10 ml buffer was added. Cells were scraped loose with a rubber policeman and the cell suspension was placed on ice in a DNAse/RNAse free 1.5 ml centrifuge tube (TreffLab) and agitated regularly. Next, the lysate was homogenised with a conical crusher and spun down for 20 min at 4000g at 4°C. The pellet was discarded and the supernatant was transferred into a new 1.5 ml centrifuge tube and stored at -80°C.

2.2.1.8.2 Determining protein concentration

The protein concentration of each sample was determined using the Bradford method (595 nm) (Bio-Rad). Bio-Rad colour reagens (Bio-Rad) is first diluted (1/5) in Milli-Q (MQ) ultrapure water (Millipore) and filtered. Then a standard curve was made by diluting Albumin Standard with BSA in NaOH 0.1 N. 40 µl of the standard curve, 40 µl of the blanc (NaOH 0.1 N) or 40 µl of the diluted samples were mixed with 2 ml colour reagens and the absorbance at 595 nm was measured with a spectrophotometer (Genesys 6, Thermo Spectronic). The protein concentrations were calculated according to the standard curve (with a standard curve y = b + ax, concentration = ((absorbance – b) / a)*(1/dilution)).

2.2.1.8.3 Electrophoresis and blotting

The -80°C stored samples were thawed on ice and the samples were diluted in MQ and pipetted in a DNAse/RNAse free 1.5 ml centrifuge tube, reaching a total volume of 13 µl. 4.9 µg and 1.36 µg proteins of the samples were loaded for Müller glia and microglia respectively. Subsequently, 5 µl XT Sample Buffer 4x (Bio-Rad) and 1 µl XT Reducing Agent 10x (Bio-Rad) were added to the tube. The tubes were vortexed and spun down quickly before they were heated in a heating block at 70°C for 10 min. Meanwhile the Criterion XT 3-8% Tris-Acetate Precast Gel (Bio-Rad) was rinsed with AD and mounted in the electrophoresis apparatus (BioRad), which was filled with XT Tricine (Bio-Rad) diluted 1/20 in AD. The 26-well gel was loaded with 10 µl of a molecular weight marker (Precision Plus Protein Dual Color Standards (Bio-Rad)) and 15 µl sample per well. Next, the electrophoresis apparatus was connected to the power source and the electrophoresis was set for 55 min at 200 V and 400 mA. After electrophoresis, the proteins were blotted onto a Nitrocellulose membrane with the Trans-Blot Turbo Transfer Pack, Midi format, 0.2 µm Nitrocellulose membrane (Bio-Rad) for 10 min with a Trans-Blot Turbo Transfer System (Bio-Rad).

2.2.1.9 Lava purple (LP) total protein stain

After blotting, the membrane was rinsed in 1x tris buffered saline (TBS) (10x TBS (0,1 M Tris (pH 7,6), 15 M NaCl and 0,015 M Triton X-100) diluted 1/10 in AD) protein side down. From this step on, the blot with lava purple was kept in abscence of light as much as possible. Next, the membrane was placed in Lava purple (Serva) in staining solution (6.3 g boric acid and 3.85 g NaOH in 1l MQ) diluted 1/800 and rocked for 10 min protein side down. This staining detects proteins in the blot and can be used in order to verify whether the electrophoresis and blotting is successful or not. After the staining step, the blot was washed 3 times in MQ and then 30 min with 1x TBS. The blot was dried in a dark space and imaged using the cy3 fluorophore detecting function in a ChemiDoc MP imager (BioRad), using the Image Lab 4.1 software (Biorad).

2.2.1.9.1 Immunological detection

After the lava purple stain, the blot was washed 30 min with 1x TBS and blocked for 2h in 5% milk powder (Nestlé) in TBS. Afterwards, the blot was incubated with the primary Ab (Table 2) ON at 4°C. Besides immunolabeling of ROCK1 and ROCK2, also vimentin was stained. The next day, the excess primary Ab was washed away by rinsing the blot 3 times 10 min in TBS. Then the corresponding secondary antibody, GAM-HRP (P0477, Dako) for Vimentin and ROCK1 or GAR-HRP (P0488, Dako) for ROCK2 (Table 2), diluted in milk in TBS was added for 45 min, after which the excess secondary Ab was removed by washing 2 times 10 min with TBS and 10 min with 1x Tris (10x Tris (0.5 M tris(hydroxymethyl)aminomethaan with (pH 7,4) HCl) diluted 1/10 in AD). To visualise the detected proteins, the Thermo Scientific SuperSignal West Dura Extended Duration Substrate kit (Thermo) was used. This is a luminol-based enhanced chemiluminescence HRP substrate that gives stable light output for imagers. When the two reagentia in this kit (luminol and H_2O_2) react with the HRP from the secondary Ab, a signal at the spot where the secondary Ab is bound is detectable by the imager.

To immunolabel another protein on the same blot, the primary and secondary Ab were removed by stripping the blot. First the blot was rinsed for at least half an hour in 1x TBS, and then it was stripped by incubating in Restore PLUS Western Blot Stripping Buffer (Thermo) for 15 min at RT. The blot was rinsed for at least 30 min in TBS, after which exactly the same immunological detection procedure was followed as before, starting with blocking for 2h and incubating with the primary Ab overnight. To analyse the intensity of the immunodetected bands on the WB, the Image Lab 4.1 software was used.

Table 2: Primary and corresponding secondary Abs and their dilution used to detect proteins on WB. ROCK1, ROCK2 and Vimentin proteins were detected on the WBs of cellular samples.

Detected antigen	Primary Ab	Firm	Product number	Dilution	Secondary Ab	Dilution
ROCK1	monoclonal mouse anti-ROCK1	BD Bioscience	611136	1/250	GAM-HRP	1/50000
ROCK2	polyclonal rabbit anti-ROCK2	Abcam	ab71598	1/400	GAR-HRP	1/35000
ROCK2	monoclonal rabbit anti-ROCK2	Abcam	ab125025	1/1000	GAR-HRP	1/25000
Vimentin	monoclonal mouse anti-vimentin	Sigma	v5255	1/5000	GAM-HRP	1/25000

2.2.2 *Ex vivo* adult porcine explants

For the validation of the adult porcine explant model, porcine explants from fresh pig eyes were extracted and RGC densities after different culturing periods were analysed. All materials and products used in the culturing procedure were sterile. All preparations were made under a biohazard laminar flow.

2.2.2.1 Isolation of adult porcine explants

The eyes were dissected in Neurobasal medium (Gibco, Life Technologies) and opened by making an incision with a scalpel size 22 in the cornea close to the limbus. Next, sharp curved scissors (F.S.T) were used to cut along the limbus to remove the anterior chamber. After removal of the anterior chamber, the lens and the vitreous were dissected and 4 cuts were made with the curved scissors along 4 large blood vessels, to avoid the visual streak. 4 retinal explants were punched in the visual streak of a single retina at equal distance from the optic nerve using a 4 mm biopsy punch needle (Kai medical). The punches were carefully separated from the RPE by a soft fluid spurt with neurobasal medium.

2.2.2.2 Culturing of adult porcine explants

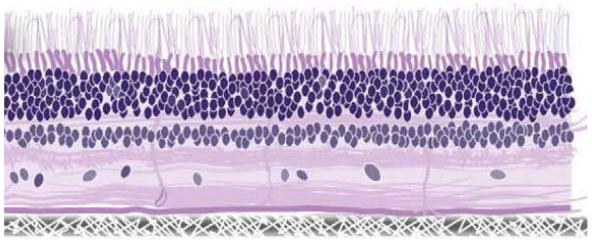

Figure 10: Illustration of the positioning of a porcine retinal explant, with the RGCL facing the culturing membrane (Taylor et al., 2014).

The explants were divided over 6 well plates (Nunc, Thermo Scientific) filled with 1.2 ml porcine explant culture medium (0.2 mM L-glutamine (Invitrogen), 0.25 µg/ml Fungizone (Invitrogen), 100 U/ml Penicillin (Invitrogen), 100 µg/ml Streptomycin (Invitrogen) and 2% B27 supplement (Invitrogen) in Neurobasal medium) and 0.4 µm pore size culture plate inserts (Millipore), thereby carefully transferring 3 explants of different eyes per insert. The explants were oriented with the RGC layer facing the Millipore insert (Figure 10). They were spread far apart from each other, taking care that they did not touch the edge of the wells. Finally, the excess fluid in the insert was removed. The explant medium was refreshed and a drop was added on the explant right before incubating the plate at 5% CO_2 and 37°C. The explants were incubated for different culturing periods: 0, 1, 3, 5 or 7 days in vitro (DIV), with the day of dissection as 0 DIV. The explant medium was completely refreshed every two days. After the incubation period, the explants were snapfrozen and lysed for western blot analysis or fixated and embedded in agarose (Invitrogen) for IHC (Taylor et al., 2013).

2.2.2.3 Western blot

2.2.2.3.1 Lysis of adult porcine explants

To prepare the explants for lysis, they were removed from the culture plate and dropped per 3 explants in a 1.5 ml centrifuge tube. The tube with the tissue was quickly snapfrozen by placing it in liquid nitrogen. The frozen tubes were stored at -80°C until lysis.

For the lysis, the samples were placed on ice and 150µl lysisbuffer (300mM NaCl, 0.5% Igepal, 0.5% sodium deoxycholate, 1mM EDTA (Sigma) and 0.1% SDS in 50mM tris HCl pH 8.0), supplemented with 1 mini tablet EDTA-free protease inhibitor cocktail per 10 ml buffer, was added to the explants. This was followed by rupturing the tissue with a rotating

conical crusher and sonicating the samples to disrupt the membranes. Next, the samples were centrifuged during 15 min at 13000 rpm at 4°C and the supernatans was transferred to a fresh 1.5 ml centrifuge tube.

Proteïn concentration was determined following the Bradford method as previously described in paragraph 2.2.1.8.2.

2.2.2.3.2 Electrophoresis and blotting

Electrophoresis was similar to the procedure that was previously described, with some exceptions. For porcine retinal samples, always 20 µg proteins of the samples were loaded on a 4-12% Criterion XT Bis-Tris Gel, 26 well (Biorad). A XT MOPS buffer (Biorad) 1/20 diluted in AD was used for electrophoresis for 50 min at 200 V and 400 mA. The blotting procedure was executed as previously described.

Next, a lava purple total protein stain was performed and different proteins were immunologically detected with different primary (and secondary) Abs, all summed up in Table 3. Detection of neuronal nuclei (NeuN) proteins should give an indication of the amount of GCL neurons in the explants. Detection of β-tubulin also gives an indication of the amount of GCL neurons in the explants. GFAP is a marker for Müller glia and astrocytes and its expression level is commonly used as a hallmark for gliosis induced in a diseased retina (Johansson et al., 2010). Analysis was identical to WBs analysis in paragraph 2.4.

Table 3: Primary and corresponding secondary antibodies and their dilution used to detect proteins on WB. NeuN, β-tubulin and GFAP proteins were detected on WBs of porcine explant samples.

Detected antigen	Primary Ab	Firm	Product number	Dilution	Secondary Ab	Dilution
NeuN	monoclonal mouse anti-NeuN	Millipore	MAB377	1/500	GAM-HRP	1/25000
β-tubulin	monoclonal mouse anti-β-tubulin	Sigma	T8660	1/500	GAM-HRP	1/25000
GFAP	polyclonal rabbit anti-GFAP	Dako	Z0334	1/20000	GAR-HRP	1/100000

2.2.2.4 Immunohistochemistry (IHC)

2.2.2.4.1 Fixation an embedding adult porcine explants

The retinal explants were fixated with 4% PFA for 2h at RT, after which they were rinsed twice with 1x PBS. Then the explants were placed in gradually increasing sucrose concentrations in 1x PBS for cryoprotection: first in 10% sucrose for 2h, secondly in 20% sucrose for the next 2h, finally in 30% sucrose overnight. The fixated porcine adult retinal explants were then embedded in agarose. Therefore, 1.25% agarose was solved in 30% sucrose in PBS. 30% sucrose was added to the explant on the culture plate insert to dislodge the explant. Then 450 µl agarose was added to a cryomold (15 x 15 x 5 mm, Thermo Scientific) and the dislodged explant was transferred on the agarose. After removing the

excess fluid, another 450 µl agarose was added. When the agarose is solidified, a second explant can be transferred to the cryomold and covered with agarose. The agarose blocks solidified at 4°C and were stored in 30% sucrose till sectioning.

2.2.2.4.2 Cryosectioning and staining of explants

The agarose embedded explants were sectioned serially using a cryostate (Microm HM 560) at -30°C. The 20 µm thick sections were placed on Superfrost plus slides (Thermo Scientific) and stored at -20°C. These sections are used to study retinal histology and to perform IHC labelling.

2.2.2.4.2.1 H&E staining

To visualise the morphology of the tissue, a Hematoxilin & Eosin (H&E) staining was used. At first, the slides were hydrated in AD for 5 min, then immersed in Hematoxylin solution (Sigma) for 3 min, to stain the nucleic acid rich structures, and thoroughly rinsed under running tap water for 10 min. Eosin solution (Sigma), which stains eosinophilic structures, was applied for 10 min. After this, the slides were rinsed twice in AD, and dehydrated by an alcohol series of ethanol 50%, ethanol 70%, ethanol 96% and two times 3 min in Ethanol 100% absolute for analysis (Millipore). In a last step, the slides were put two times 5 min in Xylene (Klinipath), after which the slides were mounted with Distyrene Plasticizer Xylene (DPX) mountant for histology (Sigma) using rectangular cover slips (Menzel-Glässer) and dried overnight on a heat plate at 37°C.

2.2.2.4.2.2 NeuN staining

The NeuN staining visualises nuclei of neuronal cells. The staining on the porcine retina proved to highlight neuronal cells in the GCL, yet RGCs more strongly than amacrine cells, more than the other neuronal cells in the retina (Bull et al., 2011; Taylor et al., 2014). The protocol starts by hydrating the cryosections for 5 min in AD, then washing solution (0.1% X-100 Triton in 1x PBS) was put on the slides for 5 min. After a blocking step of 20 min in blocking solution (0,1% X-100 Triton and 1% BSA in 1x PBS), the primary Ab (Table 4) diluted in blocking solution was placed on the slides ON at 4°C. The next day, the slides were washed five times for 5 min with washing solution, after which 500 µl of the secondary Ab (Table 4) diluted in blocking solution, was added to the slides for 45 min. Afterwards, the slides were washed 3 times 5 min with washing solution, next 30 min DAPI and finally mounted with mowiol and stored at 4°C in absence of light.

2.2.2.4.2.3 β-tubulin and GFAP stainings

The protocol of the β-tubulin and the GFAP staining starts with the rehydration of porcine explant sections by placing them 5 min in AD and 5 min in TBS. After this, the sections are submerged in citrate buffer (10 mM citric acid, 0.05% Tween-20 and NaOH to pH 6 in AD) and heated in an oven at 95°C for antigen retrieval. This heat treatment takes care of breaking the protein cross-links, which could interfere with staining, that arise from PFA fixation to

unmask epitopes to which the Abs bind (Shi et al., 2011). After the slides were allowed to cool down for 20 min, they were rinsed 3 times 5 min in TBS. Then the sections were blocked for 45 min in 20% PIG in Tris NaCl buffer (TNB) (0,5% blocking reagent (PerkinElmer) in 1x TBS), followed by ON incubation with the primary Ab diluted in TNB, as listed in Table 4. The next day, the slides were washed 3 times 5 min in TBS, after which the sections were incubated for 2h in the secondary Ab diluted in TNB, as listed in Table 4. This step was followed by 3 times 5 min washing in TBS, 30 min incubation in DAPI, mounting with mowiol and storage at 4°C.

Table 4: Primary and corresponding secondary antibodies and their dilution used to detect proteins in IHC stained porcine explant slides. NeuN, β-tubulin and GFAP proteins were detected.

Detected antigen	Primary Ab	Firm	Product number	dilution	Secondary Ab	dilution
NeuN	monoclonal mouse anti-NeuN	Millipore	MAB377	1/100	GAM-Alexa 488	1/250
β-tubulin	monoclonal mouse anti-β-tubulin	Sigma	T8660	1/600	GAM-Alexa 488	1/300
GFAP	polyclonal rabbit anti-GFAP	Dako	Z0334	1/1000	GAR-Alexa 488	1/300

2.2.2.4.3 Visualisation of the stainings

For the H&E, NeuN, GFAP and β-tubulin visualisation, stained sections of 4-5 different explants per condition were randomly selected, always using 3-4 sections per explant. Two pictures were taken of the peripheral part of the one section (the peripheral retina) (for GFAP only one picture) and one picture was taken of the central part of one the section.

To visualise the H&E and GFAP stained slides, an Axio imager Z1 (Carl Zeiss) controlled by ZEN Pro software was used with respectively brightfield microscopy and an AxioCam MR3 black and white camera. The pictures were taken using a 20x objective. The explant sections of the NeuN and β-tubulin staining were visualised using an inverted confocal fluorescence microscope using a 20x objective and parameters were kept constant. The pictures were taken as stacks of images over the z-axis, merged into a single projection and saved as tiff and oib files.

2.2.2.4.4 Analysis

The cells of the GCL in the NeuN stained sections were counted over a length of 500 µm using a CellCounter in Fiji software. On top of that, thickness of retinal layers was measured on the H&E pictures. The β-tubulin stained sections were not further analysed. And the intensity of the GFAP signal was compared between conditions by measuring the mean gray value of a 500µm wide selection area of the different retinal layers with Fiji.

2.3 Axonal regeneration

2.3.1 *Ex vivo* P3 mouse retinal explants

The postnatal *ex vivo* retinal explant model from P3 mouse eyes can be used to investigate the effects of ROCK inhibitors on neurite initiation and elongation. All materials and products used in the culturing procedure were sterile. The mice were sacrificed by decapitation, followed by dissection of the eyes with Dumont #7 forceps.

2.3.1.1 Isolation of P3 mouse explants

All preparations were made onder a biohazard laminar flow. One day prior to dissection, sterile 4-well culture plates were coated with 0.25 mg/ml Poly-L-lysine hydrobromide (Mw 70000-150000, Sigma) in 1x PBS. 300µl of the poly-L-lysine solution was added per well and the well plates were kept overnight in a 37°C incubator with 5% CO_2 supply. The mouse explant culture medium (1 mM L-glutamine, 0.25 µg/ml Fungizone, 100 U/ml Penicillin, 100 µg/ml Streptomycin, 2% B27 supplement and 0.4% Methylcellulose (Sigma) in Neurobasal-A medium (Gibco, Life Technologies)) was prepared and filtered with a sterile 40 µm cell strainer. Right before the dissection, the poly-L-lysine was aspirated and the wells were incubated with 300 µl laminin solution (2 µg/ml Laminin in 1x PBS) and incubated at 37°C for 2h. Afterwards, the laminin solution was aspirated and the wells were rinsed twice with PBS. Furthermore, specific P3 explant condition media (0.1 % DMSO with or without one or more of these components: 5 µM Y-39983 (AMA0076, Amakem NV), 1 µM AMA0428 (Amakem NV), 2ng/ml CNTF (PeproTech) and/or 5 ng/ml BDNF (PeproTech) in explant culture medium) were made containing explant culture medium with or without ROCK inhibitors (Y-39983 and AMA0428) and neurotrophic factors (CNTF and BDNF) as shown in Table 5 and the wells were filled with 250 µl of the specific P3 explant condition media and stored in the incubator upon use. In every explant experiment, more than one third of the wells were filled with explant culture medium without supplements, which served as a control condition. The data of these control samples were used as a baseline that enabled comparison amongst different experiments.

Table 5: All twelve possible specific P3 explant condition media used in the P3 explant experiments, obtained by supplementing the explant culture medium with a combination of ROCK inhibitors (Y-39983 and AMA0428) and/or neurotrophic factors (CNTF and BDNF).

Condition media	**-**	**AMA0428**	**Y-39983**
-	Control	AMA	Y3
CNTF	CNTF	AMA + CNTF	Y3 + CNTF
BDNF	BDNF	AMA + BDNF	Y3 + BDNF
CNTF + BDNF	C/B	AMA + B/C	Y3 + B/C

The eye was dissected in neurobasal-A medium. First a small puncture was made in the limbus of the mouse eye with a 23G needle. Then, Vannas spring scissors were used to cut

along the limbus to remove the anterior chamber. After removal of the anterior chamber and the lens, the slera and RPE were ruptured to expose the retina and the retinal cup was carefully removed after pinching off the optic nerve. The retinal cup was fixed by putting pressure on the ONH with a blunt straight forceps and the 750 µm FUE standard punch needle (Mediquip Surgical) was placed at the periphery of the retina. The retinal explants were punched out of the retina by gently pressing down the punch needle. On average, six to eight explants were harvested from one retina and one 4-well plate was filled with explants from two eyes from one mouse.

2.3.1.2 Culturing of P3 mouse explants

The explants were carefully transferred to a 4-well plate (3 to 4 explants per well), containing 250 µl specific explant condition medium per well. The explants were oriented with the RGC layer facing the coated surface using a blunt forceps, thereby avoiding touching the other explants and the edge of the wells. An additional 250 µl of the specific condition medium was added to each well. The plates were incubated at 5% CO_2 and 37°C during 72h, while 250 µl of the medium was refreshed every 24h. Hereafter, explants were washed with icecold 1x PBS and fixated in 4% PFA for 30 min. After washing 3 times with PBS, the explants were stored at 4°C in PBS containing 0.01% NaAz (Buyens et al., 2014).

2.3.1.3 β-tubulin IHC staining

The simple indirect IHC staining to detect β-tubulin in P3 explants is used in order to visualise the outgrowing neurites. First, the explants were washed 3 times 10 min in 1x TBS. The subsequent blocking step was performed by incubating the explants in 20% pre-immune goat (PIG) serum in TNB during 1h. Then, the primary Ab, mouse anti-β-tubulin (Sigma), diluted 1/500 in TNB, was incubated ON at RT. The next day, the tissues were washed 3 times 10 min in 1x TBS, followed by 2h incubation at RT with secondary Ab GAM-Alexa 488, 1/500 in TNB. Then the explants were washed once more with 1x TBS and DAPI for 30 min. Finally, they were stored in absence of light at 4°C in PBS with 0.01% NaAz.

2.3.1.4 Neurite outgrowth visualisation

The explants were visualised using an inverted confocal fluorescence microscope, FV1000 IX-82 (Olympus), with a motorised stage using a 20x objective. The DAPI stain was excited by a 405 nm laser, while the Alexa 488 fluorophore was excited by a 488 nm laser. In every experiment, laser power, gain and other microscopic parameters were maintained to minimise variation. Mosaic pictures of whole retinal explants were taken as stacks of images over the z-axis, merged into a single projection and saved as tiff and oib files.

2.3.1.5 Neurite outgrowth quantification

For the neurite outgrowth analysis, two custom-made explant analysis scripts were selected. A first script was compatible to Axiovision software (Zeiss) (Gaublomme et al., 2013), which is

not up to date anymore. Because Fiji software is consistently mentioned in literature, this software was a good candidate to write a second script for. The new script, written by Emiel Geeraerts, was mainly based on the basic principles of the Axiovision script.

2.3.1.5.1 Script with Axiovision

In the Axiovision analysis software automated script, tiff files were used from pictures taken on the confocal microscope with a resolution of 800 by 800 pixels. To measure the Immunodetected Neurite Area (INA), three input values had to be set on the first picture of the images of one experiment and they determined the local tresholding parameters. With these parameters set, the images of the entire experiment were analysed automatically. Each image was split into two colour channels. The blue channel visualised the DAPI signal, detecting the explant body. Then binarisation of the image followed, depending on the set threshold. Next, some filtering steps ensure closing of the explant edge, deletion of excess nuclei, selecting for circular objects and smoothening of the explant body. This generated an explant picture from which the explant area and perimeter were measured. The green channel visualised the β-tubulin signal, detecting the neurites. In this channel, the neurite network was detected using the two other thresholds and the signal from the explant itself was removed. The background noise and artefacts were filtered out, generating a picture with binarised neurites (Figure 11 B).

The total neurite area is categorised in different segments: from 0 to 100 µm, from 100 to 200 µm, from 200-300 µm and more than 300 µm from the explant edge (Figure 11 C). In addition, the Neurite Outgrowth Area (NOA) was determined by outlining the neurite area and substracting the explant body (Figure 11 A). The values from INA, NOA, different segments of the neurite area and the image name are exported to excel. In excel, INA and NOA and the segments of each explant were calculated relatively to the perimeter of the explant. Then those values were grouped per condition (Table 5). For each condition the mean and the SEM were calculated for INA and its different segments and for NOA.

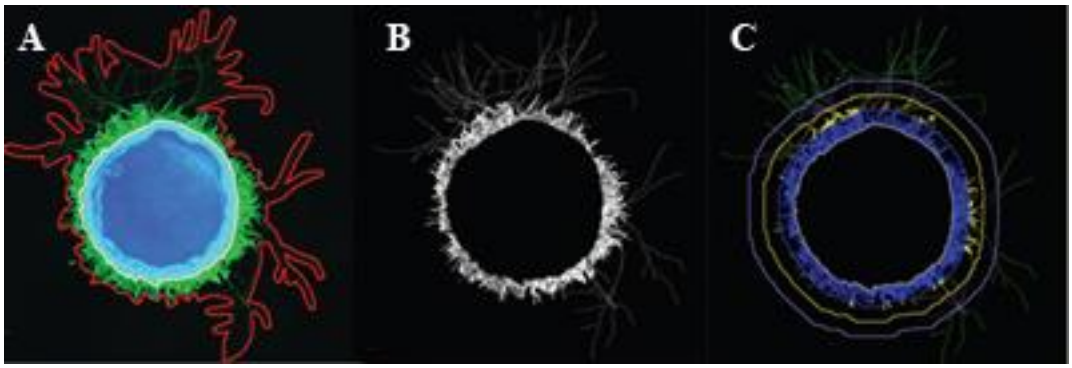

Figure 11: The explant analysis script in Axiovision. A: The explant body and the neurites in blue (DAPI) and green (β-tubulin), respectively. The Neurite Outgrowth Area (NOA) is outlined in red. The area of the explant body is outlined in yellow. B: The Immunodetected Neurite Area (INA) is shown in white. C: The different concentric circles of 100 µm width, in blue, yellow, purple and green represent neurite outgrowth from 0-100, 100-200 and 200-300 µm, and further than 300 µm from the explant body, respectively (Gaublomme et al., 2013).

2.3.1.6 ROCK double IHC staining

To localise the expression of ROCK protein to specific cell types within the explants, double IHC stainings with either β-tubulin or GFAP were performed. The protocol for this staining was similar to the β-tubulin IHC staining for P3 explants (see 2.3.1.3), starting with the same washing and blocking step. Next, ROCK2 was stained with a monoclonal and a polyclonal primary Ab, shown in Table 6. After incubation with the first primary and secondary Abs with green fluorophore (GAR-Alexa 488), the washing and blocking steps were repeated. Next, ROCK2 staining was combined on one hand with a β-tubulin primary Ab and corresponding secondary Ab with red fluorophore GAM-Alexa 568 (A-11004, Invitrogen), to examine if ROCK2 was colocalised with the neurites. On the other hand, ROCK2 staining was combined with GFAP primary Ab and corresponding secondary Ab, with the same red fluorophore, to examine if ROCK2 was colocalised with the glial fibres. After application of the secondary Ab, the explants were washed again, stained with DAPI and stored.

Table 6: Primary and corresponding secondary antibodies and their dilution used to detect ROCK2, ROCK1, β-tubulin and GFAP in an IHC staining of P3 retinal explants.

Detected antigen	Primary Ab	Firm	Product number	Dilution	Secondary Ab	Dilution
ROCK2	polyclonal rabbit anti-ROCK2	Abcam	ab71598	1/300	GAR-Alexa 488	1/300
ROCK2	monoclonal rabbit anti-ROCK2	Abcam	ab125025	1/100	GAR-Alexa 488	1/300
β-tubulin	monoclonal mouse anti-β-tubulin	Sigma	T8660	1/500	GAM-Alexa 568	1/300
GFAP	monoclonal mouse anti-GFAP	Sigma	G3893	1/1000	GAM-Alexa 568	1/300

Pictures were taken under the LSM 780 confocal microscope (Zeiss) by Stefan Vinckier and colocalisation was examined qualitatively.

2.4 Statistical analysis

All values were expressed as mean values ± standard error of the mean (SEM) and compared using a student's *t*-test, a one-way or two-way ANOVA in Prism 6 (Gaphpad), with Tukey or Bonferroni post hoc tests. Statistical differences were considered to be significant at $p<0.05$ (*), $p<0.01$ (**), $p<0.001$ (***) or $p<0.0001$ (****).

3 Results

3.1 Neuroprotection

Because the Rho-ROCK pathway is involved in neurological diseases, inhibition of this pathway can be beneficial as a therapy for these diseases (Liao et al., 2007; Noma et al., 2006). However, a better knowledge of these components, might lead to more efficient targeting and therapies. To investigate the role of ROCK1 and ROCK2 in neurodegeneration, *in vitro* porcine retinal cell models and an *ex vivo* porcine explant model were optimised, validated and ROCK expression was or will in the future be determined in these neurodegenerative models.

3.1.1 *In vitro* retinal cell models

The main objective in this section is to perform a detailed *in vitro* study of ROCK1 and ROCK2 expression in healthy and pathological porcine retinal cell cultures. However, before ROCK expression levels can be determined, it is crucial to validate the microglia and Müller glia cell culture purity. Next, to mimic the pathological retinal environment, we will apply cytotoxic stressors to the cells and validate the glial response.

3.1.1.1 Validation of cell culture purity

To evaluate cell culture purity, healthy microglia were stained for Iba-1 and healthy Müller glia for GS. The amount of Iba-1 or GS positive cells was compared to the total cell number, as indicated by the DAPI positive nuclei. Comparison of DAPI and Iba-1 stained cells in microglia cultures (Figure 12 A-C) lead to an estimation of >80% cell culture purity. Comparison of DAPI and GS stained cells in Müller glia cultures (Figure 12 D-F) lead to an estimation of >95% cell culture purity.

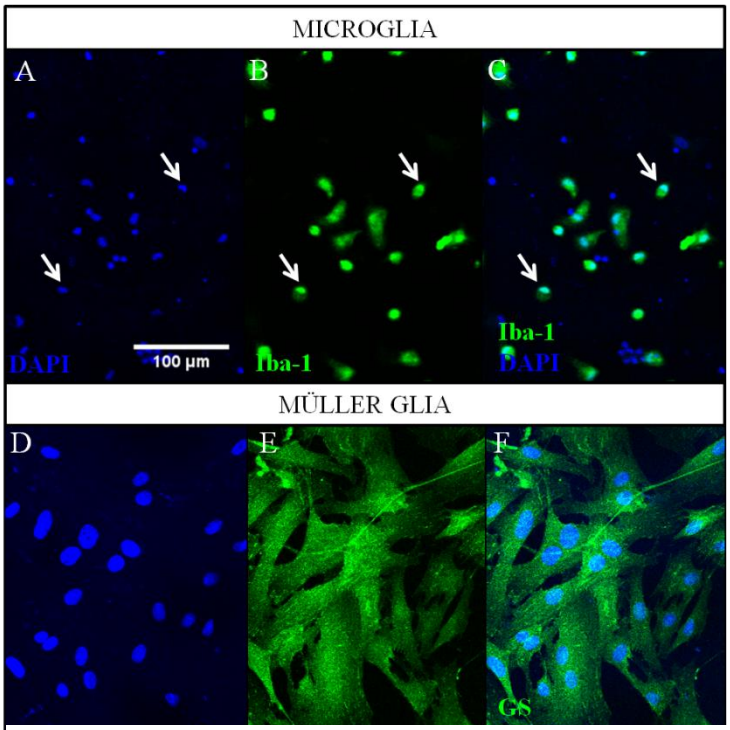

Figure 12: Iba-1 and GS ICC of microglia and Müller glia, respectively. A: blue channel revealing DAPI signal of all cells in microglia culture. B: green channel showing Iba-1 positive microglia. C: overlay of both channels (DAPI and Iba-1) indicates around 80% overlap (2 examples denoted by white arrows) of blue and green signal. D: blue channel revealing DAPI signal of all cells in Müller glia culture. E: green channel showing GS positive Müller glia. F: overlay of both channels (DAPI and GS) indicates around 95% overlap of blue and green signal. All pictures have the same scale and there was a notable difference in nuclear size between Müller glia and microglia.

3.1.1.2 Validation of stress induction in Müller glia cell cultures

To validate cytotoxic stress, stressed and healthy Müller glia were subjected to ICC and WB for vimentin, which is a marker that is upregulated in stressed glial cells in a process called reactive gliosis (Bringmann et al., 2009a). Müller glia were exposed to 100µM $CoCl_2.6H_2O$ or H_2O_2 for 6 hours *in vitro* (HIV) or 24HIV for the induction of oxidative stress (Kesherwani et al., 2014), to 5, 10 or 20mM glutamate for 6HIV or 24HIV for the induction of excitotoxic stress (Challenor et al., 2015), or to 30mM glucose for 24HIV for the induction of hyperglycemia (Devi et al., 2012). In control conditions in healthy Müller glia, no stressor was added, except in the hyperglycemia experiment, where the control cells were grown in 5mM glucose, corresponding to normal glycemia levels that are needed for cell proliferation in culture (Devi et al., 2012; Matteucci et al., 2015). In microglia cultures, the same concentrations were used.

Representative pictures of cells with and without stressors during 24HIV are shown in Figure 13. The negative control, where primary Abs were omitted, did not show any vimentin signal (green signal), although Müller glia are present, as can be seen from the DAPI positive nuclei (blue signal). After induction of oxidative stress with 100µM of both $CoCl_2.6H_2O$ and H_2O_2,

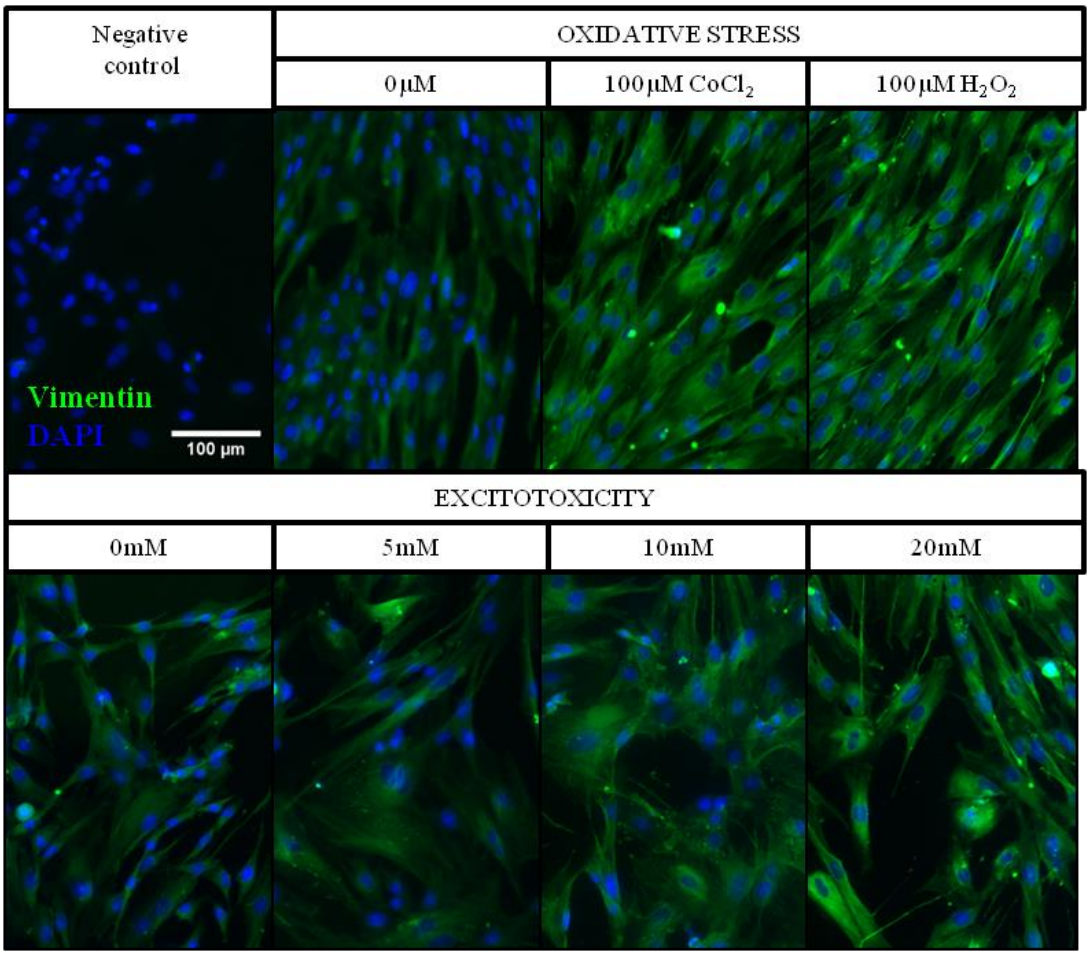

Figure 13: Representative pictures of vimentin ICC of healthy and stressed Müller glia during 24HIV. The DAPI signal is displayed in blue and the vimentin signal in green. The left upper picture is a negative control. The three other upper pictures demonstrate increased levels of vimentin in oxidative stressed cells. Similarly, vimentin levels are accumulating in cells exposed to excitotoxicity, as shown in the four lower pictures.

the vimentin signal was stronger as compared to the healthy situation (0µm). After excitotoxicity, the vimentin signal was slightly stronger with increasing concentrations of glutamate as compared to the healthy situation. Vimentin ICC on hyperglycemic Müller glia was not performed. These pictures suggest that vimentin is upregulated in cultured Müller glia subjected to cytotoxic stress.

Semiquantitative WB analysis of Müller glia cell lysates subjected to excitotoxicity demonstrated an 11 ± 6% higher vimentin expression as compared to healthy Müller glia (Figure 14 A), yet this difference was not significant. Vimentin expression was 37 ± 13% higher for $CoCl_2.6H_2O$ and 5 ± 8% higher for H_2O_2 oxidative stress, relative to the control condition (Figure 14 B and C). The H_2O_2 oxidative stress condition did not differ significantly, whereas induction of $CoCl_2.6H_2O$ induced a significant vimentin upregulation. Hyperglycemic cells showed a similar (2 ± 6% higher) vimentin expression in stressed cells compared to the control condition (Figure 14 D). Vimentin expression was also assessed at other time points (6HIV for excitotoxicity and oxidative stress) and with increasing stresscompound concentrations (10mM and 20mM for excitotoxicity). These results were similar (data not shown).

Although WB data did not clearly show an augmented vimentin expression for all the stressors, ICC already suggested an increased vimentin expression after excitotoxicity and both oxidative stressors. Based on these results and the concentrations indicated in literature, these concentrations and time points meantioned in the beginning of the paragraph were used for all other *in vitro* experiments (Challenor et al., 2015; Devi et al., 2012; Kesherwani et al., 2014).

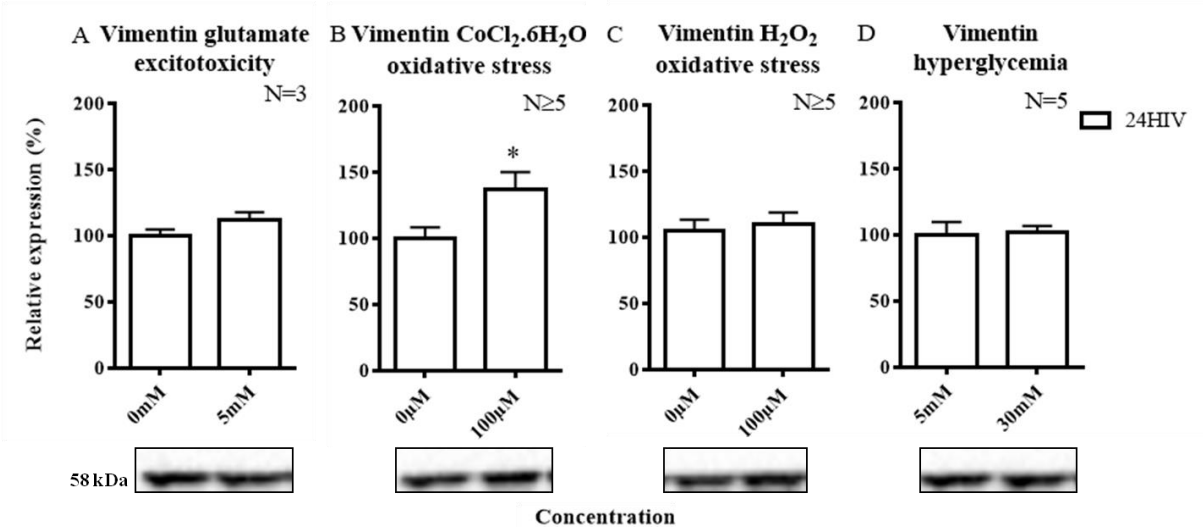

Figure 14: Semiquantitative WB analysis of vimentin expression in Müller glia subjected to hyperglycemia, excitotoxicity and oxidative stress during 24HIV. Densitometric analysis of vimentin expression showed that vimentin was not altered after exposure of Müller glia to glutamate (A), H_2O_2 (C) and hyperglycemia (D), but was significantly increased after exposure to $CoCl_2.6H_2O$ (B). Representative WBs are shown under each graph. Data are represented as percentage relative to vimentin expression in the respective control condition (mean ± SEM). N: number of biological replicas per condition. Conditions were compared by using a student's *t*-test, *: $p<0.05$.

3.1.1.3 Detailed study of ROCK2 and ROCK1 expression in healthy and pathological retinal cell cultures

Both vimentin ICC data and literature indicate a glial reactivity in Müller glia after adding stressors as described above. To examine the presence of ROCK2 and ROCK1 in healthy and reactive (pathological) Müller glia and microglia, ICC and WB analysis were performed. Especially ROCK2 expression in the CNS is documented, yet its role in the healthy and diseased retina is not completely clear (Koch et al., 2014a; Schofield & Bernard, 2013). The ICC staining of healthy Müller glia for ROCK2 (Abcam) is displayed in Figure 15, in which ROCK2 is clearly present in the cytoplasm of healthy Müller glia.

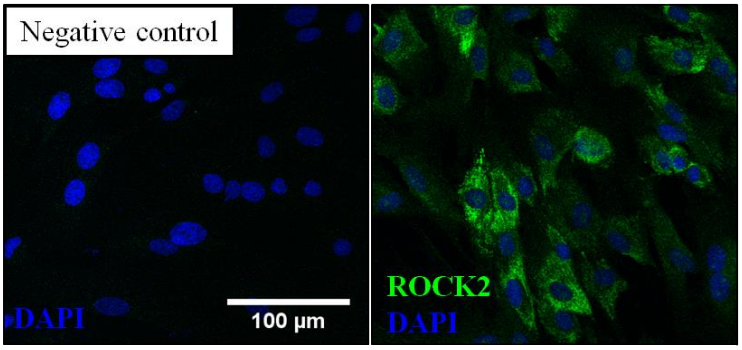

Figure 15: ROCK2 ICC on healthy Müller glia. ROCK2 (green) is clearly present in the cytoplasm of cultured, healthy Müller glia, of which the nuclei are stained with DAPI (blue). The left picture is a negative control, without primary Ab.

The presence of ROCK2 (Abcam) in healthy Müller glia was further confirmed via WB (0mM condition in Figure 16).

Moreover, the ROCK2 expression in Müller glia cell cultures was examined at 6 and 24HIV (Figure 16). 6HIV after 5mM glutamate excitotoxicity induction, ROCK2 expression was significantly higher (33 ± 9%) than in the control condition. ROCK2 expression of Müller glia 6HIV after 10mM and 20mM glutamate excitotoxicity induction was comparable to control levels. Stressed Müller glia under 5mM and 10mM glutamate during 24HIV demonstrated a 13 ± 3% and 48 ± 1% higher ROCK2 expression as compared to the control condition, respectively. Only induction of 10mM glutamate was significantly higher than the control 24HIV conditions. The expression 24HIV after 20mM was comparable to control levels.

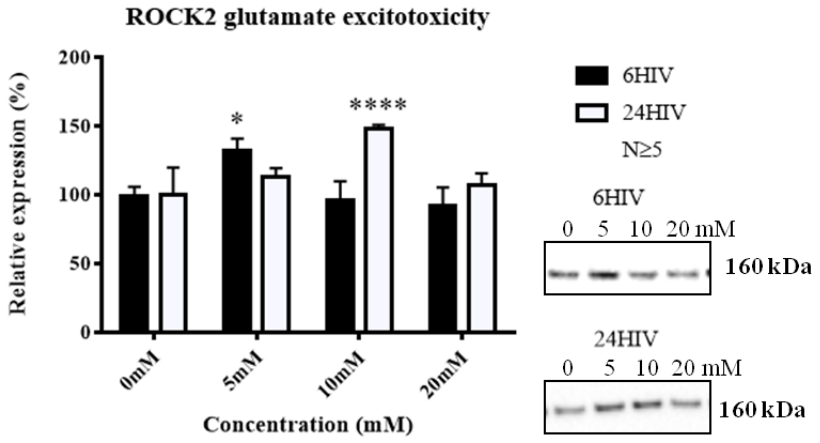

Figure 16: Semiquantitative WB analysis of ROCK2 expression in Müller glia subjected to excitotoxicity during 6 and 24HIV. Densitometric analysis of ROCK2 expression showed no altered expression after 6HIV under 10 and 20mM and a slight upregulation after 24HIV under 5 and 20mM glutamate, but was significantly increased after exposure of Müller glia for 6HIV to 5mM glutamate and for 24HIV to 10mM glutamate. Representative WBs are shown on the right side of the graph. Data are represented as percentage relative to ROCK2 expression in the control condition (mean ± SEM). N: number of biological replicas per condition. All stress conditions of one time point were compared by using a one-way ANOVA statistical analysis with a Tukey's test or using a student's *t*-test, *: $p<0.05$, ***: $p<0.001$, ****: $p<0.0001$.

ROCK2 expression in Müller glia subjected to oxidative stress was examined at 6 and 24HIV with both $CoCl_2.6H_2O$ and H_2O_2. Semiquantitative WB analysis of ROCK2 expression showed only a slightly increased expression (15 ± 11%) after 6HIV under 100µM $CoCl_2.6H_2O$ as compared to the control condition (Figure 17 A). Administration of 100µM H_2O_2 after 6 and 24HIV and 100µM $CoCl_2.6H_2O$ after 24HIV did not differ from the control condition (Figure 17 B).

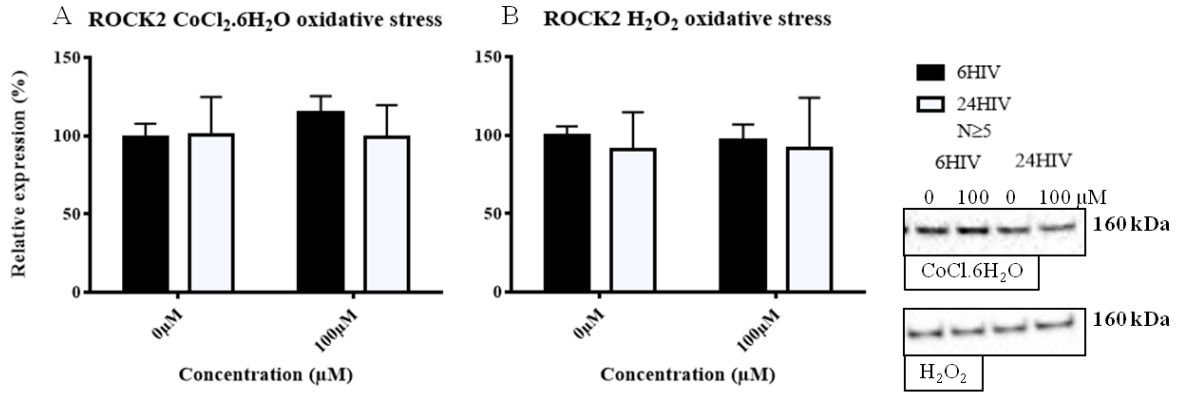

Figure 18: Semiquantitative WB analysis of ROCK2 expression in Müller glia subjected to $CoCl_2.6H_2O$ and H_2O_2 oxidative stress during 6 and 24HIV. A: Densitometric analysis of ROCK2 expression showed that ROCK2 was slightly increased after exposure of Müller glia to 6HIV and 24HIV $CoCl_2.6H_2O$, yet this difference was not significant. B: Densitometric analysis of ROCK2 expression showed that ROCK2 was not altered after exposure of Müller glia to H_2O_2. Representative WBs are shown on the right side of the graphs. Data are represented as percentage relative to ROCK2 expression in the control condition (mean ± SEM). N: number of biological replicas per condition.

Next to excitotoxic and oxidative stress, high glucose (30mM) after 24HIV exposure showed a 19 ± 14% increase in ROCK2 expression (Figure 18 A). However, this ROCK2 elevation was not significant due to high variability in the samples. A similar analysis was performed for microglia and for this WB, equal protein concentrations of both healthy and stressed microglia samples and one Müller glia sample as a positive control were loaded (Figure 18). Although a clear band for ROCK2 was demonstrated in healthy Müller glia, ROCK2 bands in microglia were very faint.

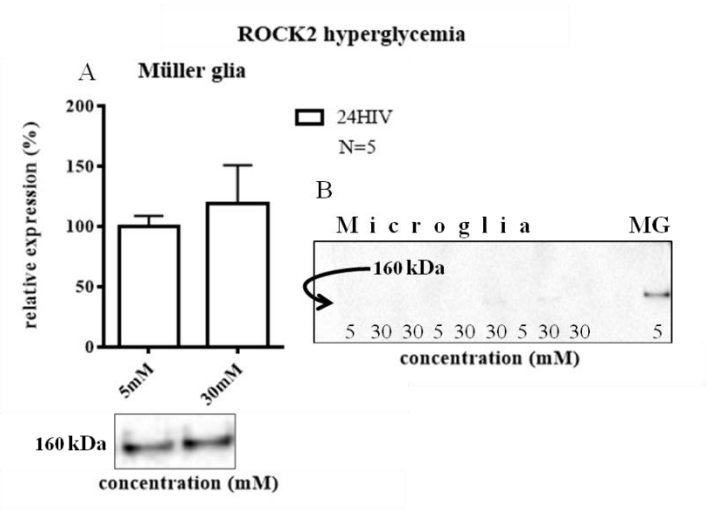

Figure 17: WB analysis of ROCK2 expression in Müller glia and microglia subjected to hyperglycemia during 24HIV. A: Densitometric analysis of ROCK2 expression in Müller glia subjected to hyperlycemia is depicted on the left and shows a non significant ROCK2 increase after hyperglycemia induction. A representative WB is shown below the graph. Data are represented as percentage relative to ROCK2 expression in the control condition (mean ± SEM). N: number of biological replicas per condition. B: The WB of microglia with one Müller glia (MG) sample shows a clear band for ROCK2 in the MG sample, yet very faint bands in microglia.

Since ROCK2 was more abundant in Müller glia than in the microglia, we discontinued the study of ROCK expression in stressed microglia in this thesis, yet we focussed on ROCK expression in stressed Müller glia.

The expression of ROCK1 in the CNS is discussed to a lesser extent in literature. ROCK1 expression was also examined in healthy and stressed Müller glia using only WB analysis. However, due to practical issues of the ROCK1 antibodies (mouse monoclonal anti-ROCK1 (BD Bioscience) and mouse monoclonal anti-ROCK1 (Santa Cruz)), ICC did not disclose a clear ROCK1 expression in the Müller glia. The presence of ROCK1 (BD Bioscience) in healthy Müller glia was already demonstrated via WB (0mM condition in Figure 19).

ROCK1 expression in Müller glia cell cultures was also examined after induction of excitotoxicity, more specifically at 6 and 24HIV (Figure 19). ROCK1 expression after induction of 5mM and 10mM glutamate at 6HIV showed a significant increase (55 ± 19% and 29 ± 10%, respectively) compared to the control condition. The ROCK1 expression levels 24HIV after glutamate showed a similar, but less pronounced trend.

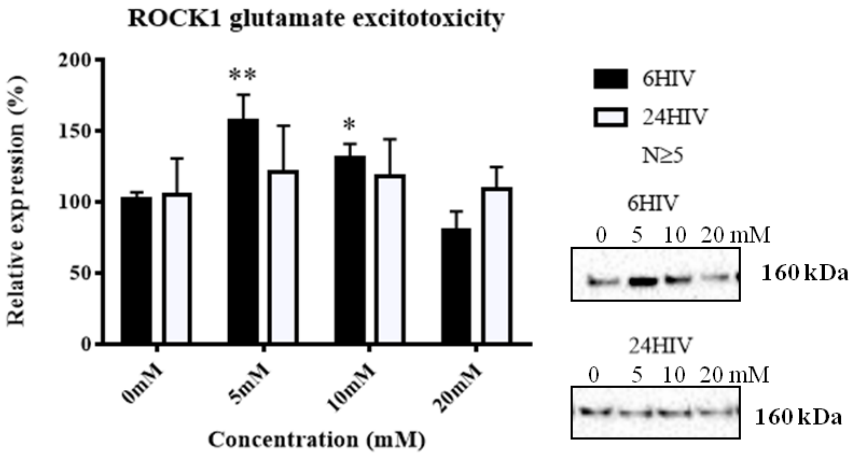

Figure 19: Semiquantitative WB analysis of ROCK1 expression in Müller glia subjected to excitotoxicity during 6, 24 and 48HIV. Densitometric analysis of ROCK1 expression showed that ROCK1 was not significantly altered after 6HIV under 20mM and after 24HIV under 5, 10 and 20mM glutamate, but was significantly increased after exposure of Müller glia for 6HIV to 5 and 10mM glutamate. Representative WBs are shown on the right side of the graph. Data are represented as percentage relative to ROCK1 expression in the control condition (mean ± SEM). N: number of biological replicas per condition. Conditions were compared by using a student's *t*-test, *: $p<0.05$, **: $p<0.01$.

ROCK1 expression after oxidative stress was examined at 6 and 24HIV with both 100µM $CoCl_2.6H_2O$ and H_2O_2, ROCK1 expression showed a slight increase (12 ± 13%) at 6HIV following $CoCl_2.6H_2O$ treatment as compared to the control (Figure 20). At 24HIV with $CoCl_2.6H_2O$ and at 6 and 24HIV under H_2O_2, no significant differences in expression levels were observed as compared to the control (Figure 20).

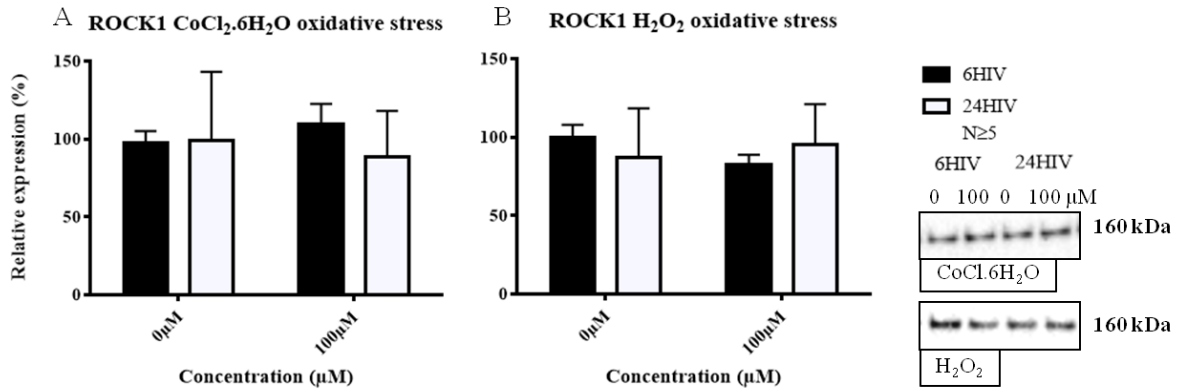

Figure 20: Semiquantitative WB analysis of ROCK1 expression in Müller glia subjected to $CoCl_2.6H_2O$ and H_2O_2 oxidative stress during 6 and 24HIV. A: Densitometric analysis of ROCK1 expression showed that ROCK1 was slightly increased after exposure of Müller glia to 6HIV $CoCl_2.6H_2O$, yet this difference was not significant. B: Densitometric analysis of ROCK1 expression showed that ROCK1 was not significantly altered after exposure of Müller glia to H_2O_2. Representative WBs are shown on the right side of the graphs. Data are represented as percentage relative to ROCK1 expression in the control condition (mean ± SEM). N: number of biological replicas per condition.

Next to excitotoxic and oxidative stress, high glucose (30mM) after 24HIV exposure showed a clear (30 ± 14%) increase in ROCK1 expression (Figure 21). However, this ROCK1 increase was not significant. Given the limited number of samples available, repetition of this experiment is necessary to check the consistency of these findings.

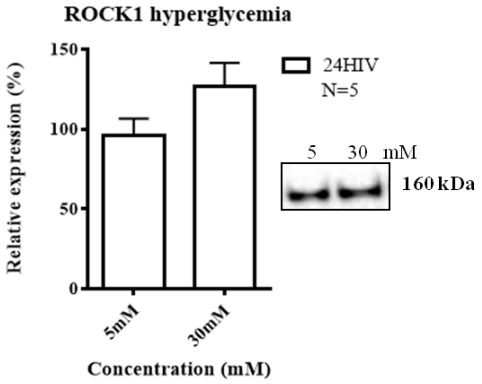

Figure 21: Semiquantitative WB analysis of ROCK1 expression in Müller glia subjected to hyperglycemia during 24HIV. Densitometric analysis of ROCK1 expression shows a non significant ROCK1 increase after hyperglycemia induction. A representative WB is shown on the right side of the graph. Data are represented as percentage relative to ROCK1 expression in the control condition (mean ± SEM). N: number of biological replicas per condition.

Overall our findings revealed that both ROCK2 and ROCK1 were present in healthy and pathological Müller glia and were upregulated in excitotoxic, hyperglycemic and oxidative stress conditions.

3.1.2 *Ex vivo* adult porcine explant model

The adult porcine explant model was introduced in our lab in order to develop an *ex vivo* model that mimics pathological neurodegeneration in the eye, thereby intending to use this neurodegenerative model for the evaluation of new neuroprotective strategies, for example ROCK inhibition.

Two hallmarks of neurodegenerative eye diseased are decreased neuronal cell survival and increased glial reactivity. In order to validate the porcine explant model as a neurodegenerative model, these two parameters were assessed immediately after dissection (0 days *in vitro* (DIV)) and at 1, 3, 5 and 7DIV. In addition, the morphological changes in the explant were examined via H&E staining.

3.1.2.1 Neuronal cell survival is decreased with time during culturing

3.1.2.1.1 NeuN

The neuronal nuclei (NeuN) protein is specifically expressed in post-mitotic mature neurons. The NeuN Ab primarily stains the neuronal nucleus, but also the cytoplasm and dendrites can be more faintly stained. NeuN immunoreactivity decreases in degenerating mature neurons, and therefore can be used to monitor neuropathogenesis (Lavezzi et al., 2013). NeuN specificity for RGCs is contradictory in literature (Smedowski et al., 2014); according to Johansson et al. (2010), NeuN strongly labels RGCs, but also weakly labels displaced amacrine cells in the porcine GCL.

WB and IHC analysis for NeuN (Millipore) were performed to quantify degeneration of RGCs in the GCL. WB (Figure 22 A) showed a gradually decreasing NeuN expression, with significant differences between control (0DIV) and 1, 3, 5 and 7DIV. The NeuN IHC analysis, performed by counting NeuN positive cells over a distance of 500µM in the RGC layer (Figure 22 B and C), also revealed a decrease in NeuN positive cells, with significant differences between control (0DIV) and 1, 3, 5 and 7DIV. This gradual decrease of NeuN positive cells over time confirmed the WB data. Furthermore, a thinning of the inner retina was observed on the NeuN stained pictures, but will be further discussed in paragraph 3.1.2.3.

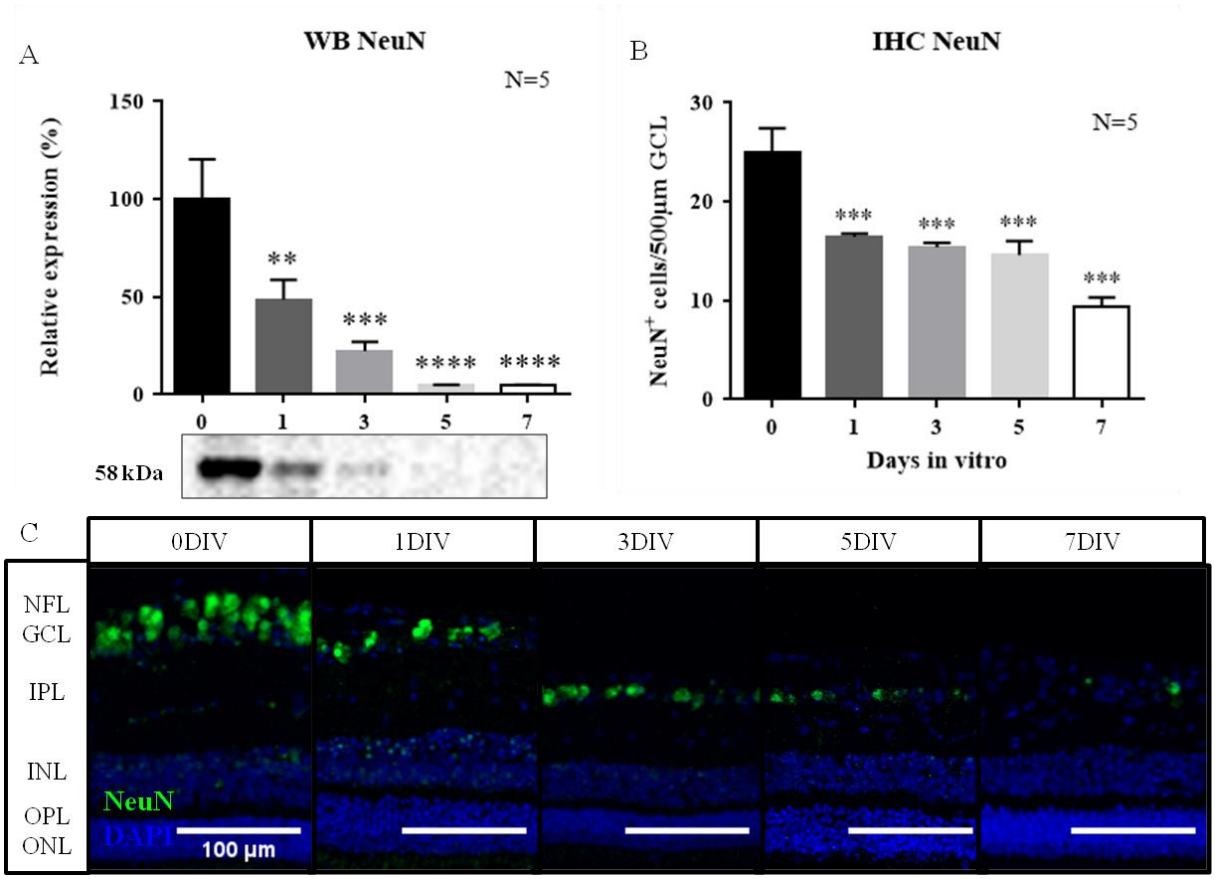

Figure 22: Semiquantitative WB analysis and IHC analysis of NeuN expression in porcine explants after 0, 1, 3, 5 and 7DIV. A: Densitometric analysis of NeuN expression demonstrated a significant decrease in NeuN expression over time. A representative WB is shown under the graph. Data are represented as percentage relative to NeuN expression in the control condition (0DIV: 100%). N: the amount samples of the same condition, each containing a pool of 3 different explants. B: Counting of NeuN positive cells over a distance of 500µm in the GCL confirmed this decrease in NeuN signal. N: the amount of explants per condition from different eyes. C: NeuN (green) IHC stained porcine explant cryosections of all time points, with DAPI in blue and retinal layers of the 0DIV explant picture indicated on the left. A thinning of the retina is visible. Data in the graphs are represented as mean ± SEM. Conditions were compared to the control using a one-way ANOVA statistical analysis with a Tukey's test, *: $p<0.05$, **: $p<0.01$, ***: $p<0.001$, ****: $p<0.0001$.

3.1.2.1.2 β-tubulin

β-tubulin is a neural specific protein of the tubulin family, which comprises proteins that form the microtubule of the cytoskeleton. According to most sources, β-tubulin is proven to be a trustworthy RGC marker in the rodent retina (Cui et al., 2003; Jiang et al., 2015).

WB and IHC analysis for β-tubulin (Sigma) were performed to quantify RGC degeneration (Figure 23). WB demonstrated a decreasing β-tubulin expression, although differences were not significant. IHC staining for β-tubulin on porcine explant cryosections did not appear to be restricted to RGC somata and rather stained RGC axons. Therefore, cell counting was not possible.

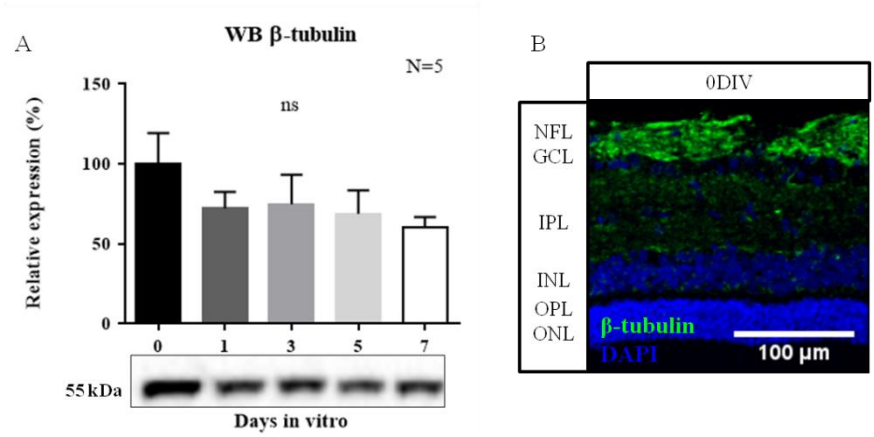

Figure 23: Semiquantitative WB analysis and IHC analysis of β-tubulin expression in porcine explants after 0, 1, 3, 5 and 7DIV. A: Densitometric analysis of β-tubulin expression demonstrated a slightly decreasing β-tubulin expression over time, yet differences were not significant. A representative WB is shown under the graph. Data are represented as percentage relative to β-tubulin expression in the control condition (0DIV: 100%) B: β-tubulin (green) IHC stained porcine explant cryosections of 0DIV, DAPI in blue and retinal layers indicated on the left. Cell somata were not clearly defined and also RGC axons were stained. Data in the graph is represented as mean ± SEM. N: the amount samples of the same condition, each containing a pool of 3 different explants.

3.1.2.1.3 H&E

The Hematoxilin & Eosin (H&E) staining visualises the nuclei with basophilic hematoxylin and the cytoplasm with eosinophilic eosin. This H&E staining is commonly used in literature to evaluate differences in cell number (RGCs, displaced amacrine cells and astrocytes in the GCL) (Johansson et al., 2010). The H&E pictures of the porcine explants at 0, 1, 3, 5 and 7DIV are depicted in Figure 25. However, cell counting in the GCL was not possible due to the laminar organisation of NFL, GCL and IPL that is not clearly distinguishable at later time points (5 and 7DIV) (Figure 25). Cell counting in the ganglion cell complex (GCC), i.e. the NFL, GCL and IPL together, was feasible, but this analysis is still ongoing.

3.1.2.2 Glial reactivity is increased with time during culturing

3.1.2.2.1 GFAP

Glial fibrillary acidic protein (GFAP) is an intermediate filament that is strongly present in astrocytes, but also in the radial Müller glia of the porcine retina (Johansson et al., 2010; Taylor et al., 2014). Moreover, GFAP expression is commonly used as a hallmark for gliosis induced by disease or injury (Ghosh et al., 2007).

Porcine explants showed a significantly increased glial reactivity after one week in culture, as indicated by the significantly higher GFAP expression (Dako) in a WB analysis at 3, 5 and 7DIV compared to the control (Figure 24 A). GFAP IHC staining demonstrated a very clear labeling of astrocytes and Müller glia endfeet in the GCL and NFL and faint labelling in the thin vertical Müller glia fibres troughout the retina at 0DIV. The intensity of the GFAP signal in Müller glia endfeet and astrocytes in the GCL and NFL augmented at 1DIV and reached its peak at 3DIV, and declined at 5 and 7 DIV, although differences were not significant (Figure 24 C and E). Furthermore, GFAP intensity per pixel was significantly elevated with time (5

and 7DIV) in the combination of INL, IPL and ONL, in which the radial glia fibres were more intensely stained (Figure 24 D and E).

3.1.2.2.2 Vimentin

Vimentin is another intermediate filament that can be used as a marker for reactive gliosis. Semiquantitative WB analysis of relative vimentin expression (Figure 24 B), shows a clear

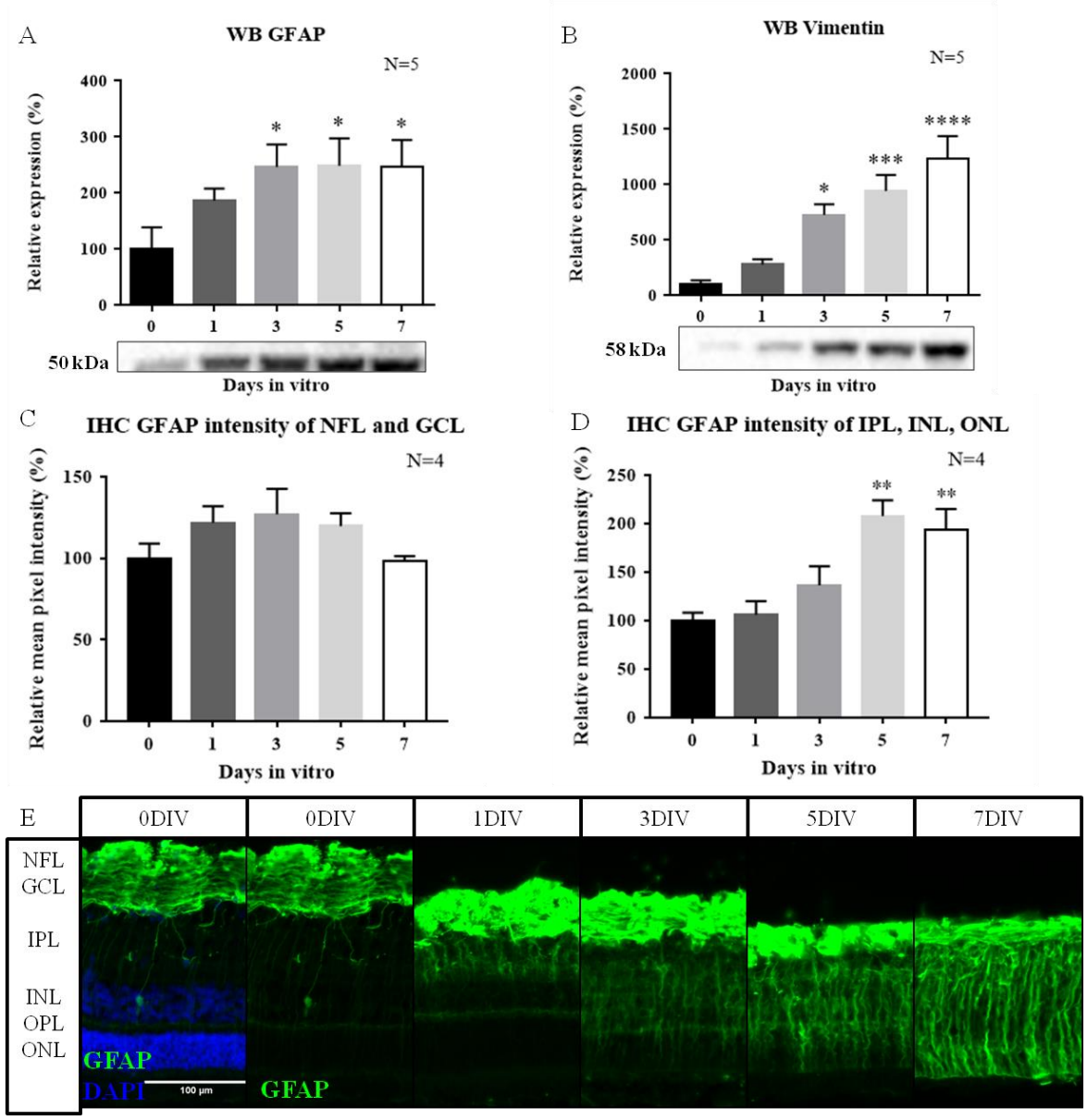

Figure 24: Semiquantitative WB analysis of GFAP and vimentin expression and IHC analysis of GFAP expression in porcine explants after 0, 1, 3, 5 and 7DIV. A: Densitometric analysis of GFAP expression demonstrated a significant increase in GFAP expression over time. B: Densitometric analysis of vimentin expression demonstrated a clear significant and gradual increase in vimentin expression over time. Representative WBs are shown under the graph. N: the amount samples of the same condition, each containing a pool of 3 different explants. C: Relative mean pixel intensity of the green signal in the NFL and GCL (B) showed a peak at 3DIV and declined afterwards. D: Relative mean pixel intensity of the green signal in the IPL, INL and ONL was elevated over time. N: the amount of explants per condition from different eyes. E: NeuN (green) IHC stained porcine explant cryosections of all time points, with DAPI in blue and retinal layers of the 0DIV explant picture indicated on the left. A thinning of the retina is visible. Data are represented as percentage relative to GFAP expression or intensity in the control condition (0DIV: 100%) (mean ± SEM). Conditions were compared to the control using a one-way ANOVA statistical analysis with a Tukey's test or using a student's *t*-test, *: $p<0.05$, **: $p<0.01$, ***: $p<0.001$, ****: $p<0.0001$.

and gradual upregulation of vimentin over time, with significant differences at 3, 5 and 7DIV as compared to control.

3.1.2.3 Morphological changes in laminar architecture and retinal thinning

The H&E staining is also commonly used to visualise retinal morphology. General retinal laminar organisation was preserved over time, yet in the GCC, i.e. NFL, GCL and IPL together, a slow disturbance of laminar architecture was observed the longer the time *in vitro* (starting from 3DIV, but more pronounced at 5 and 7DIV) (Figure 25 C). Moreover, the total thickness of the retinal layers declines and representative pictures are displayed in Figure 25 A. To asses differential thinning of the layers, retinal thickness was assessed for each of the three separate layers: GCC, INL and ONL (Figure 25 B). The GCC contributed most to the thinning over time, its thickness already declined significantly from 0 to 1DIV. The INL also thinned slightly from 0 to 1DIV, without any significant differences, while the thickness of the ONL remained constant.

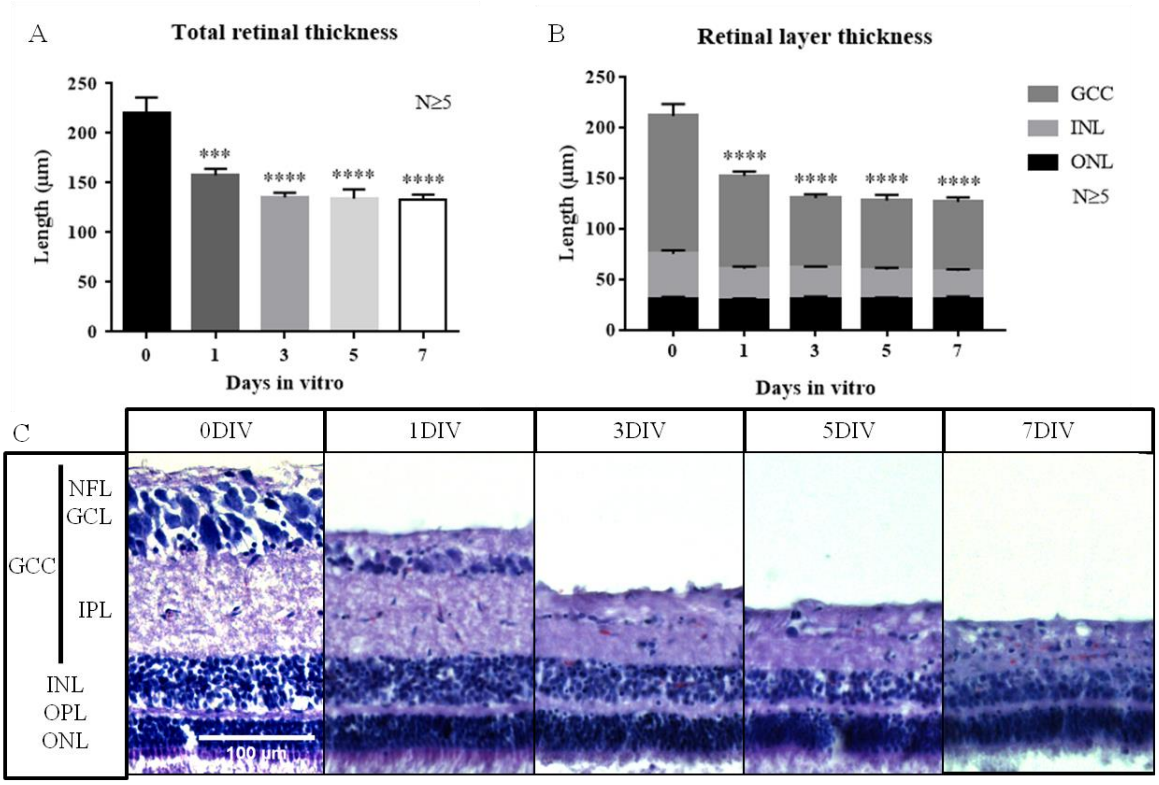

Figure 25: H&E morphological analysis of the retinal thickness in porcine explants after 0, 1, 3, 5 and 7DIV. A: Thickness of the total retina (from NFL to ONL) in µm decreases significantly over time. Conditions were compared using a one-way ANOVA statistical analysis with a Tukey's test. B: Thickness of retinal layers GCC, INL and ONL over time. Significant decline in GCC thickness is observed, the INL thickness decreases very slowly and differences are not significant, while the ONL thickness remains constant. Conditions were compared using a two-way ANOVA statistical analysis with a Tukey's test. C: H&E stained porcine explant cryosections of all time points. Retinal thinning and reorganisation of cells in the GCC is visible. Data are represented as mean ± SEM. N: the amount of explants per condition from different eyes. Significancies compared to the control (0DIV) are shown as *: $p<0.05$, **: $p<0.01$, ***: $p<0.001$, ****: $p<0.0001$ above the error bars of that condition.

3.2 Axonal regeneration

Because regeneration of injured axons in the CNS remains elusive, reliable models are necessary to screen regeneration-promoting agents, such as neurotrophic factors and ROCK inhibitors.

3.2.1 *Ex vivo* P3 mouse retinal explants

An explant culture of neonatal mouse retinas was used, in combination with an automated standardised analysis script that allows rapid and detailed analysis of neurite outgrowth of the explants. Detection of neurites was achieved by immunostaining for β-tubulin, which labels neurites outgrowing from retinal explants (Gaublomme et al., 2013). The objective of this part was to assess neurite outgrowth after ROCK inhibition in combination with neurotrophic factors. But first, the presence and localisation of ROCK was demonstrated in the explants.

3.2.1.1 Localisation of ROCK

To identify the cellular localisation of ROCK2, explants after 3DIV were double stained with one of the following two ROCK2 antibodies, the rabbit polyclonal anti-ROCK2 antibody (Abcam, ab71598) or the rabbit monoclonal anti-ROCK2 antibody (Abcam, ab125025), in combination with either GFAP or β-tubulin. GFAP is a marker for macroglia, while β-tubulin is a marker for neurites.

The double staining of the polyclonal ROCK2 antibody and β-tubulin is shown in Figure 26 A. The orange color marks the locations where both ROCK2 and β-tubulin are present in the triple-stained (DAPI (blue), ROCK2 (green), β-tubulin (red)) explant in the lower right panel. All neurites were stained orange, which suggests ROCK2 expression in all neurites. However, not all ROCK2 expression was restricted to these neurites, suggesting that ROCK2 is also present in (the processes of) other cell types. More detailed pictures of the lower right panels of Figure 26 A, B, C and D are shown in the addendum as Figure 31. The double staining of monoclonal ROCK2 and β-tubulin is shown in Figure 26 B. The monoclonal anti-ROCK2 staining is more faint, compared to the polyclonal anti-ROCK2 staining. However, this monoclonal antibody is more specific for the ROCK2 protein, whereas the polyclonal ROCK2 antibody also has affinity for the ROCK1 protein to a certain extent. Nevertheless, the observations are similar to the ones in Figure 26 A. The double staining of polyclonal ROCK2 and GFAP is shown in Figure 26 C and of monoclonal ROCK2 and GFAP in Figure 26 D. For both antibodies, the orange staining suggests colocalisation of ROCK2 and GFAP, suggesting that ROCK2 is present in glial fibres. However, it is clear that ROCK2 signal is not only restricted to GFAP positive structures, since a clear ROCK2 signal is detectable in non-GFAP positive structures, which might be neurites in the lower right panel of Figure 26 C.

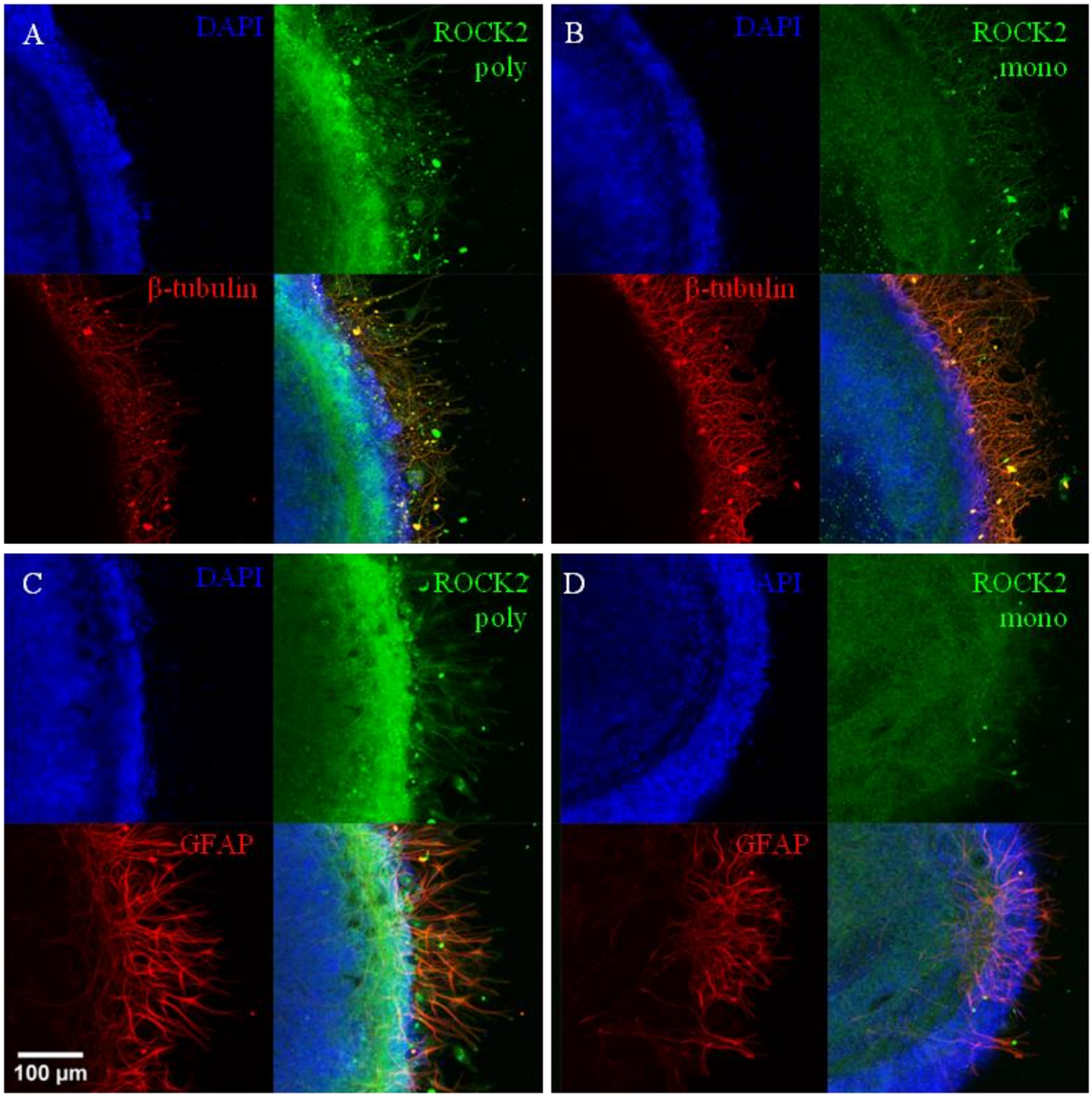

Figure 26: ROCK2, GFAP and β-tubulin ICC double staining on P3 explants. In pictures A, B, C and D, the upper left panel displays the blue channel (DAPI), the upper right panel displays the green channel (ROCK2), the lower left panel displays the red channel (β-tubulin or GFAP) and the lower right panel displays all three simultaneously.

3.2.1.2 Optimisation of the neurite outgrowth quantification method

Because the Axiovision software, used for an older Axiovision script, was outdated, there was a need for a new neurite outgrowth quantification method. Free Fiji software is consistently mentioned in literature, this software was used to write a new script, based on the previously used Axiovision script (Gaublomme et al., 2013). In the new Fiji automated script, oib files (Olympus image binary files) were used from pictures taken on a confocal microscope (FV1000 IX-82, Olympus). It was possible to take pictures in several resolutions, since this script extracts information from the oib file and scales the picture based on pixel size and resolution.

To start processing, the input picture (Figure 27 A) was converted into grays and the contrast was normalised. Then the blue channel, i.e. the explant body, was processed and converted to a binary (black and white) image (Figure 27 B). The edge was

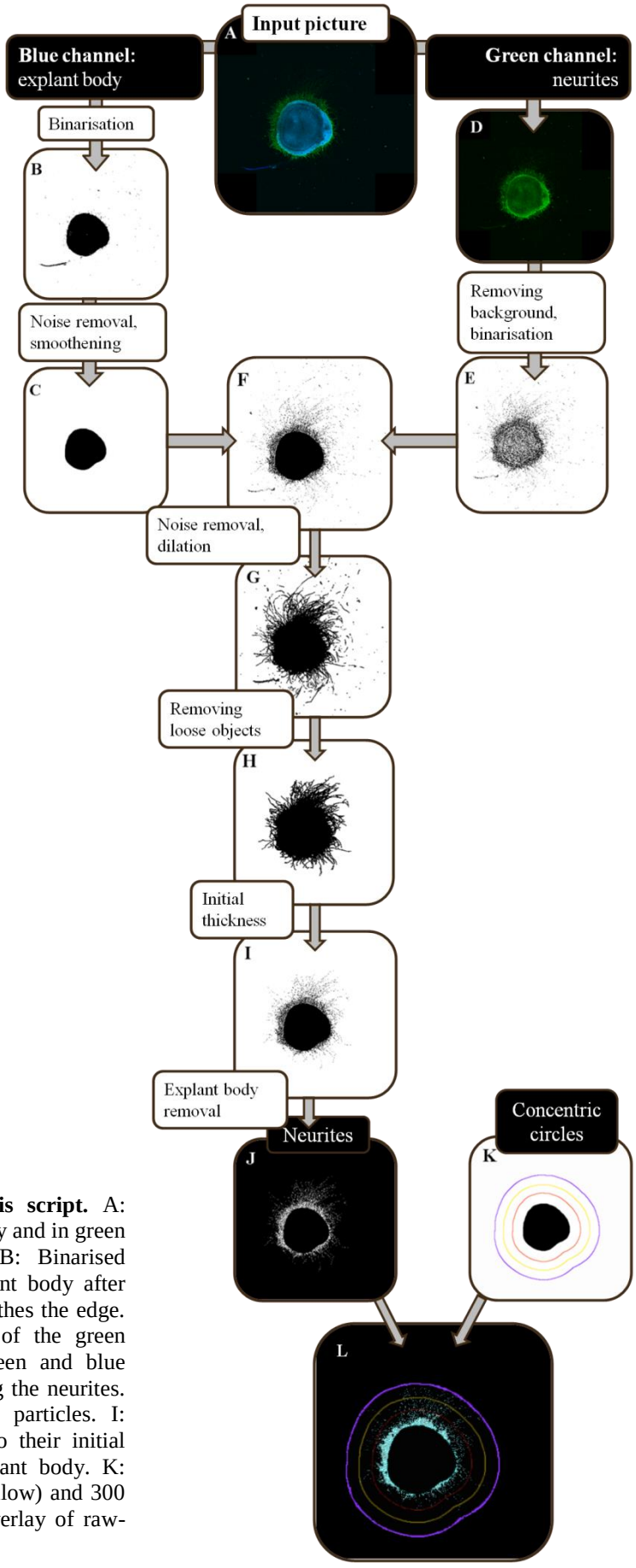

Figure 27: Steps in the Fiji P3 analysis script. A: Explant picture with in blue the explant body and in green the β-tubulin immunopositive neurites. B: Binarised picture of the blue channel. C: The explant body after processing, which removes noise and smoothes the edge. D: Green channel. E: Binarised picture of the green channel. F: Binarised pictures of the green and blue channels. G: Binarised picture after dilating the neurites. H: Dilated neurites without unconnected particles. I: Binarised picture with neurites returned to their initial thickness. J: Inverted image without explant body. K: Three concentric circles 100 (red), 200 (yellow) and 300 (purple) µm from the explant body. L: Overlay of raw-neurites (light blue) and concentric circles.

smoothed and small particles were removed, creating the explant body image (Figure 27 C). Next, the green channel (Figure 27 D), with the neurites, was processed. It was also binarised after removing the background by using the treshold tool (Figure 27 E). The explant body image from the previous step and the neurite image were merged, so explant body, neurites and some debris remained on the processed image (Figure 27 F), after which pixel noise was removed. Because neurites are thin and elongated structures, the more circular (circularity, a measure of how closely a shape of an object resembles that of a circle) particles were removed via the addition of a circularity restriction (circularity <0.8). Physiologically, neurites are always connected to the explant body and therefore, only objects connected to the explant body can be counted as neurites. However, staining or imaging imperfections can cause small gaps between two neurite pieces. To account for these artefacts, the next steps include dilating neurites to bridge small gaps (Figure 27 G), thereby only keeping only the items connected to the explant body (Figure 27 H) and returning the neurites to their initial thickness (Figure 27 I). Another restriction step of rather circular objects, mostly debris (circularity <0.6), was performed. Next, the explant body was substracted from the neurite image, keeping only the neurites and occasionally some debris (Figure 27 J). When too much debris was still visible, the user was able to remove the remaining debris manually, by erasing or encircling the debris with a pencil tool. Whether or not the image was edited, the resulting image was analysed as described below.

The explant area and perimeter were measured in Fiji. The neurite data was calculated by drawing 3 concentric circles, each 100 µm further from the explant body (Figure 27 K). The total neurite area (the INA) and the neurite area inside the 3 concentric circles (100 µm from explant body, 200 µm from explant body and 300 µm from explant body as shown in Figure 27 L) were also measured in Fiji. All neurite data was collected and further processed in excel and divided by the explant perimeter to correct for variation in explant size. Next, outliers from the neurite data were removed and mean and SEM were calculated per condition, as a % relative to control (100%) for INA and neurite area inside 0-100µm, 100-200µm, 200-300µm and >300µm from the explant body.

3.2.1.3 Validation of the neurite outgrowth quantification method with Fiji

Because differences exist between the Fiji script (for the processing of the confocal pictures of retinal explants) and the Axiovision script, we compared the functionality of the Fiji script to the Axiovision script. One set of P3 explant pictures was analysed with both Axiovision and Fiji script (Figure 28). Explants were grown for 3 days in predetermined conditions. In this experiment, two ROCK inhibitors were used, AMA0428 (AMA) and Y-39983 (Y3), with or without the combination of two neurotropic factors, BDNF and CNTF. Addition of none (control), one (AMA, Y3), two (BDNF/CNTF) or three (AMA + B/C, Y3 + B/C) compounds resulted in 6 conditions, of which neurite outgrowth area relative to the explant perimeter was

calculated. Since these results are very similar, this shows that the Fiji script is able to detect the neurite outgrowth as good as the Axiovision script. On top of that, the Fiji script resulted in a graph with 3 significantly different values from the control condition, in stead of one with the Axiovision script. This might suggest that better consistency in the Fiji script could lead to a lower variance and a higher statistical power.

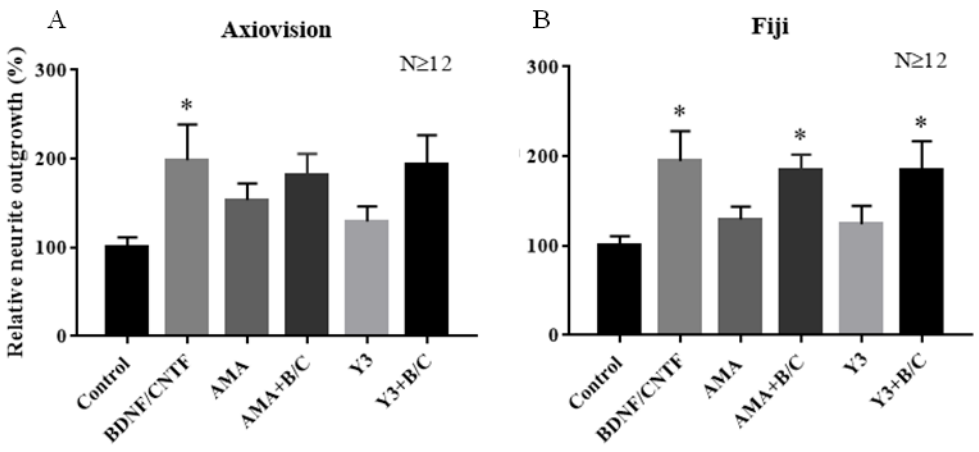

Figure 28: Immunodetected neurite outgrowth area relative to the perimeter. A: INA detected with the Axiovision script. B: INA detected with the Fiji script. Data are represented as percentage relative to neurite outgrowth in the control condition (100%) (mean ± SEM). N: the number of explants per condition. Conditions were compared to the control using a one-way ANOVA statistical analysis with a Tukey's test, *: $p<0.05$.

3.2.1.4 Screening the effects of neurotrophic factors, ROCK inhibitors and the combination of both on neurite outgrowth

Literature states that neurotrophic factors BDNF and CNTF promote axon regeneration (Benowitz & Yin, 2007; Logan et al., 2006). Accordingly, BDNF and CNTF were expected to promote neurite outgrowth in this P3 explant model. Since ROCK is implicated in neurodegeneration, investigating the effect of ROCK inhibitors on neuroprotection and axon regeneration could provide promising results (Van de Velde et al., 2015). The effect of the combinatorial treatment of BDNF and CNTF (B/C), as well as the effect of ROCK inhibitors, AMA and Y3, whether or not in combination with the neurotrophic factors, was investigated in detail. Firstly, the total immunodetected neurite area (INA) was analysed, secondly, the immunodetected neurite area in 4 segments from close to far from the explant body was measured.

The results of the Fiji analysis of explants under different conditions over 5 different, independent experiments are shown in Figure 29 and Figure 30. INA showed that B/C alone, and both ROCK inhibitors in combination with BDNF or B/C proved to have a striking positive effect on overall neurite outgrowth (Figure 29). The ROCK inhibitors alone also have a slightly positive effect on overall neurite outgrowth, yet this difference was not significant.

To get a closer look at different aspects of neurite outgrowth, the neurite outgrowth was assessed in different segments ranging from close (0-100µm) to further (>300µm) from the explant body. A high percentage of neurite outgrowth in the area close to the explant body indicated stimulation of neurite outgrowth initiation, while high neurite outgrowth in the area far away from the explant body was indicative for stimulation of neurite elongation.

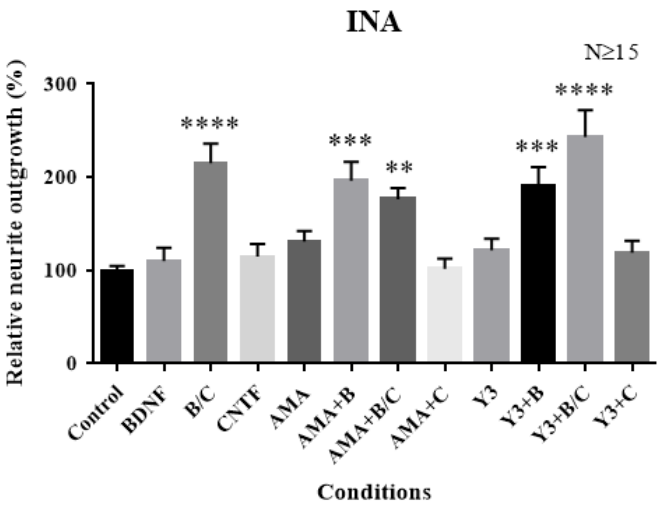

Figure 29: Immunodetected neurite outgrowth area in different conditions. A clear increase in neurite outgrowth in explants cultured in B/C, AMA+B, AMA+B/C, Y3+B and Y3+B/C was detected. Data are represented as percentage relative to neurite outgrowth in the control condition (100%) (mean ± SEM). N: the number of explants per condition. Conditions were compared to the control using a one-way ANOVA statistical analysis with a Tukey's test, *: $p<0.05$, **: $p<0.01$, ***: $p<0.001$, ****: $p<0.0001$.

In the 0-100µm segment, significantly more neurite outgrowth was observed in all conditions with the B/C combination, in AMA treatment with and without BDNF and in Y3 treatment with BDNF. Neurite outgrowth initiation (Figure 30 A) after 3DIV with the two neurotrophic factors combined was similar to the initiation after AMA and Y3 administration. However, if they were combined with both neurotrophic factors, or with BDNF alone, outgrowth was even higher. The difference in neurite outgrowth 0-100µm from the explant body was significant among Y3 treatment and Y3+B/C, yet, AMA+B/C did not differ significantly from AMA treatment alone, neither did B/C and AMA+B/C or B/C and Y3+B/C.

A significantly increased neurite outgrowth was observed after administration of B/C, AMA+B, Y3+B and Y3+B/C between 100 and 200µm from the explant body (Figure 30 B) and significant neurite elongation stimulation was shown in the segment 200-300µm (Figure 30 C) and >300µm (Figure 30 D) after culturing in B/C or Y3+B/C, with both treatments performing equally wel. The combinatorial treatment of BDNF and CNTF clearly stimulated axon elongation, yet ROCK inhibitors seemed to have a negative influence on the neurite elongation potential of these neurotrophic factors.

BDNF treatment, with or without ROCK inhibitor, generally promotes neurite outgrowth more than CNTF treatment, yet, we cannot compare both factors directly because they were added in two separate concentrations, 5ng/ml BDNF and 2ng/ml CNTF. However, an additional experiment was performed in which equal concentrations (5ng/ml) of BDNF and CNTF were tested and again, BDNF was identified as the strongest outgrowth promoter (data not shown). Additionally, the combination of both neurotrophic factors, especially during

elongation is even better. Strikingly, Y3 treatment with both neurotrophic factors had a very strong positive effect on both neurite outgrowth initiation and elongation compared to the control, while AMA treatment mainly seemed to promote neurite outgrowth initiation.

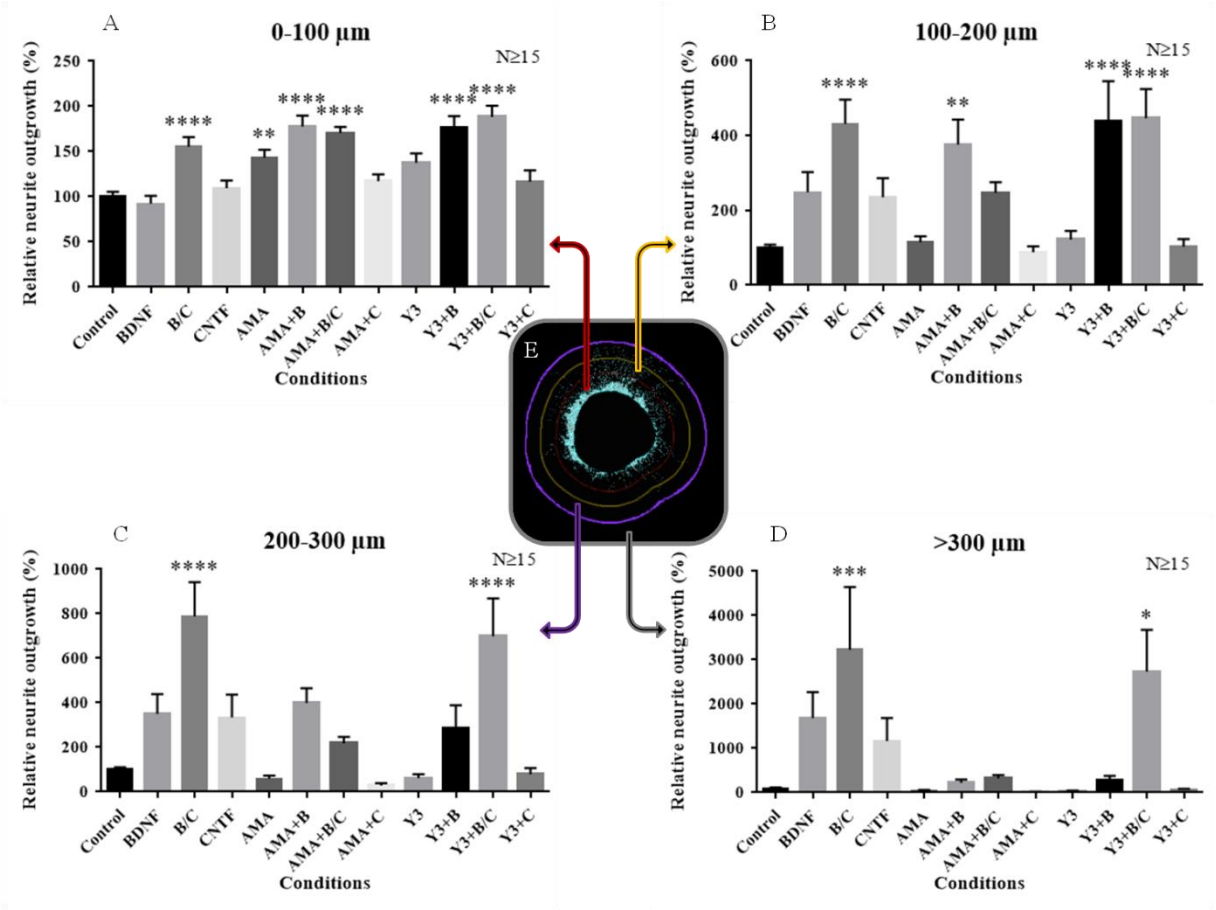

Figure 30: Immunodetected neurite outgrowth divided in segments 0-100µm, 100-200µm, 200-300µm and >300µm in different conditions. A: A clear increase in neurite outgrowth in explants cultured in B/C, AMA, AMA+B, AMA+B/C, Y3+B and Y3+B/C was detected in the 0-100µm segment. Neurite outgrowth initiation under B/C was similar to the initiation after AMA and Y3 administration. However, if they were combined with both neurotrophic factors, or with BDNF, outgrowth was even higher. B: A significantly increased neurite outgrowth was observer after administration of B/C, AMA+B, Y3+B and Y3+B/C between 100 and 200µm from the explant body. C and D: significant neurite elongation stimulation was shown in the segment 200-300µm and >300µm after culturing in B/C and Y3+B/C. E: Overlay of raw neurites and the three concentric circles used to calculate the four segments with arrows indicating which segment is used to calculate the values in the corresponding graph. Data are represented as percentage relative to neurite outgrowth in the control condition (100%) (mean ± SEM). N: the number of explants per condition. Conditions were compared to the control using a one-way ANOVA statistical analysis with a Tukey's test, *: $p<0.05$, **: $p<0.01$, ***: $p<0.001$, ****: $p<0.0001$.

4 Discussion

Because more and more people are at risk of developing neurodegenerative (eye)diseases as a consequence of the increased life expectancy and because current treatments fail to stop or reverse neurodegeneration, the development of novel therapies, including neuroprotective and axon regenerative therapies is urgent and highly desirable (Beal et al., 2005). Recently, the selective inhibition of Rho-associated coiled-coil kinase (ROCK) was put forward as a very promising approach for the treatment of glaucoma, diabetic retinopathy and other neurodegenerative diseases, holding potential to promote neuroprotection, axonal regeneration and to suppress glial reactivity in future therapies (Arita et al., 2009; Koch et al., 2014a; Van de Velde et al., 2015). ROCK is a crucial regulator of the cytoskeleton and cell polarity and has two isoforms, ROCK2 and ROCK1 (Amano et al., 2010). Because the exact working mechanism of ROCK signalling and the differential regulation of its two isoforms remains elusive in the healthy and pathological retina, the main objective of this thesis was to unravel the underlying cellular mechanism of ROCK in the healthy and pathological retina. Therefore, three models were employed, two to study neuroprotection and one to study axon regeneration. First, in an *in vitro* model of porcine primary retinal cells, expression levels for ROCK2 and ROCK1 were determined in a healthy *versus* pathological state. Stress-related processes, as those occurring in the pathological retina, were mimicked *in vitro* by inducing stress in these cells. Next, an *ex vivo* porcine retinal explant model that mimics neurodegeneration was developed and optimised. Both *in vitro* and *ex vivo* models will be used for future study of neuroprotective capacities of ROCK inhibitory compounds. Secondly, in an *ex vivo* postnatal mouse retinal explant model, the localisation of ROCK2 in Müller glia and neurites was determined and the axon regenerative capacities of neurotrophins, ROCK inhibition and the combination of both were investigated.

4.1 Neuroprotection

To elucidate how ROCK signalling affects neuronal apoptosis, *in vitro* porcine retinal cell models and an *ex vivo* porcine retinal explant model were optimised and validated.

4.1.1 *In vitro* retinal cell models

In vitro cell models have been widely used as low cost screening methods for a variety of compounds in different biomedical research domains such as oncology, toxicology and neurology (Katt et al., 2016; Lesuisse & Martin, 2002). With this approach, cells can be cultured in large quantities at a relatively low cost and they, as well as their environment, can by easily manipulated. At the same time the use of culturing techniques reduces the amounts of laboratory animals needed for drug screening. Moreover, the porcine eyes used in these experiments yield more retinal tissue, and thus cells, than smaller rodent eyes for example. The eyes were collected from a slaughterhouse and as a consequence, the use of laboratory animals in this thesis is even further reduced, thereby diminishing the ethical concerns.

Besides RGCs, also other retinal cell types and their interactions with RGCs are assumed to play a crucial role in the neurodegenerative pathology. There is accumulating evidence suggesting that the increase in reactivity of microglia, astrocytes and Müller glia is a key process in neurodegenerative diseases and that those cell types participate in the induction of neuronal cell death (Barker & Cicchetti, 2014; Bosco et al., 2011; Bringmann et al., 2009a). Moreover, glial cells, i.e. macro- and microglial cells, have a dual role in neurodegeneration; they can both confer detrimental as well as a protective effects on neuronal survival or functioning (Bringmann et al., 2006; Vecino et al., 2015). It is crucial to understand the precise role of micro- and macroglia in neurodegeneration and therefore, the exploration and culturing of these cells is well suited to deepen our understanding in this field (Matteucci et al., 2015).

4.1.1.1 Validation of cell culture purity and stress induction

Porcine Müller glia were mechanically isolated and cell culture purity was assessed by glutamine synthetase (GS) after two weeks in culture as in Song et al. (2013). The >95% purity of the Müller glia culture was considered sufficient to obtain valid results for this cell population.

In the next step of Müller glia culture experiments, stressors were administered to the culture to mimic the pathological retina. In literature, several methods were used to induce cytotoxic stress, such as administration of compounds that induce excitotoxic stress, oxidative stress or hyperglycemia or such as the incubation of the cells in a hypoxic environment to induce oxidative stress (Challenor et al., 2015; Devi et al., 2012; Tan et al., 2015). Growing evidence indicates that glutamate excitotoxicity and/or oxidative stress is associated with mitochondrial DNA (mtDNA) damage-related mitochondrial dysfunction in retinal neurodegenerative diseases, including glaucoma (Lee et al., 2012). Furthermore, hyperglycemia is a major factor in the pathology of DR, which activates several metabolic pathways mediating oxidative stress and can induce glucotoxicity. For those reasons, excitotoxic-, oxidative stress and hyperglycemia were induced in the experiments of this thesis. Müller glia were exposed to relatively high concentrations of 5, 10 or 20mM glutamate for 6 hours *in vitro* (HIV) or 24HIV to ensure a sustained induction of excitotoxic stress, because these cells have the ability to rapidly clear extracellular glutamate (Bergles et al., 1999). In neuronal cultures, excitoxicity is usually induced with lower glutamate concentrations (200µM or 250µM) (Caprioli et al., 1996; Januschowski et al., 2015), but, due to the clearance capacity of Müller glia, a stress induction method with relatively high glutamate concentrations was adapted from Challenor et al. (2015) (inducing excitotoxicity with 5mM glutamate at 6HIV, 24HIV and 48HIV on dissociated cell cultures, which included Müller glia). Müller glia were also exposed to 100µM $CoCl_2.6H_2O$ or H_2O_2 for 6HIV or 24HIV to induce oxidative stress, based on oxidative stress induction with 100µM $CoCl_2.6H_2O$ on A 127 cells by Kesherwani et al.

(2014) and with 200µM H_2O_2 on Müller glia by Wang et al. (2015). Furthermore, Müller glia were exposed to 30mM glucose for 24HIV similar to hyperglycemia induction protocols in Müller glia established by Devi et al. (2012) and Ola (2014), while Jiang et al. (2013) used only 25mM glucose, yet Mysona et al. (2009) used 35mM glucose.

Although we applied concentrations of stressors as used in literature to induce glial reactivity of Müller glia, we aimed to confirm this stress induction in these cells by investigating vimentin, which is a marker for reactive gliosis and is specific to Müller glia (Bringmann et al., 2009a; Johansson et al., 2010; Lewis & Fisher, 2003). ICC analysis of vimentin (Figure 13) indicated successful excitotoxic stress induction with glutamate. WB analysis (Figure 14), showed slightly higher vimentin expression after glutamate induction, but could not unequivocally confirm the ICC observation. ICC analysis demonstrated increased vimentin expression with both $CoCl_2$ and H_2O_2 as oxidative stressors. WB analysis confirmed stress induction upon $CoCl_2$ treatment, whereas this was not the case after H_2O_2 treatment. It is possible that the ICC was more sensitive compared to the WB and/or that H_2O_2 treatment induces less stress because of quick H_2O_2 evaporation and decomposition when exposed to light, which is why media need to be refreshed very frequently (Cooper et al., 2007). Moreover, the original H_2O_2 concentration might have been too low, since Wang et al. (2015) used a concentration of 200µM to induce stress in Müller glia, in stead of 100µM. Another direct oxidative stressor that could have been usefull for similar experiments is tert-butyl hydroperoxide, which is frequently used to induce oxidative stress and believed to be more stable in culture than H_2O_2 (Slamenova et al., 2013). A preliminary WB analysis of Müller glia, subjected to high glucose conditions, did not reveal an increase in vimentin expression. More samples/experiments are needed to confirm these data. To further explore the stress response, another marker that is more sensitive to stress could be useful. Next to vimentin, GFAP is most frequently used as a glial reactivity marker, which also labels astrocytes, and is now being tested on our porcine Müller glia samples for ICC and WB (Lewis & Fisher, 2003). One of the first histologic changes in DR is overexpression of GFAP and furthermore, GFAP is the most sensitive non-specific response after retinal injury (Bringmann et al., 2009a; Matteucci et al., 2015).

Also microglia are present in the initial passages of Müller glia cultures. They are non-adherent cells that form loose connections to the adherent Müller glia and need these macroglia to grow. It is sufficient to tap the culturing flask in order to destroy the loose connections, in order to isolate the microglia. Supernatant containing microglia was collected and cells were obtained for seeding by centrifugation. The seeded microglia cultures showed around 80% overlap with DAPI nuclei and Iba-1 staining, which is a less compared to Iba-1 stained cultures in literature, which showed a 94% microglia culture purity (Klettner et al., 2014). The presence of RGCs and Müller glia (around 10%) in microglia cultures was

eliminated by screening the DAPI staining for larger nuclei. Indeed, pictures of both microglia cultures and Müller glia cultures on the same scale revealed larger DAPI positive nuclei for Müller glia compared to microglia, and accordingly RGCs have bigger nuclei (Figure 12). To identify the presence of other cell types in these cultures and the size of their nuclei, double stainings could be performed with specific markers for those cells, such as astrocytes, epithelial cells, pericytes or endothelial cells. The microglia culture with at least >80% cell culture purity was sufficient to obtain valid results concerning these cultures.

4.1.1.2 Detailed study of ROCK2 and ROCK1 expression in healthy and pathological retinal cell cultures

The Rho-ROCK pathway has already been suggested in literature to be an important target in retinal neurodegenerative diseases (Arita et al., 2009; Van de Velde et al., 2015; Wang & Chang, 2014). To mimic the pathological retina *in vitro*, various stress inducers were used. Increased vimentin expression already indicated stress in the Müller glia after induction of excitotoxic and oxidative stress. ROCK2 and ROCK1 expression in the cells of the CNS and the importance of the retinal cell types in the Rho-ROCK pathway are poorly described in literature and therefore, a detailed study of ROCK2 and ROCK1 expression changes in healthy and stressed cells was necessary. This is why the cellular expression of ROCK2 and ROCK1 was examined in healthy retinal cells and cells subjected to stressors, which serve as a model for the pathological retina. There was a clear ROCK2 and ROCK1 expression observed in healthy Müller glia. The very faint WB bands for ROCK expression in microglia were less clear when compared to the more pronounced and clear bands of cell lysates of healthy Müller glia. Therefore, we focused on Müller glia for this project.

Both ROCK2 and ROCK1 expression was elevated most prominently with excitotoxicity induction. At 6HIV, ROCK2 expression peaked with 5mM glutamate and dropped to control levels with 10 and 20mM glutamate. At 24HIV, the ROCK2 expression was elevated with 5mM, peaked with 10mM and dropped to control levels with 20mM. The ROCK elevation at 24HIV with 10mM was quite similar to the 6HIV 5mM condition. The aforementioned pattern could be explained by the following hypothesis: ROCK2 expression rises after sufficient stress induction with 5mM at 6HIV. After 24HIV, Müller glia deplete the medium from glutamate, taking up and degrading glutamate in physiological conditions, and subsequently this leads to a weaker effect on ROCK2 signalling (Bringmann et al., 2013; Ishikawa, 2013). Continuing this hypothesis: a higher concentration of glutamate (10mM) leads to a more prolonged stress induction (24HIV), as indicated by the ROCK2 expression results. Glutamate excess is rather toxic or too much stress induction suppresses ROCK expression, since ROCK2 levels at 20mM were not consistently elevated.

At both 6 and 24HIV, ROCK1 expression peaked with 5mM, was still elevated compared to control, but slightly decreased with 10mM and decreased even further with 20 mM. Based on these data, we hypothesise that addition of 5mM is the right concentration to induce ROCK1 expression, since 10mM and 20mM concentrations are too high, and they elicit the maximal ROCK1 stress response. Subsequently, ROCK2 and ROCK1 expression is clearly induced after glutamate stress, although in a slightly different way, indicating a strict regulation of both isoforms during excitotoxicity. Overall, a dose-dependent ROCK2 and ROCK1 upregulation in response to glutamate was observed, without upregulation after too high doses. Obviously, it is not an on/off response, because also intermediate expression levels were seen.

Significant Müller glia cell death was only observed at 48HIV with 5mM in the paper from Challenor et al. (2015) and not at 6 and 24HIV. Viabililty was explored using the dual-fluorescence cell viability assay with ethidium homodimer and calcein-AM. Toxicity after longer glutamate incubation also suggests toxicity after incubation with higher glutamate concentrations, which might explain the decrease in ROCK upregulation with high glutamate concentrations. Viability could be explored in these experiments by using the same assay, employing a lactate dehydrogenase assay or by the use of trypan blue, as in Caprioli et al. (1996), in which the blue pigment can only penetrate the permeable membrane of dead cells. In literature, an increased ROCK2 and ROCK1 at both the mRNA and protein level was observed in rat retinal explants treated with 5mM glutamate, yet this was not demonstrated for the different cell types (Huang et al., 2012). Our findings are complementary to this data, showing increased ROCK2 and ROCK1 protein expression in Müller glia cultures.

ROCK expression in Müller glia subjected to oxidative stress showed contradictory results. No upregulation was observed after H_2O_2 addition for both isoforms. On the other hand, the small increase of both isoforms at 6HIV upon $CoCl_2$ induction indicated a possible role of ROCK2 and ROCK1 in the retina after oxidative stress. However, no elevated ROCK2 and ROCK1 protein expression was observed at 24HIV, which again could indicate that increased ROCK expression is an early response after stress, or that the product is decomposed, leaving too little $CoCl_2$ in the medium to exert a response. Based on this result, induction of 100µM $CoCl_2$ confirms being a good stressor, in accordance with (Kesherwani et al., 2014). Apoptosis, as a result of excessive stressor concentration can be verified via a viability assay. Based on the lack of increased vimentin expression from WB data, but increased expression via ICC, one could assume that the concentration of H_2O_2 was too low to elicit a maximal stress response in Müller glia. This was possibly due to some of the reasons mentioned earlier (paragraph 4.1.1.1). In future experiments, the H_2O_2 concentration could be increased and the medium could be refreshed more frequently. There might be slight differences in oxidative stress responses due to the way of inducing oxidative stress in these cultures, since $CoCl_2$ as

chemical inducer of hypoxia-like reponses indirectly evokes oxidative stress, while H_2O_2 as one of the reactive oxygen species itself evokes oxidative stress directly (Lopez-Sanchez et al., 2014).

After hyperglycemia, both ROCK2 and ROCK1 expression was elevated after 24HIV, although not significantly. However, 24HIV is the time point and 30 mM is the concentration that is most commonly used in literature to apply hyperglycemia. Since no glial reactivity was demonstrated at this specific time point and concentration, additional WB and ICC analyses for GFAP could clarify this and different time points (for example 6HIV, comparable to excitotoxicity and oxidative stress induction time points) and other concentrations could be tested.

Overall, oxidative stress, excitotoxicity and hyperglycemic stess conditions demonstrated a clear and early response of ROCK upregulation in Müller glia, with a differential expression pattern of ROCK2 and ROCK1. Still, more experiments are needed to complement these data. Although monoclonal Abs were used it would be recommended to perform a real time PCR (RT-PCR) analysis in the near future, on one hand to confirm the data and on the other hand to investigate the specificity for the two isoforms as there is a very high similarity in amino acid sequences between ROCK2 and ROCK1. However, a differential ROCK2 and ROCK1 expression pattern was already demonstrated in this thesis, suggestive for a certain level of specificity of the Abs.

4.1.2 Optimization of an *ex vivo* adult porcine explant model

An *ex vivo* adult porcine explant as a model for neurodegeneration was introduced very recently in the host lab. Retinal explants or organotypic cultures are punches of the retina that are brought in culture. Such *ex vivo* approaches have the major advantage over *in vitro* studies that cell-cell interactions and the extracellular matrix remain intact, notwithstanding that it is less complex and less expensive compared to *in vivo* studies and the use is more ethically relevant since a smaller number of laboratory animals is needed. Additionally, the environment can be controlled in a more standardised way and explants are easier to manipulate compared to an *in vivo* situation (Bull et al., 2011; Katt et al., 2016).

This model is applied to closely mimic the *in vivo* situation in a pathological neurodegenerative retina, with the aim of studying neuroprotection at a later stage. Since the hallmarks of a neurodegenerative retina are mainly slow and progressive apoptosis of the RGCs, together with activation of micro- and macroglia, we aimed for these characteristics in our neurodegenerative model. Therefore, porcine explants were cultured according to Taylor et al. (2013) with slight modifications. Culturing the porcine explants with the ganglion cell layer (GCL) facing an insert membrane ensures proper support of the inner retina, while

neurodegeneration progresses more slowly and gradual in comparison to floating cultures or cultures with the photoreceptor layer facing down, as has been described in literature (Ghosh et al., 2016; Taylor et al., 2014). Moreover, culturing an explant that is not submerged in medium (in contrary to the postnatal mouse explant), but resides on an insert, results in both good gas exchange and absorbance of nutrients (Winkler et al., 2002). The explants were dissected by the use of a punch needle with a standard diameter and always punched out of the central part of the visual streak of the porcine retina to standardise size and RGC density. This part is the area of highest visual acuity, which is homologous to the human fovea. In contrast to Taylor et al. (2013), the explant dissection was not random and into irregular parts, but similar to the technique used by Osborne et al. (2016), who also punched circular explants using on equidistant location from the macula in the human retina.

4.1.2.1 Neuronal cell survival is decreased with time during culturing

To study neuron/RGC survival in the RGCs in this model, different neuron or RGC markers were used. NeuN is specifically expressed in post-mitotic mature neurons and the Ab primarily stains the neuronal nuclei. However, the cytoplasm can also be more faintly stained. According to Johansson et al. (2010), it is a good RGC marker for the porcine retina, therby strongly labelling RGCs, but also weakly labelling displaced amacrine cells in the GCL. In rats, NeuN is considered an ideal marker to visualise RGCs (Bull et al., 2011). IHC of NeuN showed clear and strong immunopositive staining only in the GCL, while also non-stained DAPI nuclei were present in the GCL, which could be astrocytes and/or displaced amacrine cells. Both IHC cell counting and WB analysis revealed a clear decrease in the amount of RGCs with time, with a faster decrease in NeuN expression in the WB analysis (Figure 22). Examining the IHC NeuN pictures showed a lot of strongly labelled RGCs in the control, but progressively less and more weakly labelled RGCs were observed with time, up to 1 week in culture. The decreased cell number was most pronounced at 1DIV, a plateau at 3 and 5DIV and more pronounced again at 7DIV (Figure 22). This is consistent with a literature report, showing a similar result in NeuN-stained cells in the GCL of rats, with a strong cell number decrease at 1DIV, a plateau at 2, 3 and 4DIV and a slightly stronger reduction again at 5, 6 and 7DIV (Bull et al., 2011). Furthermore, our experiments confirmed that NeuN IHC analysis was an ideal tool to determine RGC survival (Bull et al., 2011). According to Lavezzi et al. (2013), NeuN immunoreactivity diminishes in degenerating mature neurons and the expression is decreasing before apoptosis, making NeuN a good marker to monitor neuropathogenesis, since it can reflect an early phase of degeneration (Lavezzi et al., 2013). The reduction in the amount of NeuN positive RGCs (Figure 22 B) as well as the loss of NeuN intensity (Figure 22 C), could clarify the rapid decline in NeuN expression in the WB analysis (Figure 22 A), meaning that WB did not provide a clear reflection of the amount of RGCs left after the indicated days in culture. However, NeuN still remains a very powerful indicator for the pathological state of neurons.

Another specific and trustworthy RGC marker that does not label amacrine cells in the GCL in the rodent retina is β-tubulin, which is claimed to be unaffected by injury (Cui et al., 2003; Jiang et al., 2015). Contradicting reports point out that β-tubulin can cross react with ligands expressed on amacrine cells (Mead et al., 2014; Sharma & Netland, 2007). However, this cross reactivity with amacrine cells was less apparent in the human retina, suggesting that β-tubulin is in fact a specific marker for porcine RGCs (Osborne et al., 2016). WB analysis also showed a clear decrease of β-tubulin with time, but this decrease was less pronounced as compared to the NeuN WB analysis (Figure 23). Strikingly, the β-tubulin WB analysis and the NeuN IHC analysis revealed a very similar pattern, together confirming the slow and progressive decrease in RGC number with both markers, most prominently at 1DIV and 7DIV, with a 40% decline of β-tubulin signal and a 60% decreased amount of NeuN positive cells after one week in culture. Confirmation of this WB analysis with β-tubulin IHC analysis was not yet possible because the β-tubulin antiboly also labels the RGC processes on sections for IHC. Constistent with literature, this disorganised staining pattern was not quantified for RGC somata (Bull et al., 2011). However, in the GCL, Smedowski et al. (2014) counted β-tubulin positive somata successfully. In contrast to our approach, they only counted RGCs at the periphery, wheras we analysed RGCs in the central part of the retina. They claimed that axons in the periphery are thinner, and therefore, RGC cell bodies are better visible (personal communication). Furthermore, it is regularly reported that β-tubulin IHC stainings are performed on wholemount explants, counting the RGC somata as small dots on the wholemount (Mead et al., 2014; Osborne et al., 2016).

Brn3a is a widely used marker, while RNA-binding protein with multiple splicing (RBPMS) is a more recent marker for specific RGC labelling *in vivo* (Kwong et al., 2011; Mead et al., 2014). Yet, their reliability for *ex vivo* culturing is not well documented and previous in-house experiments suggested diminished expression of both markers as a result of *ex vivo* culturing.

Additionally, in a next approach, it would also be very informative to stain for cell death markers to confirm apoptosis and to verify whether or not RGC death is complementary to RGC survival in the GCL. According to Adamiec-Mroczek et al. (2015), RGC apoptosis mainly occurs secondary to caspase-dependent pathways. Besides caspase-3 stainings, indicative of caspase-dependent apoptosis, the terminal deoxynucleotidyl transferase dUTP nick-end (TUNEL) labeling method has already been tested in the porcine explant model by Taylor et al. (2014) and can be used to detect DNA fragmentation during the late phase of apoptosis (Kyrylkova et al., 2012).

4.1.2.2 Glial reactivity is increased with time during culturing

Next, glial reactivity was assessed by investigating GFAP and vimentin expression. Upregulation of these intermediate filaments is frequently used as hallmark for glial reactivity induced by disease or injury (Bringmann et al., 2009a; Ghosh et al., 2007). GFAP is an early

marker of gliosis and is strongly upregulated in activated astrocytes, but also in activated Müller glia of the porcine retina (Johansson et al., 2010; Taylor et al., 2014). In our data, an increased glial reactivity with time in culture was clearly visible, which is also observed in rat and porcine retinal explants (Bull et al., 2011; Winkler et al., 2002). However, they contradict the attenuation of GFAP expression at 10DIV as compared to 0DIV in porcine explants with inner retinal support, as reported by Taylor et al. (2014). WB analysis showed initially augmenting GFAP levels, yet they plateaud at 5 and 7DIV (Figure 24 A). GFAP IHC staining in the control also demonstrated GFAP expression mainly in the Müller glia endfeet and astrocytes (in the NFL and GCL) and also less pronounced in the radial glia (Müller glia) (in the INL, IPL and ONL). Furthermore, the GFAP intensity increased with time, especially in the radial glia, and to a lesser extent in the Müller glia endfeet and astrocytes (Figure 24 E). GFAP intensity of the different layers was analysed, to look at the glial fibres in the INL, IPL and ONL and to look at astocytes and Müller glia endfeet in the GCL and NFL. Intensity in the radial glia continued to rise, while intensity in astocytes and endfeet at first increased (until 3DIV), but then decreased (Figure 24 C and D). Possibly, this drop in intensity can be attributed to downregulation of GFAP in chronically stressed astrocytes, a phenomenon that was also described in the hippocampus by Araya-Callis et al. (2012), and might be compensated by the increasing GFAP intensity in radial fibres, resulting in the observed plateau of total explant GFAP expression in the WB analysis at 5 and 7DIV.

Vimentin is specific for Müller glia, in contrast to GFAP, and is upregulated in stress conditions (Ghosh & Arner, 2010). WB analysis displayed a very clear and gradual upregulation of vimentin over time (Figure 24 B). The rise in vimentin expression indicates increasing Müller glia reactivity, which confirms the progressively increasing Müller glia reactivity in glial fibres in the earlier mentioned GFAP analysis. This vimentin and GFAP augmentation was also confirmed in the porcine explants used by Winkler et al. (2002).

4.1.2.3 Morphological changes in laminar architecture and retinal thinning

The H&E morphological staining is used to investigate retinal morphology, laminar architecture and retinal thickness of the porcine retinal explants during their time in culture. It revealed thinning of the total explant thickness over time, while in different retinal layers, thinning was mostly confined to the ganglion cell complex (GCC), slight thinning occurred in the INL, while there was no apparent thinning in the ONL (Figure 25). The latter is in contrast to the ONL of a rat retinal explant, which does show retinal thinning (Bull et al., 2011). Moreover, our data showed that there was a preservation of the general retinal laminar organisation, with a slow disturbance of the laminar architecture in GCC after longer durations *ex vivo* (Figure 25 C). Explants with similar inner retinal support in the study of Taylor et al. (2014) maintained their laminar architecture up to 10DIV and showed only slight thinning at that time point.

Overall, the porcine retinal explant model showed a significant decrease in neuronal/RGC cell survival in the GCL and an increase in glial reactivity, mainly in Müller glia, after one week in culture. Moreover, retinal laminar organisation was generally maintained, underpinning the applicability of this model in neuroprotective research, possibly in parallel with *in vivo* studies. It can be used to monitor the effects of several compounds or inhibitors on RGC degeneration, glial reactivity and morphology and to examine whether or not injured RGCs can be rescued from apoptosis. This model now allows us to assess the neuroprotective potential of ROCK inhibitors.

4.2 Axonal regeneration

CNS neurons lose their axon regenerative potential early in development, which is why regeneration of injured axons in the CNS remains impossible (Benowitz & Yin, 2008; Bosse, 2012; Huebner & Strittmatter, 2009). As a result, reliable and validated models are necessary to screen regeneration-promoting agents, such as neurotrophic factors and ROCK inhibitors. Since retinal explants are commonly used to study axonal regeneration (Bull et al., 2011; Buyens et al., 2014) and because of more effective neuronal axon regeneration in a younger mammalian retina, compared to an adult retina (Benowitz & Yin, 2007), the postnatal mouse retinal explant model was used to unravel the role of ROCK inhibition in axon regeneration.

4.2.1 Localisation of ROCK

To identify the cellular localisation of ROCK2, double stainings were performed with GFAP, as a marker for glial fibres, or with β-tubulin, which preferably stains RGC neurites (Figure 26). ROCK2 staining with the monoclonal anti-ROCK2 antibody (Abcam, ab125025), which is claimed to be specific for ROCK2 and does not recognise ROCK1, was overall faint. This is why stainings with the rabbit polyclonal anti-ROCK2 antibody (Abcam, ab71598) were also performed, an antibody that poved its usefulness in IHC on retinal sections after optic nerve crush. Both Abs showed cellular localisation of ROCK2 in both glial fibres and neurites. This confirms the ROCK2 expression found in Müller glia in the *in vitro* part of this thesis, which is very interesting, because information about the cellular expression of ROCK2 and ROCK1 is lacking in literature. Furthermore, the localisation of ROCK2 in neurons was documented in literature (Koch et al., 2014a), which was confirmed in our experiments more specifically ROCK2 was also present in neurites. Even more, the localisation of ROCK2 was confirmed *in vivo*, via IHC procedures for ROCK2 on mouse retinal sections after optic nerve crush. These IHCs demonstrated ROCK2 expression in the NFL, where RGC axons are located and also in Müller glia in both the healthy and stressed (after optic nerve crush) state.

4.2.2 Optimisation of the neurite outgrowth quantification method

The β-tubulin neurite staining on postnatal day 3 (P3) retinal explants was analysed with a new Fiji-software based in-house script written with some modifications compared to the outdated Axiovision-software based script according to Gaublomme et al. (2013). Unlike the Axiovision script, the Fiji script uses scaled filters with a variable amount of pixels, based on image resolution, which makes processing of images of different size and resolution possible, contrasting to the filters of a fixed amount of pixels in the Axiovision script. Also, the picture is binarised using global Fiji thresholding tool after subtraction of the background, instead of using local thresholding. A third difference is that the Fiji script includes the definition of neurites as objects (nearly) connected to the explant body, which is why loose objects were removed, while this was not the case in the Axiovision script. From a biological perspective, neurites are objects connected to the explant body, as they will always grow from the explant body. However, numerous small gaps can arise due to the fixation, staining and imaging procedures. This is why the bridging step (by inflating the explants) is required and this provided very good results (Figure 27 G, H and I).

Because the Fiji script does not completely function the same way the Axiovision script does, there was still a need to validate the functionality of the Fiji script and compare it to the Axiovision script from Gaublomme et al. (2013) prior to general use. Comparison of the two scripts in Figure 28 showed very high similarity in data analysis, with even more significancy in the new script, which might suggest that better consistency in the Fiji script could lead to a lower variance and a higher statistical power.

4.2.3 Screening the effects of neurotrophic factors, ROCK inhibitors and the combination of both on neurite outgrowth

To screen the neuroregenerative capacity of ROCK inhibitors, whether or not in combination with neurotrophic factors, the P3 explant model was used and the Fiji script was used to analyse the explants. The neurotrophins were administered to postnatal mouse retinal explants during culturing and neurite outgrowth was compared to control conditions. The ROCK inhibitors AMA0428 (AMA) and Y-39983 (Y3) were chosen because AMA is a novel and potent ROCK inhibitor (Hollanders et al., 2015; Van de Velde et al., 2015), while Y3 is a commercially available ROCK inhibitor and is proven to be more potent than Y-27632 (Y2) (Hove et al., 2015; Sagawa et al., 2007; Van de Velde et al., 2015). Several neurotrophic factors were proven to stimulate both axon outgrowth initiation and elongation in several *in vitro* and *ex vivo* settings (Buyens et al., 2014; Johnson et al., 2011; Van de Velde et al., 2015).

In terms of neurite outgrowth initiation, both ROCK inhibitors performed better compared to the control (Figure 30 A and B), in agreement with the literature, in which Y3 is also a neurite outgrowth initiator (Van de Velde et al., 2015). This effect was even more profound in

combination with the growth factors. In more detail, the ROCK inhibitors, supplemented with BDNF or the combination of BDNF and CNTF exerted a synergistic effect on neurite outgrowth initiation. Interestingly, this effect was even stronger than the combination of BDNF and CNTF without ROCK inhibitors. On the contrary, supplementation of ROCK inhibitors with solely CNTF worked rather antagonistically on the initiation of neurite outgrowth. These findings contradicted Lingor et al. (2008), claiming the synergistic effect of CNTF and ROCK inhibitors in *in vitro* and *in vivo* studies, yet Y2 was used in these experiments. However, ROCK inhibitors alone did not promote axon elongation (Figure 30 C and D). Moreover, neurotrophic factors alone did induce neurite elongation, however, this effect was diminished when combined with ROCK inhibitors, this time confirming the data reported by Lingor et al. (2008). Administration of growth factors (in combination with ROCK inhibitors), especially the combination of BDNF and CNTF, evoked prominent elongation. However, CNTF in combination with the ROCK inhibitors had weaker effects on elongation than CNTF alone and BDNF or BDNF+CNTF in combination with ROCK inhibitors. Furthermore, the neurite outgrowth and elongation potential was more pronounced upon Y3 treatment, compared to AMA treatment, demonstrating overall stronger neuroregenerative capacities of Y3. This study indicates that ROCK inhibition (in combination with both neurotrophic factors) can clearly support the inial stage of axon regeneration, while ROCK inhibitors have a negative influence on the neurite elongation potential of the neurotrophic factors.

5 Conclusion and future perspectives

Up till now, a combination of complementary *in vitro*, *ex vivo* and *in vivo* studies have been performed to identify ROCK as a negative regulator of neurite outgrowth, axon guidance and neuronal survival. Furthermore, accumulating evidence indicates distinct responses of ROCK2 and ROCK1 in the cells of the CNS and in neurodegenerative processes. However, ROCK expression studies of these isoforms in the retina and in the different retinal cell types are lacking. To unravel the cellular sources of both ROCK isoforms and their response to cytotoxic stress, a hallmark in many ocular pathologies, expression and inhibition studies were performed in models of the healthy and/or pathological retina, using both *in vitro* and *ex vivo* approaches.

In vitro retinal cell cultures revealed more pronounced expression levels of ROCK2 in healthy and stressed porcine Müller glia as compared to its expression levels in microglia. Overall, in Müller glia, oxidative stress, excitotoxicity and hyperglycemic stess conditions demonstrated a clear and early response: ROCK2 and ROCK1 upregulation. After induction of excitotoxic stress, a dose dependent ROCK2 and ROCK1 upregulation was observed with clear differences in expression pattern of both isoforms, yet no upregulation after high doses was observed. This suggests the different stress sensitivity of ROCK2 and ROCK1 in modulating retinal pathology, confirming the importance of selective ROCK inhibitors for ROCK2 and ROCK1. To further investigate the differential expression pattern of both isoforms in healthy and pathological conditions, ROCK expression studies will also be performed for other retinal cell types, such as RGC neurons. Furthermore, since our *ex vivo* data indicated ROCK expression in RGCs, it would be interesting to co-culture glia and neurons, to assess interactions and crosstalk between glial cells and neurons and the resulting effect on ROCK signalling. Moreover, these co-cultures could then be subjected to ROCK inhibitors or to glial inhibitors, to unravel ROCKs function in glial reactivity or neurodegenerative processes.

To study neurodegeneration in an ex vivo model, the porcine explant model was developed to mimic neurodegeneration. This model showed a significant decrease in RGC cell survival and an increase in glial reactivity, mainly from Müller glia, after one week in culture. However, general retinal laminar organisation was maintained. After development and optimisation of this neurodegeneration mimicking model, it will be implemented for use in neuroprotective research. We aim to verify and compare the neuroprotective effects of different ROCK inhibitors in this neuroprotection assay. RGC degeneration, glial reactivity and morphology will be explored with and without the addition of ROCK inhibitor to examine whether or not injured RGCs can be rescued from apoptosis.

To explore the outgrowth promoting capacities of ROCK inhibitors and neurotrophins, the postnatal mouse *ex vivo* retinal explant model was used. In this model ROCK2 was expressed in glial fibres and neurites. To analyse neurite outgrowth, a novel in-house developed Fiji

script for automated neurite outgrowth analysis was successfully evaluated in comparison to the previously used in-house developed Axiovision script, of which the software was outdated. Postnatal mouse retinal explant data confirmed the potential of ROCK inhibitors to promote the axonal outgrowth that was even more pronounced when supplemented with neurotrophic factors. Moreover, these experiments implicate that ROCK inhibition (in combination with both neurotrophic factors) can support the earlier stages of axon regeneration, neurite outgrowth initiation, while the ROCK inhibitors have a negative influence on the neurite elongation potential of the neurotrophic factors. More research is necessary to determine the *in vivo* capacities of these ROCK inhibitors in combination with neurotrophins.

In this thesis, *in vitro* mouse retinal cell models indicated the involvement of Müller glia in the stress response and that the Rho-ROCK pathway signals via these Müller glia. Furthermore, the optimisation of the *ex vivo* porcine retinal explants resulted in a suitable model to study neuroprotection. Moreover, *ex vivo* postnatal mouse explants confirmed the neurite outgrowth potential of ROCK inhibitors and neurotrophic factors, while the combination of both demonstrated that ROCK inhibition could clearly support neurite outgrowth initiation, while negatively influencing the neurite elongation potential of neurotrophic factors. Furthermore, this study highlights the necessity of further unravelling the cellular mechanisms of the Rho-ROCK pathway before applying ROCK inhibition as an innovative therapy for glaucoma, diabetic retinopathy and other neurodegenerative diseases.

Addendum

A. Risk analysis

In the context of Health, Safety and Environment (HSE), risks concerning the experimental practiced described in this thesis were briefly assessed.

In vitro and *ex vivo* experiments were carried out in a separate cell culture room with containment level 2 (L2), while all other practical experiments were performed in a laboratory with containment level 1 (L1) and). To protect the researcher, **lab coat** and **gloves** were continuously obligated when working in the lab and consumation of food and drinks were not allowed in the lab. Researchers entering the mouse facility always wore an additional mask, overshoes and a hair net to prevent transfer of infections and exposure to allergens to provide an optimal personal hygiene. The use of individual filtertops on mouse cages when working in proximity to the cages is appropriate for the same reasons. Correct waste disposal is important to guarantee safety and minimise impact on the environment. **Hazardous** and **non-hazardous waste** were separated, the latter being contained in normal dustbins. Extra attention was payed to **sharp objects**, such as the needle to punch a hole in the mouse eyes during dissection or blades to cut open the porcine eyes. These objects obviously held an extra physical risk. After use, sharp objects were disposed in a needle container. Hazardous **chemical waste** was consequently collected in the correct waste category. Hazardous **biological waste** in pasty or liquid form, such as fluids used in cell or explant cultures or organs and tissues from eye dissections, were collected in plastic PE barrels. Hazardous biological waste in solid form, such as empty culture bottles, well plates, tissue and gloved, were collected in Cordi boxes.

The Müller glia and microglia **cell cultures** were non-pathogenic biological agents. These cells were only manipulated in the L2 cell culture room with new gloves under a sterile horizontal flow while equipped with a sterile lab coat to protect the researcher, yet also to prevent the cells from getting infected by pathological micro-organisms.

In the experimental lab work, several hazardous chemical compounds were used. Risks of the most relevant products will be defined with the necessary precautions to handle these risks. Two of the stressors of the Müller glia were $CoCl_2.6H_2O$ and H_2O_2. **$CoCl_2.6H_2O$** (special liquid waste, category 5) is most likely a carcinogenic substance that is harmful by ingestion and can lead to reduced fertility and skin and eye irritations. On top of that, it is harmful to the environment. This substance was always handeled carefully and kept away from heat. Additional mask and safety goggles were continuously used while handling this product. **H_2O_2** (category 5), a strong oxidiser was kept away from flames and heat because it can evoke serious skin burns. To fixate the tissue, **4% paraformaldehyde** (PFA) was used (category 5). PFA is a toxic substance and is potentially carcinogenic. It is also harmful and can irritate

when inhaled, ingested or makes contact with eyes and skin. Therefore PFA was always handled with care under a fume hood and additional protection with mask and safety goggles was advised. During the H&E stain on porcine explants, **xylene (**non-halogenated organic liquid waste, category 3) is used in the dehydration series. This product is highly flammable, possibly carcinogenic and also harmful when inhaled or when it comes in contact with skin, which forces the user to continuously handle this product under a fume hood. **Boric acid** (acid inorganic liquid waste, category 1) was used in the lava purple stain of Western Blotting (WB). It is a substance that may impair fertility and cause harm to the unborn child. The WB stripping buffer, which effectively removes antibodies from the membrane, contains **sodium dodecyl sulphate** (SDS) (category 3). This product is harmful when it comes in contact with the skin and with ingestion and is irritable for skin and eyes. **Triton X-100** (category 3) is a component of TBS and the lysis buffer for cells and explants. This product is harmful by ingestion, can cause serious eye damage and is slightly irritating to the skin. Therefore, safety goggles were used and after handling, hands were thoroughly washed. Because BDNF and CNTF, two neurotrophic factors used to promote axon regeneration in mouse explants, are not soluble in water, **dimethyl sulfoxide** (category 5) was used. This product is irritable to the skin and eyes, which is why it needed to be carefully handled. **ROCK inhibitors** Y-39983 and AMA0428 were administered to investigate axonal regeneration in mouse explants. Protective clothing and gloves are advised when working with these producs. They can be harmful when inhaled, swallowed and after coming in contact with the skin and eyes. Finally, **liquid nitrogen** is an extremely cold substance (freezing point -210°C), used to snapfreeze porcine explants and to freeze Müller glia for later use. It can supersede oxygen in the surroundings and can build up pressure very quickly, which is why it is important to provide good ventilation and not containing the substance without pressure safety. Researchers can not touch the liquid nitrogen with their bare skin because this would cause freeze wounds. For this reason, centrifuge tubes or vials are always removed from the nitrogen with an appropriate gripper.

B. Extra figures

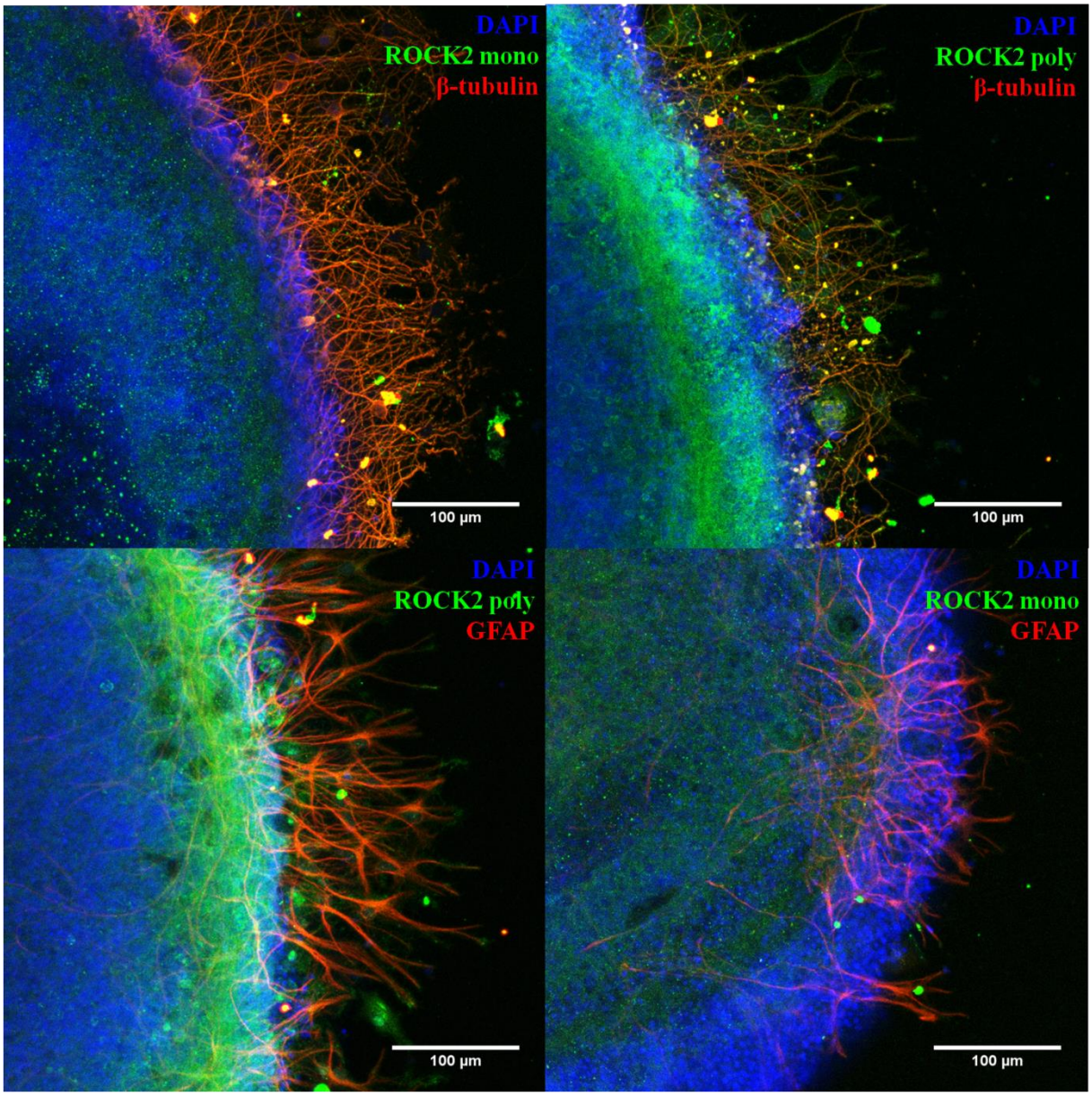

Figure 31: ROCK2, GFAP and β-tubulin ICC double staining on P3 explants. Overlay of the blue channel (DAPI), the green channel (ROCK2) and the red channel (β-tubulin or GFAP).

ANIMAL PHYSIOLOGY AND NEUROBIOLOGY SECTION
Naamsestraat 59 box 2465
3000 LEUVEN, BELGIUM
tel. + 32 16 33 02 83
fax + 32 16 32 39 02
www.kuleuven.be